Title

IDENTIFICATION OF ORAL CANCER SPECIFIC LIGANDS FROM ONE-BEAD ONE-COMPOUND COMBINATERIAL LIBRARIES TO DEVELOP THERANOSTIC AGENTS AGAINST ORAL SQUAMOUS CELL CARCINOMA

Permalink

https://escholarship.org/uc/item/9w14k8p4

Author

Yang, Fan

Publication Date

2016

Peer reviewed|Thesis/dissertation

IDENTIFICATION OF CANCER SPECIFIC LIGANDS FROM ONE-BEAD ONE COMPOUND COMBINATORIAL LIBRARIES TO DEVELOP THERANOSTICS AGENTS AGAINST ORAL SQUAMOUS CELL CARCINOMA

by

Frances (Fan) Yang

DISSERTATION

Submitted in partial satisfaction of the requirements for the degree of

DOCTOR OF PHILOSOPHY

in

Oral and Craniofacial Sciences

in the

GRADUATE DIVISION

of the

UNIVERSITY OF CALIFORNIA, SAN FRANCISCO

ACKNOWLEGEMENTS

ABSTRACT: IDENTIFICATION OF ORAL CANCER SPECIFIC LIGANDS FROM ONE-BEAD ONE-COMPOUND COMBINATERIAL LIBRARIES TO DEVELOP THERANOSTIC AGENTS AGAINST ORAL SQUAMOUS CELL CARCINOMA

Background: Oral squamous cell carcinoma (OSCC) is one of the most prevalent diseases worldwide and the patients have a particular low 5-year survival rate. The cause of this outcome is likely multifactorial and may be related to the late detection and lack of effective tumor specific therapies. In addition, the special structure of the tongue that is poorly equipped to protect itself from invasion and metastasis of cancer cells, also contribute to the poor prognosis. Therefore, development of early detection techniques and subsequent innovative OSCC specific targeting therapeutic are greatly needed. One-bead one-compound (OBOC) combinatorial technology is a powerful method to identify peptidomimetic ligands against a variety of receptors on cell surfaces. We therefore **hypothesized** that cancer specific ligands against OSCC might be identified through the high throughput screening of OBOC combinatorial libraries. The OSCC ligands can be conjugated to optical dyes or nanocarriers to develop theranostic agents against OSCC.

Material and methods: twenty four OBOC combinatorial peptide libraries were generated using split-mix synthesis approach. A rainbow beads assay was utilized to select proper OBOC libraries for the large-scale screening.   Live OSCC cells were incubated with OBOC libraries and beads with cell binding were sorted and re-incubated with different OSCC cell lines. The peptide-beads that were able to bind different OSCC cells were then screened with normal human keratinocyte, endothelial cell lines, fibroblast cells and granulocytes. The peptide-beads exhibiting property of binding to

different OSCC cell lines but no binding to normal human cells were finally identified. The chemical structures of these compounds were determined by Edman sequencing. Hemolytic assay and MTT assay were employed to evaluate potential cytotoxicity of identified compounds. The molecular probes of OSCC (named as LLY1, LLY2, LLY5, LLY12 and LLY13) were developed by conjugating OSCC ligands to biotin via a hydrophilic linker on the carboxyl end of the peptides. *In vitro* peptide-histochemistry study as well as *In vivo* and *ex vivo* mice orthotropic models were employed to evaluate OSCC probes' targeting efficacy and specificity. OSCC ligand induced cell endocytosis assay was used to assess the OSCC ligands' cell penetration property by incubating ligand-biotin/streptavidin-fluorophor complex with live OSCC cells. To investigate the corresponding receptor involved in the binding of OSCC ligands with OSCC cells, a panel of anti-integrin antibodies was evaluated for their ability to block OSCC cells binding to these ligand beads. Suspected integrin was further confirmed by receptor transfected cells confirmation assay. OSCC theranostic agents were developed by synthesizing ligand conjugated and PEG/cholic acid (CA) containing amphiphilic telodendrimer (Ligand-PEG^{5k}-CA$_8$) and then mixed with PEG^{5k}-Por$_4$-CA$_4$ telodendrimer. After lyophilization, ligand-telodendrimer and porphyrin-telodendrimer were self-assembled in aqueous solution to form targeting micellar nano-porphyrins (NPs). OSCC orthotopic bioluminescent tumor model was established in nude mice, and used to study the biodistribution and targeting efficiency of OSCC optical probe as well as OSCC theranostics.

Results: Among twenty-four OBOC combinatorial libraries screened, six OBOC combinatorial libraries were identified for possessing OSCC cell binding beads.

Following the large-scale high throughput screening assays, six ligands were discovered from ~45,000,000 compound beads with ability to bind strongly to four different human OSCC cell lines but not bind to human NHK, fibroblast cells, endothelial cells and granulocytes. The amino acid sequences of these peptides were determined by Edman sequencing. Even with the small number of ligands identified, a motif was observed among these ligands. These six peptides were re-synthesized in soluble form, purified by HPLC and the molecular weights were confirmed by mass spectroscopy. Initial peptide-histochemistry study indicated that LLY12 and LLY13 were able to detect OSCC cells grown on chamber slides at the concentration of 1 μM, while there were weak bindings to the human keratinocytes and endothelial cells. In addition, LLY13 was found to have the property to penetrate into OSCC cells and accumulate in the cytoplasm as well as in the nucleus. After screened with anti-α1, α2, α3, α4, α5, α6, αV, β1 antibodies, only anti-α3 antibody was able to block most of OSCC cells binding to the LLY13 compound beads. Furthermore, the α3 transfected K562 cells were able to bind to the LLY13 compound beads, while parent K562 cells did not bind to LLY13 compound beads, thereby indicating that α3 integrins are indeed involved in the interaction between the LLY13 and OSCC cells. OSCC theranostic agents developed using targeting LLY13 micelles (25± 4nm in diameter) were more efficient in binding to HSC-3 cancer cells compared to non-targeting micelles. *Ex vivo* images demonstrated that both non-targeted micelles and targeting micelles exhibited relatively high uptake in the HSC-3 orthotopic tumor compared to normal organs except for liver, while xenografts from the mice with targeting micelles appeared to have higher signals than

the non-targeting groups, i.e., the median fluorescence intensity of tumors for targeting

micelles is 2.44 folds higher than that for non-target micelles.

Conclusion: LLY13 has promising *in vitro* and *in vivo* targeting activity against OSCC.

In addition, LLY13 is also able to penetrate into cancer cells via endocytosis. Initial

study indicated that α3 integrin might partially be the corresponding receptor involved

for LLY13's binding to oral cancer cells. OSCC ligands developed from this study may

become potential candidates for the development of OSCC targeted theranostic agents

after further optimization. This work also demonstrates that the combinatorial strategy of

OBOC libraries in conjuncture with high throughput screening assays can be adopted in

the field of oral cancer targets discovery. Work is currently underway to evaluate

LLY13's binding affinity and specificity against pre-cancerous lesions and OSCC from

human tissues, including leukoplakia, erythroplakia or combined pathologies, oral

cancer, as well as normal human oral tissues.

TABLE OF CONTENTS

CHAPTER 3. IDENTIFICATION OF ORAL CANCER SPECIFIC LIGANDS FROM ONE-BEAD ONE-COMPOUND COMBINATORIAL LIBRARIES AGAINST OSCC –

LIST OF TABLES

CHAPTER 3. IDENTIFICATION OF SPECIFIC LIGANDS FROM OBOC COMBINATERIAL LIBRARIES AGAINST OSCC

CHAPTER 4. DEVELOPING OSCC OPTICAL PROBES – *In vitro* and *in vivo* STUDIES OF THEIR TARGETING EFFICACY

CHAPTER 5. INVESTIGATION OF CORESPONDING RECEPTOR INVOLVED FOR LLY13 AND OSCC CELLS

LIST OF FIGURES

CHAPTER 5. INVESTIGATION OF OSCC LIGANDS–RECEPTOR INTERACTION—

CHAPTER 6. DEVELOPMENT OF TARGETING NANO PORPHYRINS WITH BOTH IMAGING AND THERAPEUTIC POTENTIAL AGAINST OSCC

CHAPTER 1. INTRODUCTION

1.1. Dissertation motivation and clinical significance:

Oral cancers ranks the eighth to tenth most common cancer worldwide, accounting for about 4% of all cancers, (1,2, 3). Histopathologically, OSCC is by far the most common cancer type of the oropharynx and oral cavity, representing more than 90% of all oral cancers (4, 5). Oral tongue squamous cell carcinoma (OTSCC) is the most common subtype cancer diagnosed in the oral cavity comprising 25-40% of oral carcinoma, and along with the closely related cancer of the floor of the mouth (15-20%) can account for more than half of all oral carcinomas when excluding those affecting the lips (6, 7). Patients diagnosed with oral cancer have a particularly poor prognosis, which might be related with the compounding factors of later detection and lack of truly effective therapies. In addition, the special structure of the tongue that is poorly equipped (rich lymphatic network and highly muscularized structure) to protect itself from invasion and metastasis, might also contribute to the poor prognosis of OSCC patients. OSCC of the tongue is thus more frequently associated with metastasis to draining lymph nodes than any other cancer of the oral cavity (8). Despite the intensity of treatment with chemotherapy, radiation therapy and surgery, oral cancer remains the third most lethal cancer, accounting for 18% of all cancer deaths and a 5-year survival of less than 50% (9, 10). Current diagnostic techniques involved light-based detection systems, fluorescent visualizations and brush cytology (11, 12, and 13). Unfortunately, only 35% of cases are caught early in time. So far, there are no specific biomarkers for oral cancer. Therefore, there is an urgent need to look for specific biomarker for OSCC to improve its early detection techniques and subsequent innovative therapies. I

hypothesized that one bead one compound combinatorial strategy can be employed to identify cancer specific ligands to develop theranostic agents against OSCC.

This research project involves the discovery of cancer specific ligands against OSCC. The OSCC specific ligands can be used to develop tumor imaging probes that can be applied for primary clinical screening as well as tumor imaging on direct biopsy samples. Furthermore, OSCC specific ligands can be conjugated to nano-carriers to enhance specific delivery of chemotherapy drugs to tumor sites while sparing the normal organs. If proven successful, the new technology can be translated into novel and effective therapeutic agents for human oral carcinoma. As a result, we expect that patients with refractory oral carcinoma will benefit from such novel strategies of diagnosis and treatments.

1.2. Oral squamous cell carcinoma

OSCC is ranked from the eighth to tenth most common among the cancers in various studies with incidence of more than 500,000 cases per year worldwide (1,2,3). The survival rate of OSCC greatly depends upon the tumor stage at the time of diagnosis. Patients with stage I tumors have a 5-year survival rate of 75%, that dramatically decreases in patients with stage III or IV disease, to 49% and 30%, respectively (14,15).

OSCC is a malignancy of the squamous epithelium of the oral cavity and includes tumors found in the tongue, lip, gingival, palate, floor of mouth and buccal mucosa. Histopathologically, OSCC is by far the most common cancer type of the oropharynx and oral cavity, representing more than 90% of all oral cancers (4, 5). Oral tongue squamous cell carcinoma (OTSCC) is the most common cancer diagnosed in

the oral cavity comprising 25-40% of oral carcinoma, and along with the closely related cancer of the floor of the mouth (15-20%) can account for more than half of all oral carcinomas when excluding those affecting the lips (6, 7). It is the advanced form of precancerous lesions, which develop in the form of benign or malignant tumors. Precancerous lesions can be in the form of leukoplakia (white lesions), erythroplakia (red lesions), erythroleukoplakia (combination of white and red lesions), or oral submucosa fibrosis (deposition of collagen on fibromuscular connective tissue) and all of these potentially give rise to primary tumor in the oral cavity (16, 17, 18). Oral cancer (OC) is known to have a multi-factorial etiology; tobacco, alcohol and betel quid being the major risk factors, especially in combination with smoking and heavy alcohol consumption (19, 20). The consumption of alcohol may lead to a multiplication effect, most likely by enhancing the penetration of tobacco carcinogens in laryngeal tissue. Furthermore, infections with human papilloma virus (HPV) are associated with oropharyngeal carcinogenesis (21, 22).

The diagnostic pathway for suspicious lesions in the oral cavity usually starts with the comprehensive oral examination (COE) based on inspection and palpation of the oral mucosa with the support of an incandescent light available on the dental chair. It is well known that COE mainly depends on a subjective interpretation, which is a consequence of the experience of the operator. Moreover, oral epithelial dysplasia (OED) and early OSCC may already be present within areas of macroscopically normal oral mucosa, as well as within the context of oral lesions with malignant potential, such as leukoplakia, erythroplakia, submucous fibrosis and oral lichen planus. The gold standard for the diagnosis of oral dysplastic and neoplastic malignant lesions is

histological examination. Incisional or excisional biopsy techniques are the most reliable methods to collect a surgical specimen suitable for microscopic evaluation. Many other noninvasive techniques to date have been applied for the earlier detection of OSCC, e.g. light-based detection system, fluorescent visualizations and brush cytology (11, 12, and 13), but they all have certain limitations. Light-based techniques, including chemiluminescence and auto-fluorescent imaging, work on the assumption that neoplastic and pre-neoplastic tissues that have undergone abnormal metabolic or structural changes and have different absorbance and reflectance properties when exposed to specific wavelengths of light. In the last decade, light-based technology has been adapted and marketed for use in the oral cavity carcinoma detection. However, only 35% of oral tumors are caught in the earlier stage (23). Among the approaches to the treatment of OSCC such as surgery, radiation therapy (external beam radiotherapy and/or brachytherapy), and adjuvant therapy after surgical resection (chemotherapy with agents such as cisplatin, carboplatin, 5-fluorouracil, paclitaxel and docetaxel), the mortality rates for OSCC remain high and the prognosis of OSCC is generally poor with an overall survival rate less than 50% (14, 15), as well as an estimated recurrence rate of 30% (24). In general, oral cancer is one of the most common cancers in the world, with a delayed clinical detection, poor prognosis, without specific biomarkers for the disease and expensive therapeutic alternatives. Therefore, there is urgency for the development of novel and sensitive probes, as well as efficacious therapeutic agents for the early diagnosis and treatment alternative of OSCC.

1.3. Rationale for the development of theranostic agents for OSCC

Targeted molecules have become important for cancer diagnostics and treatment because of their specificity in attacking cancer cells instead of normal tissues by focusing on trying to combine targeting molecules with diagnostic imaging agent and/or therapeutics into a single entity, enhancing their site-specific tumor imaging and delivery while reducing off-targeting agents. Furthermore, more emphasis is now focused on identification of peptidomimetic molecules instead of monoclonal antibodies for better cell surface-targeting agents because they are a) smaller and therefore can penetrate large tumors better; (b) less likely to bind to the reticuloendothelial system such as liver, spleen, and bone marrow; and (c) easy to derivatize chemically (25). Therefore, peptidomimetic molecules are well suited as OSCC biomarkers for the development of the theranostic agents for cancer disease. The OBOC combinatorial strategy has been proven to be a powerful tool for the identification of synthetic ligands against specific biological targets (26, 27, 28, 29, 30). In this method, the OBOC library is prepared by a "split-mix synthesis" approach using polystyrene beads (88 micron diameter) as a solid support. As a result, each bead displays only one chemical entity and there are approximately 10^{13} copies of the same chemical entity. The schematic illustration of the generation of a OBOC combinatorial library is shown in Figure 1.1. This one-bead one-compound feature enables one to rapidly screen hundreds of thousands to millions of library beads with an on-bead binding or functional assays. The exact chemical nature of the compounds on selected beads with specific biological function can be determined with an automatic micro-sequencer. This technique has been applied to the discovery of targeting ligands against various biological targets, such as cancer cell surface receptor (27, 28, 29, 30), protein kinase substrates and inhibitors, (31, 32) protease substrates

and inhibitors(33, 34), artificial enzymes, (35, 36) and various ligands for the preparation of affinity column media(37, 38).

However, targeted therapy not only needs specific recognition of cancer cells but also need specific delivery of anti-cancer drugs to the tumor site as well. Hence, nanotechnology is an emerging field that has shown great promise for the development of novel diagnostic imaging and therapeutic agents for a variety of diseases including cancer. Recently, my mentor, Lam et al. and his colleagues developed several novel nano-carriers for the delivery of paclitaxel (PTX) or other hydrophobic anti-cancer drugs (39, 40, 41, 42, 43). Using a reversible disulfide crosslinked micelle system named nano porphyrins (NPs), (PEG^{5k}-Cys$_4$-CA$_8$ teloderdrimers), hydrophobic drugs can be encapsulated and triggered to be released at the tumor site and inside the cancer cells with high reductive potential. PEG^{5k}-Cys$_4$-CA$_8$ loaded with PTX and decorated with ovarian cancer binding ligands (discovery through OBOC library screening), exhibit superior anti-tumor efficacy and lower systemic toxicity profile in dude mice bearing ovarian cancer tumor xenografts, when compared with equivalent doses to non-targeted PTX nanoparticles as well as clinical PTX formulation (Taxol ^{R}) (44).

In this project, we have used OBOC combinatorial library technology to identify cancer specific ligands for the improvement of screening and diagnostic techniques in parallel with the development of new therapeutic molecules against OSCC.

1.4. Research hypotheses and specific aims

The overall goal of the proposed research is to discover cancer specific ligands using

the OBOC combinatorial strategy to develop targeting theranostic agents against OSCC. **Our hypothesis** is that specific ligands against OSCC might be identified through the high throughput screening OBOC combinatorial libraries. The OSCC ligands can be conjugated to optical dyes or nanocarriers to develop theranostic agents, thus enhancing the earlier detection of OSCC as well as the delivering of therapeutic drugs to the tumor sites while sparing the normal organs.

The specific **aims** of this project are as follows:

AIM 1: Identification of cancer specific ligands from OBOC combinatorial libraries against OSCC. Twenty-four OBOC libraries are generated using the split-mix synthesis method. Rainbow beads assay is used to select suitable OBOC libraries for the large-scale screening using live human oral cancer cells as well as normal cells to identify the compound beads which only bind to different oral cancer cell lines but not bind to normal human cells. MTT assay is used to evaluate potential cytotoxicity of identified ligands.

AIM 2: Development of OSCC probes and evaluation of their targeting efficacy. OSCC probes are generated by conjugation of optical dyes (Quantum Dots, fluorescent, IR, organic and etc.) using OSCC targeting ligands selected from AIM 1. These imaging probes are evaluated for their binding ability and specificity to different OSCC cell lines using peptide-histochemistry assay. The biodistribution and targeting efficacy of the OSCC probes will also be assessed by using mice bearing subcutaneous and orthotopic OSCC xenograft models.

AIM 3: Investigation of OSCC ligand-receptor interaction. The OBOC library from which we identified OSCC binding ligands is the focused library based on a cyclic peptide motif to bind preferentially to ovarian cancer with high specificity against α3 integrin, therefore, it is expected that the ligands identified might involve α3 integrin interactions. Alpha integrin blocking kit and beta integrin blocking kits are used to perform the primary screening for the corresponding receptors involved.

AIM 4: GENERATION of "ALL IN ONE" TARGETING THERANOSTIC AGENTS: *in vitro* **and** *in vivo* **STUDIES**

4.1. Develop OSCC targeting NPs by conjugating OSCC ligand with nano porphyrins. nano porphyrins (PEG^{5k}- CA_8 telodendrimers) are prepared according to Dr. lam's lab published methods (39,40,41,42,43). Click chemistry is used for the conjugation of OSCC binding ligands.

4.2. Evaluate bio-distribution of targeting NPs. OSCC orthotopic xenograft model is employed to determine *in vivo* and intra-tumoral distribution of targeting nanoporphyrin.

1.5. Figures and Tables
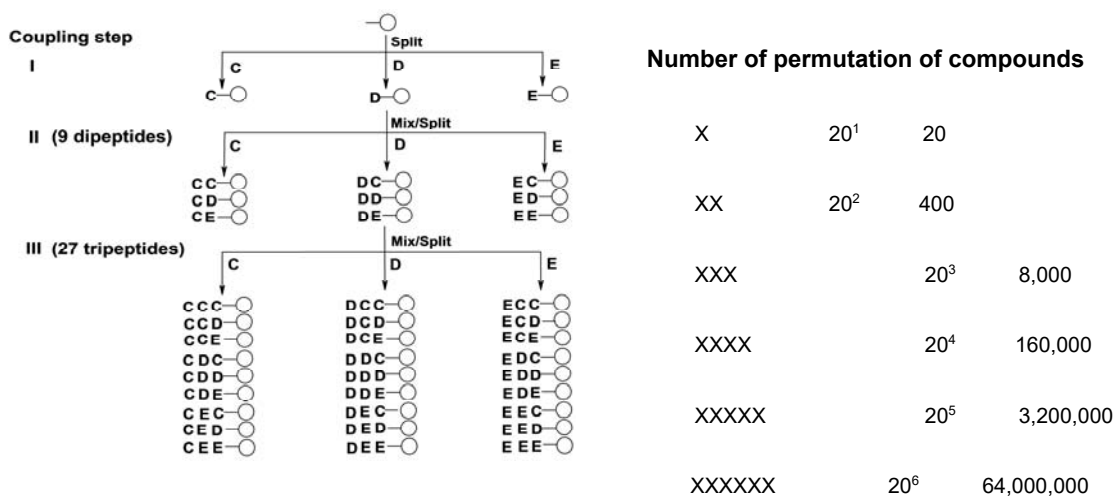
Figure 1.1. Schematic illustration of generation of one-bead one-compound combinatorial library.

CHAPTER 2. GENERAL EXPERIMENTAL TECHNIQUES

2.1. Generation of random and focused OBOC libraries. Twenty-four random and focused OBOC libraries were generated by using a split-mix synthesis approach as previous described (26). Standard solid phase peptide synthesis method with 9-Fluorenylmethoxycarbonyl (Fmoc) chemistry was used to synthesize the OBOC libraries. Briefly, the peptide was synthesized on 88 μm polyethylene glycol-grafted beads resin (loading 0.25 mmol/g), using 1-hydroxybenzotriazole/1, 3-diisopropylcarbodiimide as coupling reagents. Three-fold molar excess of Fmoc-protected amino acids to resin was used for coupling. Completion of coupling and Fmoc deprotection were monitored by the ninhydrin test. The disulfide formation was achieved with 20% DMSO in ammonia acetate buffer (pH 6.2). These libraries contained tens of millions compound beads with each carrying a peptide with distinct natural and unnatural amino acid or small organic molecule moieties. Twenty four OBOC libraries were used in these studies, including X1 focused OBOC combinatorial library, RGD based OBOC combinatorial library, seven cyclic OBOC combinatorial library and fifteen random OBOC combinatorial libraries.

2.2. Screening using rainbow bead assay. Rainbow bead assay was adopted to select suitable OBOC combinatorial libraries for subsequent large-scale screening (45). Briefly, OBOC compound beads displaying chemical compounds or families of compounds were stained with oil-based organic dyes that were used as coding tags. The color dyes did not affect cell binding to the compounds displayed on the surface of the beads. The twenty-four small samples of each OBOC combinatorial library (~15,000 beads) were color-coded and washed with PBS. In each run, four of OBOC

combinatorial library beads were combined and screened concurrently against live HSC-3 oral cancer cells for 1 hour. Those OBOC libraries having OSCC binding were selected for subsequent large-scale screening.

2.3. Large-scale screening assay. Large-scale screening assay with intact live OSCC cells was employed to identify high-affinity OSCC binding compound beads. The OBOC combinatorial libraries selected from rainbow bead assay were screened in large scale (~750,000 beads/each library) using live intact HSC-3 cells. Briefly, HSC-3 cells were grown in DMEM media with supplemented with P/S and 10% FBS. After harvested by Trypsin, HSC-3 cells were incubated with OBOC libraries for 1 hour. Beads with unique binding ligands that interacted with cell surface receptors were coated by one or more layers of the HSC-3 cells. These positive beads were isolated and the binding cells were stripped off by using 8M guanidine hydrochloride. After thorough washing with water and then PBS, the OSCC cell binding beads were then rescreened with other OSCC cells, such as SCC4, SCC10a, HOK313 and MOK101, to ensure their true positive binding properties.

2.4. Ligand specificity filtering assay. A specificity filtering assay was used to identify non-keratinocyte binding beads from the OSCC binding beads selected from large scale screening. The OSCC binding beads were incubated with live human keratinocytes, endothelial cells (Huvec), fibroblast cells (NUFF) and freshly isolated granulocytes separately. Those peptide beads with strong binding to OSCC cells that did not bind to normal human cells were finally selected. The chemical structures of selected beads were determined by Edman chemistry using an automatic ABI-protein sequencer.

2.5. Hit validation assay. Hit validation assay was used to evaluate compounds'

binding affinity and specificity using different human OSCC cell lines and normal human

cells. Those compound beads with high affinity and specificity for OSCC cells were

resynthesized in a large amount on TentaGel and were incubated with different OSCC

cell lines (HSC3, SCC 4, SCC10A, HOC313 and MOK 101) for 1 hr, as well as

incubated with normal cells, including immortalized human keratinocytes (HaCAT),

fibroblast cells (NUFF), endothelial cell (Huvec) and granulocyte for 4 hours. The

peptides with the property to bind to all of the OSCC cells tested that did not bind to

normal human cells were selected for the further cytotoxicity evaluation.

2.6. Cytotoxicity evaluation assays. Those compound beads with high binding affinity

and specificity for OSCC cells were resynthesized in a large amount in solution form.

MTT assay was used to evaluate the potential cytotoxicity of the OSCC compounds

identified on normal human keratinocytes (46, 47). Briefly, human keratinocytes were

cultured on 96-well plate overnight. The serially diluted ligands were added to each

wells and incubated for 4 hours before adding MTT (3-[4,5-dimethyl-thiazol-z-yl] 2,5

diphenyl tetrazolium bromide) solution (5μg/ml in PBS). After 4 hour incubation, DMS-

containing solution was added. The optical density at 540 nm was measured with an

auto-reader. The Hemolytic assay was used to evaluate the potential toxicity of these six

peptides (48). Briefly, six peptides were serial diluted in sterile saline (0.9 %), and

incubated with healthy human RBC ($4x10^6$ RBC/ml) for 6 hrs. and absorbance was read

by micro-plate reader at 550 nm. Triton X-100 1% was served as 100% hemolytic

positive control. RBC without added compounds was used as a negative control.

2.7. Peptide-histochemistry assay. Peptide-histochemistry assay was used to evaluate the binding efficacy and specificity of identified ligands to different human OSCC cell lines and normal cells (49). OSCC probes were generated by biotinylating the carboxyl end of the ligands via a hydrophilic linker to form ligand –linker-lysine(biotin). Human OSCC cells and normal human keratinocytes were seeded on culture chamber slides. At 70% confluency, OSCC cells were incubated with 5% BSA to block non-specific binding. After washed with PBS 3X, OSCC probes at different concentrations were added to the OSCC cells grown in the chamber slides and incubated for half an hour, then washed 3X with PBS, followed by adding 1:500 dilution of streptavidin-Alexa 488 and incubation for half hour. Specimens were washed 3X with PBS and fixed briefly with 4% formaldehyde before adding the DAPI. Confocal microscopy was then performed to observe the cell binding efficacy.

2.8. Ligand uptake assay. OSCC ligand induced cell endocytosis assay was used to investigate endocytic uptake of the targeting ligand by live OSCC cells (50, 51). Biotinylated ligand LLY13 (50 µM) was first pre-incubated with streptavidin-PE (1mg/mL) for 2 hours at RT and at 4º C overnight to form the biotin-peptides-streptavidin complexes. OSCC cells (HCS-3) were seeded in chamber slides at a concentration of $2x10^4$ cells. After 60% confluency, biotin-peptides-streptavidin complexes were added at different time intervals (30 min, one hour, two hours and three hours). By the end of experiments. 1:2000 dilution of DAPI was added to the specimens. Peptide induced endocytic uptake of OSCC was observed under confocal laser scanning microscope.

2.9. Establishment of OSCC tumor model. Establishment of subcutaneous and bioluminescent orthotopic mice OSCC models were used to evaluate ligands' targeting

efficacy. All animal experiments were performed in compliance with the institutional guidelines according to protocol No. 07-13119 and No. 09-15584 approved by the Animal Use and Care Administrative Advisory Committee at the University of California, Davis. 20 athymic nude mice (*nu/nu*) were obtained from Harlan (Hayward , CA, USA) at 5 to 6 weeks of age. OSCC subcutaneous were established by injecting HSC 3 (1×10^6 cells) into the right flank (n=10) (52, 53). To establish OSCC orthotopic bioluminescent nude mice model in tongue, HSC3 cells were infected with lentiviral vectors that express green fluorescent protein (GFP)/firefly luciferase fusion proteins. 20 μl of 1×10^5 infected HSC-3 cells mixed with Matrigel at 1:1 were implanted into mice tongue (n=10) (54, 55). Tumors were measured with calipers 2 times per week and the volume was calculated by the formula for hemiellipsoids.

2.10. NIR Optical Imaging. *In vivo* and *ex vivo* optical imaging studies were performed to evaluate the bio-distribution and efficacy of binding specificity of the OSCC targeting against OSCC xenografts (56, 57, 58, 59). OSCC subcutaneous and orthotopic mice models were established as described above. After tumors developed ($2\times2\times2$ mm^3) in mice tongues' and $8\times8\times8$ mm^3 in mice flanks, tetravalent OSCC probe-biotin-Cy.5 complex (1.8 nmol), prepared by mixing 7.2 nmol of biotinylated peptide with 1.8 nmol of streptavidin-Cy5.5 in PBS overnight at 4°C, was injected into the mice via the tail vein. Twenty four hours after injection, the mice were anesthetized by an injection of 30 μL Nembutal (50 mg/mL) and images were acquired with a Kodak IS2000MM Image Station with excitation filter 625/20 band pass, emission filter 700WA/35 band pass, and 150 W quartz halogen lamp light source set at maximum. The mice were then sacrificed

and the organs were excised for *ex vivo* imaging. Data were collected and analyzed using the Kodak ID 3.6 software by mapping the region of interest on the images.

2.11. Histological study. H&E staining of excised OSCC bearing tongues was performed to evaluate the targeting efficacy of the ligands on OSCC tissues (60). Six mice with OSCC tumors implanted in the tongue were randomly selected from each group, and sacrificed with cervical dislocation. The tumor specimens from mice tongues were excised by cutting the tongue root and bathed in a neutral buffered 10% concentrated formalin solution and embedded in paraffin embedded. The specimens were sectioned for hematoxylin and eosin staining. Histological assessment was conducted using optical microscopy.

2.12. Antibody-blocking Assay. Antibody-blocking assay was used to investigate the corresponding receptor involved for the peptide-receptor interaction (62, 63). Briefly, OSCC cells were harvested by trypsinization, washed once in phosphate-buffered saline, re-suspended in F10 buffer (1× PBS, 10% FBS, 0.1% NaN_3, 1mm $CaCl_2$, and 1mm $MgCl_2$), and then incubated with Integrin blocking kit (containing α1, α2, α3, α4, α5, α6, αV, and β1 antibody) at 1 µg per 1,000,000 cells for one hour. Integrin receptor blocked OSCC cells were washed with PBS 3X and then incubated with OSCC peptide on beads for one hour. The cell binding blocking effects of these peptide beads were observed under inverted microscope.

2.13. α3 integrin transfected cells binding study. A specific α3 integrin-transfected cells confirmation assay was employed to further confirm the suspect receptor involved for binding ligand. α3 integrin transfected K562 cells were generated by electroporation of parent K562 cell lines with a DNA construct containing full-length murine α3 cDNA

cloned from murine lung cDNA and a neomycin selectable marker. Stable transfected

cells were selected by passaging cells in culture medium containing 1 mg/ml G418

(Invitrogen) for 14 days followed by flow cytometry to isolate cells expressing the

highest level of surface-expressed murine α3 integrin. α3-transfected K562 cells were

cultured in DMEM supplemented with 4 mm L-glutamine adjusted to contain 1.5 g/liter

sodium bicarbonate, 4.5 g/liter glucose, 1.0 mm sodium pyruvate, 10% FBS, 2.5%

mouse IL-3 culture supplement, and +1.5 mg/ml active G418 (64). OSCC binding beads

were then incubated with α3-transfected K562 cells for three hours. The effect of cell

binding to compound beads was observed by microscope. Non-α3 transfected K562

parent cells were used as the control.

2.14. Generation of targeting NPs. The traditional porphyrin/CA hybrid telodendrimer

(PEG^{5k}-Por_4-CA_4), and the ligand conjugated porphyrin/CA hybrid telodendrimer (L-

PEG^{5k}-CA_8), were synthesized through solution-phase condensation reaction from

MeO-PEG-NH_2 and N_3-PEG-NH_2 using peptide chemistry as previously described (39,

40, 41, 42, 43). In brief, to make the traditional porphyrin/Ca hybrid telodendrimer,

(Fmoc)Lys(Fmoc)-OH(3 eq.) was coupled to the N-terminus of MeO-PEG^{5k}-NH_2 using

DIC and HOBt as coupling reagents until a negative Kaiser test result was obtained,

thereby indicating completion of the coupling reaction. PEGylated molecules were

precipitated by adding cold ether and then washed with cold ether twice. Fmoc groups

were removed by the treatment with 20% (v/v) 4-methylpiperidine in dimethyl-

formamide (DMF), and the PEGylated molecules were precipitated and washed three

times by cold ether. White powder precipitate was dried under vacuum and one

coupling of (Fmoc)Lys(Fmoc)-OH and one coupling of (Fmoc)Lys(Boc)-OH were carried

out, respectively, to generate a third generation of dendritic polylysine terminated with four Boc and four Fmoc groups on one end of PEG. Cholic acid-NHS ester (CA-NHS) were coupled to the terminal end of dendritic oligolysine after the removal of Fmoc with 20% (v/v) 4-methylpiperidine and the removal of Boc groups with 50% (v/v) trifluoroacetic acid in dichloromethane, and pyropheophorbide-a (12 eq.) were coupled subsequently to the leftover amino groups on the terminal end of dendritic polylysine, resulting in PEG^{5k}-Por_4-CA_4 thiolated telodendrimer. To make the ligand conjugated porphyrin/CA hybrid telodendrimer, we first prepared an azide modified telodendrimer N_3-PEG^{5k}-CA_8, using N_3-PEG^{5k}-NH_2. to generate a third generation of dendritic polylysine terminated with eight Fmoc groups on one end of PEG. Cholic acid-NHS ester (CA-NHS) were coupled to the terminal end of dendritic oligolysine after the removal of Fmoc with 20% (v/v) 4-methylpiperidine. Alkyne modified OSCC ligand LLY13 (cdG-Nle-G-Hyp-L-c-Ebes-K-alkyne) was synthesized via solid-phase synthesis on Fmoc-Rink Amide MBHA Resins using the standard Fmoc chemistry as described previously (39,40). Alkyne modified ligands was conjugated to the N_3-PEG^{5k}-CA_8 telodendrimer via Cu^I catalyzed cyclo-addition. The telodendrimer solution was filtered and then dialysed against 4 L deionized water in a dialysis tube with MWCO of 3.5 KDa; reservoir water was refreshed completely four times in 24 h. Finally, the telodendrimer was lyophilized. The conjugation was confirmed by quantitative amino acid analysis (AAA). To make targeted ligand conjugated telodendrimer with porphyrin, we mixed Ligand-PEG^{5k}-CA_8 with PEG^{5k}-Por_4-CA_4 (1:1).To prepare NP/ LNP, 20 mg porphyrin-telodendrimer or ligand-porphyrin-telodendrimer were dissolved in 1 ml PBS followed by sonication for 10 min to form NPs.

2.15. Cell targeting assay. LLY-13 NPs cell targeting assay was used to assess the OSCC ligand decorated NPs targeting efficacy (65). HSC-3 oral cancer cells were seeded in 8-well chamber slides until confluent and then incubated with 2 µM porphyrin-telodendrimer (PEG^{5k} -Por_4-CA_8) nanoparticles and ligand (LLY13)-decorated porphyrin-telodendrimer for 0, 30, 1 hr and 2 hr at 37 °C with 5% CO_2, respectively. Then, cells were washed three times with cold PBS, fixed with 4% paraformaldehyde for 10 min, and the nuclei were counterstained by DAPI. The slides were mounted with coverslips and observed by Olympus FV1000 confocal microscopy. In a separate experiment, different concentration of porphyrin-telodendrimer and ligand-porphyrin-telodendrimer (0, 0.05, 0.5, 5 µM) were incubated with HSC-3 to study the cellular uptake ability of these targeted NPs.

2.16. NIRF imaging of LLY13 NPs targeting efficacy. After orthotopic xenograft developed (~3 mm in diameter, n =10), mice were subjected to *in vivo* NIRF imaging by injecting 100 µl of LLY13-NPs via tail vein. At different time points post injection of LLY13 NPs, mice were scanned using a Kodak multimodal imaging system IS2000MM with an excitation bandpass filter at 625/20 nm and an emission at 700/35 nm under anesthesia. After *in vivo* imaging, animals were sacrificed. Tumors and major organs were then excised and imaged with the Kodak imaging station. Tumors were harvested and fixed in the cold formalin on ice. A fresh cross-section was made for LSI laser scanning confocal microscope imaging.

2.17. Statistical analysis. Statistical analysis was performed by Student's *t*-test for two groups, and one-way analysis of variance for multiple groups. All results were

expressed as the mean ± s.d. unless otherwise noted. A value of $P<0.05$ was considered statistically significant.

CHAPTER 3. IDENTIFICATION OF CANCER SPECIFIC LIGANDS FROM OBOC COMBINATERIAL LIBRARIES AGAINST OSCC

3.1 Abstract: Background: The OBOC combinatorial strategy has been proven to be a powerful tool for the identification of synthetic ligands against specific biological targets. In this method, the OBOC library is prepared by a "spit-mix synthesis method" approach using polystyrene beads as a solid support. As a result, each bead displays only one chemical entity with approximately 10^{13} copies of same compounds. We have therefore employed OBOC strategy to look for the targeting ligands against OSCC. **Material and methods**: Twenty four OBOC combinatorial libraries were designed, synthesized, and screened against OSCC cancer cells. Rainbow beads assay was used to select suitable OBOC libraries for the large scale screening. During the large scale screening OBOC libraries with live intact OSCC cancer cells, all of OSCC binding beads were physically isolated and then treated with 8 M guanidine to strip off cancer cells. They were subsequently re-incubated them with four different OSCC cell lines, (HSC-3, SCC4, SCC10a, Mok101) to confirm their true binding property. We then screened these OSCC binding beads with normal human keratinocyte, endothelial cells and granulocytes. Only those peptide-beads that bind strongly to four OSCC cell lines and not bind to normal human keratinocytes, endothelial cells and granulocytes were considered as "true positive" beads. These true positive beads were then placed in a ABI automatic protein sequencer for Edman sequencing. Once identified, the OSCC peptides were resynthesized on Tentagel beads in a large amount and incubated with human cancer cells and normal cells again to confirm their true binding property and specificity. The confirmed positive OSCC ligands were then resynthesized on Rink

resin, cleaved off the solid support and purified with reverse phase (C18) HPLC. The molecular weights of compounds were determined by mass spectrum analysis. MTT assay and hemolytic assays were used to preliminary evaluate the potential cytotoxicity of these OSCC peptides. **Result**: Six true positive OSCC peptides were determined to be non-toxic to cell culture and to bind strongly to different to OSCC cells, but not to normal human cells. **Conclusion:** Using OBOC combinatorial library strategy, we have identified six oral cancer specific ligands against OSCC. These six peptides have no any cytotoxicity *in vitro* study and were selected as lead compounds for the development of OSCC imaging probes.

3.2. Introduction

Oral cancer is a malignancy of the squamous epithelium of oral cavity. It occurs most frequently on the tongue, lip, gingival, palate, floor of mouth and buccal mucosa. The OSCC develops over many years and neoplastic transformation may take place in multiple sites within the oral cavity. OSCC is associated with multiple genetic and epigenetic alterations of oral mucosal epithelium, leading to the development of papillary hyperplasia or different stages of dysplasia, with subsequent progression to the development of carcinoma *in situ* or well-differentiated, invasive squamous cell carcinoma (66, 67). Precancerous lesions can be in the form of leukoplakia (white lesions), erythroplakia (red lesions), erythroleukoplakia (combination of white and red lesions), or oral submucous fibrosis (deposition of collagen on fibromuscular connective tissue) and all of these lesions can potentially give rise to primary tumors in the oral cavity (68, 69, 70).

The molecular and cellular mechanisms underlying the pathogenesis of oral squamous cell carcinoma (OSCC) are relatively poorly understood and remain a subject of significant importance. It is well-established that OSCC is associated with a variety of risk factors and notably, the high incidence rates of OSCC found in developing countries are attributable to exposure to different forms of smokeless tobacco. However, the way these factors contribute to the disease pathogenesis and, in particular, the transformation from oral premalignant lesions (OPLs) to primary tumors remains unknown.

Based on the anatomical location, OSCC has the advantage of been easily accessible. However, most patients are still diagnosed in advanced clinic stages. As is the case for many solid tumors, early detection and therapeutic intervention offers the best opportunity to improve the current low survival rates of OSCC. No specific biomarkers against OSCC have been reported. Therefore, there is an urgent need to search for the specific biomarker for the early detection of, and improvement in the treatment of the OSCC.

Tumor biomarkers can be any single molecule or a combination of more than one cellular molecule including DNA, RNA, proteins, peptides, carbohydrates, or small metabolites that are disease-specific and can be measured in order to analyze and monitor disease progression. Cell surface proteins are excellent biomarkers for both diagnostic imaging and targeting therapy. To target cancer cell surface proteins, several monoclonal antibodies have been used; however, their use in delivery of toxic drug or therapeutic radionuclides is limited due to non-specific binding to phagocytic immune cells (71, 72). Despite this concern, the FDA has approved a few antibody drug

conjugates in recent years (73, 74). Peptides and peptidomimetics are alternative classes of targeting agents that can be used to target cancer cell surface proteins with several advantages over antibodies. These advantages include less non-specific binding to the reticuloendothelial system (mononuclear phagocyte system which consists of phagocytic cells, mainly monocytes and macrophages), and ease of conjugation to therapeutic payloads and less expensive to manufacture. Peptides are normally susceptible to proteolytic degradation. However, with the use of D-amino acids, unnatural amino acids and organic moieties, proteolytic stable peptides and peptidomimetics can be developed for the targeting of cell surface proteins of cancer cells. In this study, we employed OBOC combinatorial library approach to identify OSCC specific peptides as the biomarkers.

3.3. Material and methods

3.3.1. Cells used for the studies. HSC-3 (Japan Health Science Research Resources Bank, site: tongue with lymph node metastasis, MD-OSCC). SCC 4 (site: tongue, T3NOMO), SCC-10A, HOC-313 and MOK 101 (site: tongues) were provided by Dr. Kramer's lab. HaCat: (ATCC, site: skin, Human adult low calcium high temperature cells), is spontaneously transformed aneuploidy immortal keratinocyte cell line from adult human skin that has the characteristics of basal epidermal keratinocytes. This cell line is currently used as a non-tumorigenic control. Human keratinocytes, human endothelial cells were purchased from ATCC. Normal human granulocytes were obtained from the healthy volunteer (Figure 3.1).

3.3.2 Generation of random and focused OBOC libraries. Twenty-four random and focused OBOC libraries were generated by using a split-mix synthesis approach as previously described (26). Standard solid phase peptide synthesis method with 9-Fluorenylmethoxycarbonyl (Fmoc) chemistry was used to synthesize the OBOC libraries. Briefly, the peptide was synthesized on 88 μm diameter Tentagel beads (polyethylene glycol-grafted beads resin, with loading 0.25 mmol/g, from Rapp Polymere), using 1-hydroxybenzotriazole/1, 3-diisopropylcarbodiimide as coupling reagents. Three-fold molar excess of Fmoc-protected amino acids to resin was used for coupling. Completion of coupling and Fmoc deprotection was monitored by the ninhydrin test. The disulfide formation was achieved with gentle mixing of the bead-library in 20% DMSO in ammonia acetate buffer (pH 6.2). These libraries contained tens of millions compound beads with each carrying a peptide with distinct natural and unnatural amino acid or small organic molecule moieties. A total of twenty-four OBOC libraries were used for these studies, including a X1 focused OBOC combinatorial library, a RGD based OBOC combinatorial library, seven cyclic OBOC combinatorial library and fifteen random OBOC combinatorial libraries.

3.3.3. Rainbow bead assay. Rainbow bead assay was adopted to select suitable OBOC combinatorial libraries for the following large-scale screening. (45). Briefly, OBOC compound beads displaying chemical compounds or families of compounds were stained with oil-based organic dyes that were used as coding tags. The color dyes did not affect cell binding to the compounds displayed on the surface of the beads. The twenty-four small samples of each OBOC combinatorial library (~15,000 beads) were color coded and washed with PBS. In each run, four of OBOC

combinatorial library beads were combined and screened concurrently against live HSC-3 oral cancer cells for 1 hour. Those OBOC libraries showed positive binding to OSCC cells were selected for large-scale screening.

3.3.4. Large-scale screening. Large-scale screening assay with intact live OSCC cells was used to identify high-affinity OSCC binding compound beads. The OBOC combinatorial libraries selected from rainbow bead assay were screened in large scale (~750,000 beads/each library) using live intact HSC-3 cells. Briefly, HSC-3 cells were grown in DMEM media with supplement with P/S and 10% FBS. After harvested by trypsin, HSC-3 cells were incubated with OBOC libraries for 1 hour. Beads with unique binding ligands that interacted with cell surface receptors were coated by one or more layers of the HSC-3 cells. These positive beads were isolated and the binding cells were stripped off by using 8M guanidine hydrochloride. After thorough washing with water and then PBS, the positive beads were then rescreened with other OSCC cell lines (SCC 4, SCC 10a, HOK 313 and MOK 101) to ensure their true positive binding properties.

3.3.5. Ligand specificity filtering assay. A specificity filtering assay was used to identify non-keratinocyte binding beads from the OSCC binding beads selected from the large scale screening. The OSCC binding beads were incubated with live human keratinocytes, endothelial cells (Huvec), fibroblast cells (NUFF) and freshly isolated granulocytes separately. Those compound beads with strong binding to OSCC cells but not bind to normal human cells were finally selected. The chemical structures of selected beads were determined by Edman chemistry using an automatic ABI-protein sequencer.

3.3.6. Hit validation assay. Hit validation assay was used to evaluate compounds' binding affinity and specificity using different human OSCC cell lines and normal human cells. Those compound beads with high binding affinity and specificity to OSCC cells were resynthesized in a large amount on TentaGel and were incubated with different OSCC cell lines (HSC-3, SCC 4, SCC10A, HOC313 and MOK 101) for 1 hr, as well as incubated with normal cells (immortalized human keratinocytes (HaCAT), fibroblast cells (NUFF), endothelial cell (Huvec) and granulocyte for 4 hours. The compounds with the property of binding to all of the OSCC cells tested but not binding to normal human cells were selected for further cytotoxicity evaluation.

3.3.7 Cytotoxicity evaluation assays. Those peptide beads with high binding affinity and specificity for OSCC cells were resynthesized in a large amount in solution form. MTT assay was used to evaluate the potential cytotoxicity of the OSCC compounds identified on normal human keratinocytes (46, 47). Briefly, human keratinocytes were cultured on 96-well plate overnight. The serially diluted ligands were added to each wells and incubated for 4 hours before adding MTT (3-[4,5-dimethyl-thiazol-z-yl] 2,5 diphenyl tetrazolium bromide) solution (5μg/ml in PBS). After 4 hour incubation, DMS-containing solution was added. The optical density at 540 nm is measured with auto-reader.

The Hemolytic assay was also used to evaluate potential toxicity of these six peptides (48). Briefly, six compounds were serial diluted in sterile saline (0.9 %), and incubated with healthy human RBC (4×10^6 RBC/ml) for 6hours and absorbance was read by micro-plate reader at 550 nm. Triton X-100 1% was served as 100% hemolytic positive control. RBC without added compounds was used as negative control.

3.4. Representative results

3.4.1 Selection OBOC libraries from rainbow bead assay. Using "split-mix synthesis method", we designed and generated twenty-four OBOC combinatorial libraries, including one X1 OBOC focused library, one RGD based OBOC library, 8 cyclic library and 14 random cyclic or linear libraries. Using the highly efficient rainbow bead assays, we rapidly surveyed all 24 OBOC libraries and selected six OBOC libraries for further large-scale screening. The six OBOC libraries all contained compound beads with the potent binding property to human HSC-3 cells, including X1 OBOC focused library, RGD based OBOC focused library, and four linear and cyclic random OBOC libraries. As shown in Figure 3.2, five of the different color coded OBOC libraries were mixed, with each color denoted for one OBOC library. Figure 3.3 showed that an OSCC binding bead was identified from one of the screened libraries (blue color coded library), therefore, this blue color coded OBOC library was selected for subsequent large-scale screening study.

3.4.2 Identification of OSCC binding beads from large-scale screening using intact live cell assay. HSC-3 cells were grown in DMEM media with antibiotics and 10% FBS. After harvested by trypsin, HSC3 cells were incubated with six different OBOC compound libraries for 1 hour in a 5% CO_2 at 50 rpm. As shown in Figure 3.4, a binding bead showed a layer of cell binding around the bead (arrow). All of the HSC3 binding compound beads were selected and treated with 8M guanidine to get rid of binding cells and re-incubated with other OSCC cell lines, including SCC4, SCC10a, Mok101 separately for 1 hours to confirm their true binding property (Figure 3.5).

3.4.3 Identification of non-human keratinocyte binding beads from the OSCC binding beads selected from 3.4.2 (specificity filtering assay). Human keratinocytes (NHK) were grown in Epi-Life media. After harvested by trypsin, keratinocytes cells were screened with OSCC cell binding beads sorted from 3.4.2 for 4 hours in 5% CO_2 shaker at 50 rpm. As shown in Figure 3.6, some OSCC binding beads has more NHK cell binding, some has less NHK cell binding, and one non-binding beads was identified from HSC-3 binding beads (arrow). All of the NHK cell non-binding beads selected from the study were then re-screened with human endothelial cells, and again the negative beads that have no endothelial cell binding were selected. Among the six OBOC libraries screened, only the X1 cyclic OBOC library showed specificity binding to OSCC cells but not bind to NHK, endothelial cells and granulocytes. A total of 137 OSCC binding beads were identified from cyclic focused X1 library, and thirteen compound beads were finally identified with the properties of binding to HSC-3 but not to normal human keratinocytes. The chemical structures of 13 peptides were determined by Edman sequencing. Even with the small number of ligands identified, a motif was observed.

3.4.4. Evaluation of OSCC ligands' binding ability and specificity using hit validation assay. Thirteen OSCC binding peptides (named LLY1-LLY13) were re-synthesized on Tentagel beads according to their structure and sequences. OSCC cell lines HSC-3, SCC4, SCC10A, HOC313, and MOK101 were incubated with each of the 13 peptide-bead samples for 1 hour in Epi-life media in non-treated petri dish. As shown in Figure 3.7, the LLY13 compound beads incubated with HSC-3 cancer cells were entirely covered by a monolayer of cells within one hour. Thirteen peptide-beads were

also challenged with normal human keratinocytes, fibroblast cells (NUFF), endothelial cell (Huvec) and white blood cells (WBC) in Epi-life media for 4 hours in non-treated petri dish. As shown in Figure 3.8, LLY13 beads do not have any normal human cells binding on them. The testing results of OSCC binding peptides against OSCC as well as human normal were summarized in Table 1. Six peptides were finally identified for their high potent binding ability to different human OSCC cell lines, but not bind to normal human cells. Sequences of six of OSCC binding compounds were available upon request. Five of the six peptides contain proline or hydroproline in position 6.

3.4.5 Potential cytotoxicity evaluation of OSCC compounds from MTT essay and hemolytic assays. Six OSCC specific binding peptides selected from Table 3.1 were synthesized in liquid form and disulfide cyclization was achieved with CLEAR-OX resin beads. The peptides were purified by HPLC and the molecular weights were confirmed by MS. The Hemolytic assay and MTT assays were used to evaluate potential cytotoxicity of these six peptides. MTT assay indicated there was no obvious cytotoxicity observed by the peptides at up to 500 μM (Figure 3.9). Hemolytic assay also showed that no hemolytic activity was observed for any of the six peptides at up to the concentration of 500 μM.

3.5. Discussion

Among the several approaches used to search for the biomarkers against cancer cells, the biological library (such as phage-display library) and OBOC combinatorial library are the two most commonly used methods to identify cancer-targeting peptide ligands (74). The OBOC combinatorial library method was developed over two decade ago by my mentor Dr. Lam. Thousands to millions of compound beads can be

generated and scanned rapidly. Each compound bead in OBOC combinatorial library displays only one chemical entity. One major advantage of the OBOC method over phage-display method is that D-amino acids, unnatural amino acids, and organic moieties can be easily incorporated into the construction of the OBOC libraries, rending the identified ligands containing such building blocks more resistant to proteolysis, while biological combinatorial libraries are generally limited to L-amino acids,

Although the OBOC combinatorial library method is highly efficient, finding the right library to screen and performing large number of cell binding assay on individual synthesized compound beads against a number of cell lines are very time-consuming. Therefore, we adopted the rainbow beads assay in a multiplex fashion (45), thus, greatly facilitating the identification of the OBOC libraries which possess significant number of OSCC targeting ligands. After preliminary screening of twenty four OBOC libraries, six libraries were quickly identified for further studies for having OSCC binding activity, including one cyclic focused X1, one-7-mer arginine-glycine-aspartic acid based cyclic OBOC library and four random linear or cyclic OBOC libraries. As shown in Figure 3.3, a binding bead showed a layer of cell binding on the bead was identified from a blue color-coded OBOC library (arrow). As a result, the blue color-coded OBOC library in this screening was selected for the following large-scale screening. One major advantage of this straightforward and yet powerful method is that only an ordinary inverted microscope is needed for the analysis, instead of a sophisticated and expensive fluorescent microscope or flow cytometer.

Among the six OBOC libraries selected for the large-scale screening studies, a total of 4,500,000 compound beads were screened, and we identified 546 OSCC cell

binding beads. Following the specificity filtering assay, only thirteen compound-beads from 137 positive compound beads were identified from X1 focused OBOC libraries, that manifested the property of strong binding to different OSCC cell lines while not binding to normal human keratinocytes, endothelial cells and granulocytes. The X1 focused OBOC library is a cyclic peptide library with a motif (cXGXGXXc) that binds preferentially to ovarian cancer with high specificity against α3 integrin (75,76). The RGD based library also yielded several OSCC strong binding beads; however, these beads also bind keratinocytes after 4 hours of incubation, making them not OSCC-specific.

A significant challenge facing OBOC screening approaches is to have a robust method to reduce or eliminate false positive or false negative compound-beads. Both of these issues need to be overcome by keeping tumor cells in a healthy and live status. To keep to this condition, we usually balanced incubation media overnight in the incubator with 5% CO, when we performed the screening assay, the shaker was equipped with 5 % CO_2. After trypsinization, the OSCC cells were usually incubated in the 37°C shaker with CO_2 for one hour to help resume the cell in healthy status before adding the OBOC library beads. A big advantage of utilizing live and healthy cells as living probes to screen OBOC libraries is to substantially increase the likelihood of identifying ligands that recognize the native conformation of the cell surface receptors.

One of the technical difficulties is not to lose the identified compound-beads during the multiple screening steps, as the beads are small (~88μm) and not easily visible to naked eye. For example, after one putative positive bead was identified, it has to be treated with 8M guanidine to strip of the binding cells and then sterilized with 70%

alcohol; washes with dd H_2O three times; washed with PBS three times before move to the next step screening. Therefore, it is not uncommon to loose important identified beads during the washed and treating steps. To overcome this issue, I first transferred the entire OSCC cell binding beads to the 1.5 ml centrifuged tube and then added 8 M guanidine and incubation for 10 mins to get rid of the binding cells. 1 ml of DD water was added to the centrifuged tube and spun for 3 mins at 1000 rpm. The beads selected were then washed for 3 $_x$ in DD water, 1 $_x$ of 70 % alcohol and 3 $_x$ PBS. Now beads are ready for the next screening or decoding. Following this step, I have not lost any of the putative positive beads.

3.6. Conclusion: Using combinatorial strategy of one-bead one-compound libraries combined with high throughput screening assays using live OSCC cells as screening probe, six cyclic peptides were identified to bind to different OSCC cell lines but not bind to normal human cells. MTT assay and hemolytic assays indicated that they were not cytotoxic to normal human cells. Therefore, the six OSCC peptides with highest binding affinity and specificity to human OSCC cells were served as the lead biomarkers for the generation of novel optical OSCC probes.

3.7. Figures and Tables
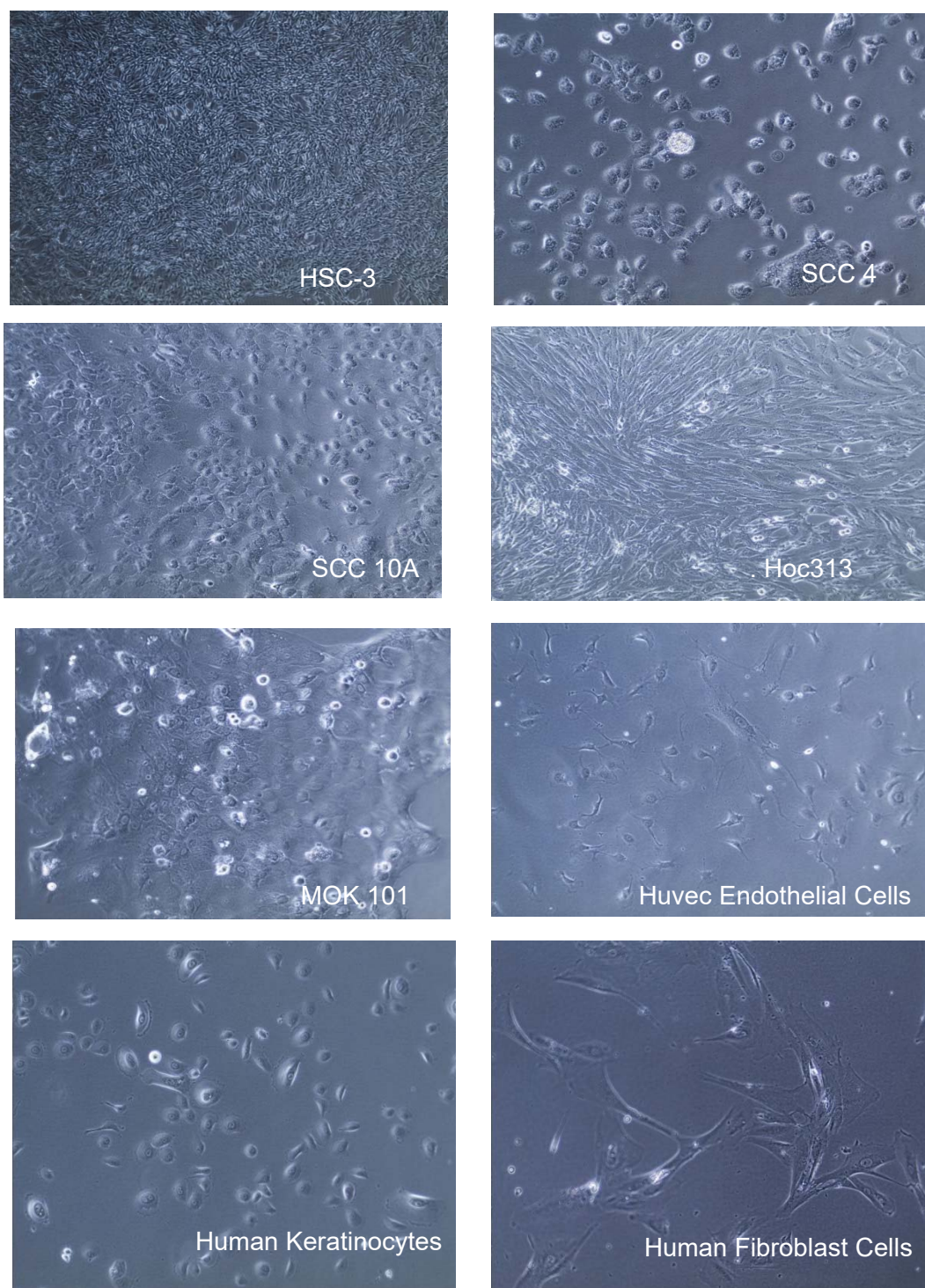
Figure 3.1: Photomicrograph of five human oral cancer cell lines (HSC-3, SCC4, SCC10A. HOC313, MOK101) and three normal cells (Huvec, keratinocytes, fibroblasts) were used for the screening of oral cancer cell binding compounds.
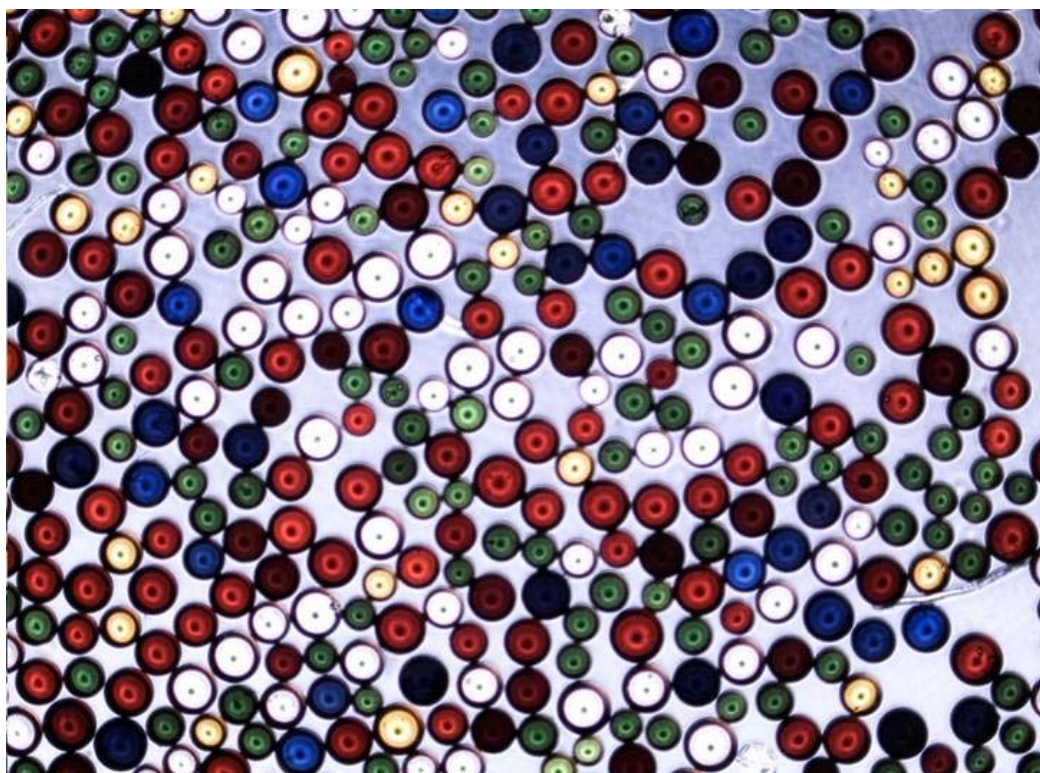
Figure 3.2: Photomicrograph of rainbow beads generated using organic dyes, one color denote for one OBOC combinatorial library.
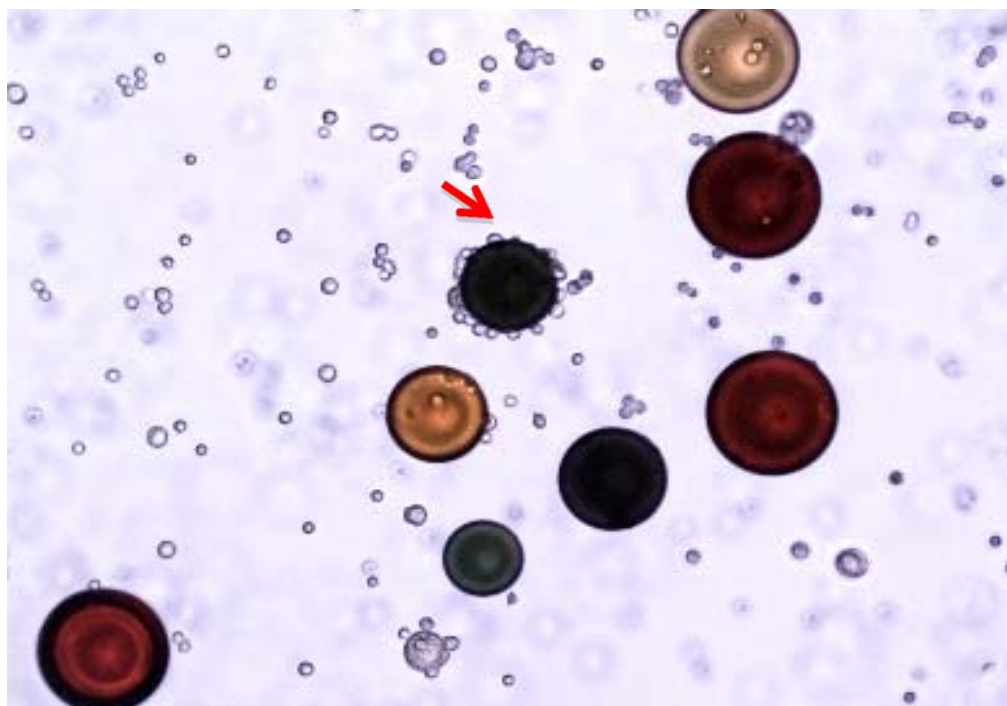
Figure 3.3: Photomicrograph of screening mixture of color coded OBOC libraries. A binding bead was identified from the blue color coded OBOC library (arrow), therefore, the blue color coded OBOC combinatorial library was selected for the large scale screening.
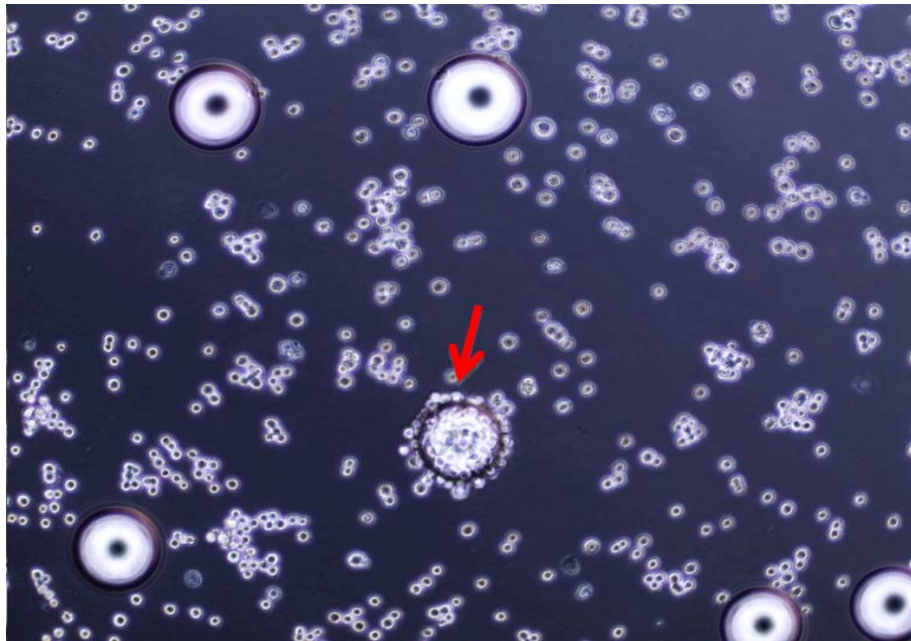
Figure 3.4: Photomicrograph of the HSC-3 cell binding bead identified from X1 OBOC library (arrow) after one hour incubation.
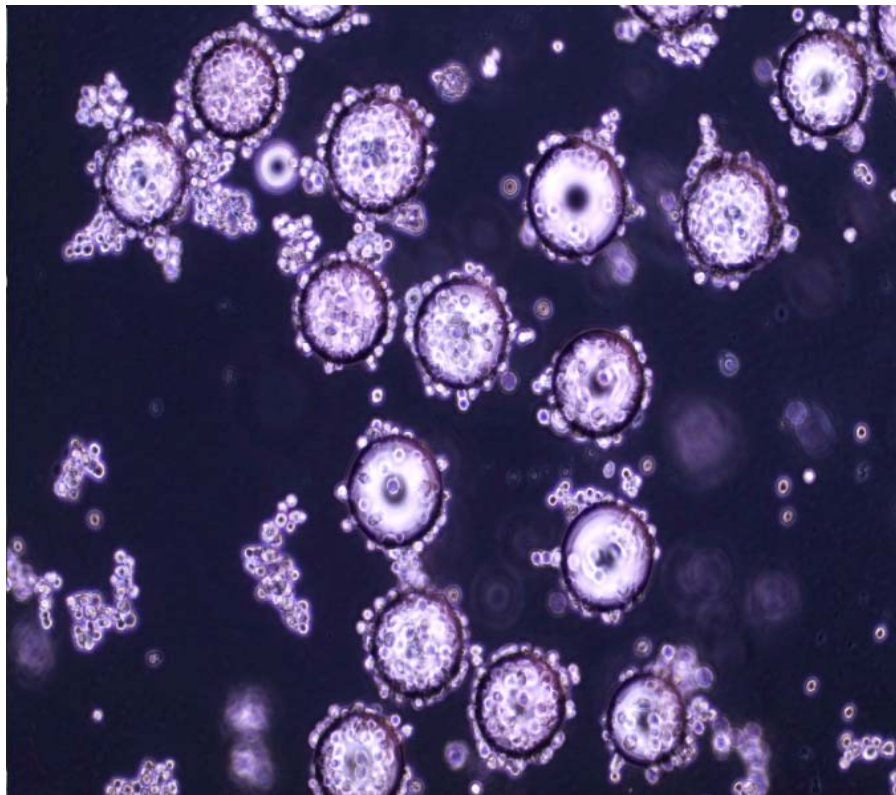
Figure 3.5.Photomicrograph of HSC-3 cell binding beads showed to have MOK101 cell binding ability.
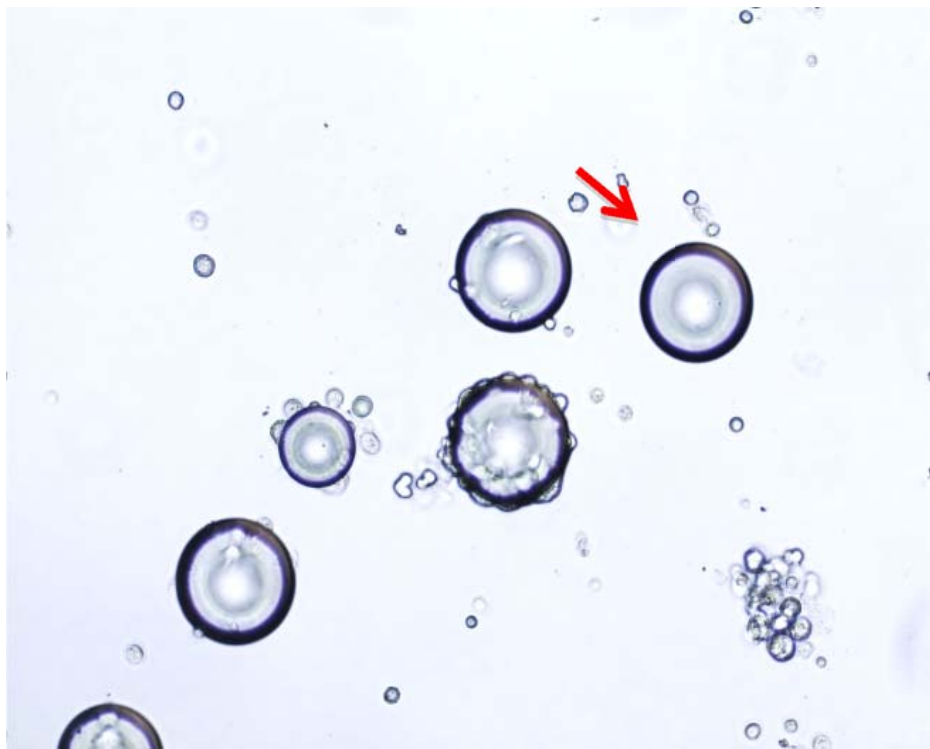
Figure 3.6: Photomicrograph of a non-NHK binding bead was identified from OSCC binding beads (arrow).
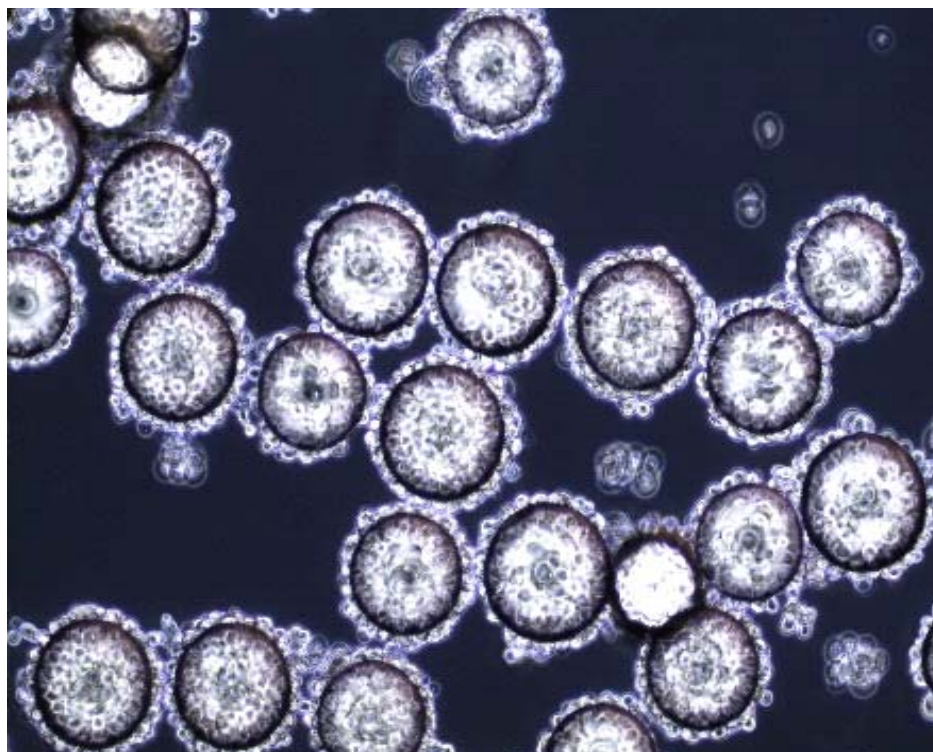
Figure 3.7: Photomicrograph of Live HSC-3 cells bound to resynthesized compound beads LLY13 after 1 hour incubation.
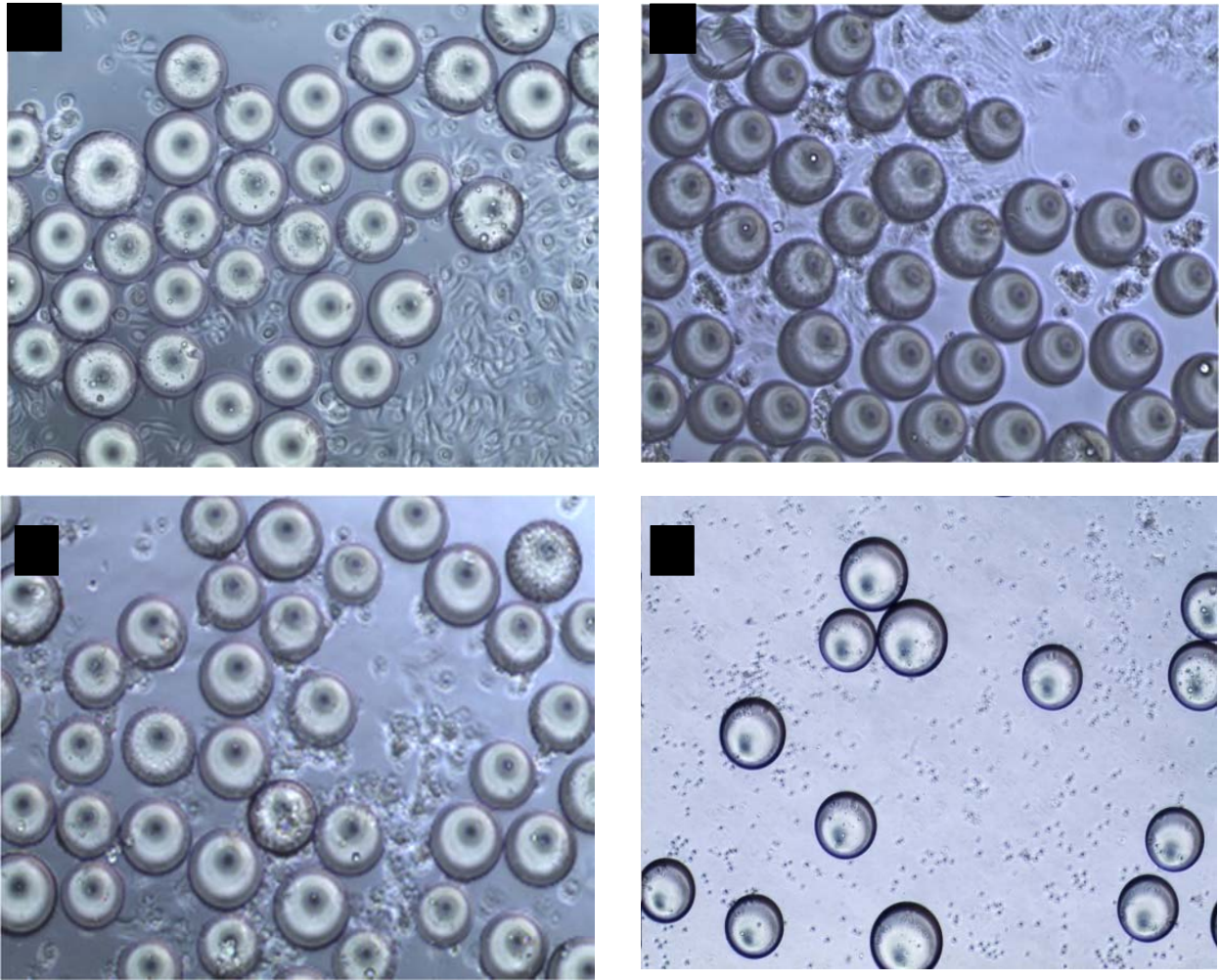
Figure 3.8: Photomicrograph of resynthesized OSCC binding compound beads challenged with normal human cells. After incubation of OSCC binding beads with human normal cells of NHK (a), fibroblast cell (b), endothelial cells (c) and granulocytes (d) for 4 hours, 6 of OSCC binding compounds were identified for not binding to these normal human cells. Some of cells attached to the surfaces of Petri dish with time (a, b, and c).

Table 3.1: Testing result of thirteen OSCC peptides on OSCC cell lines and normal human cells

Cell name	LLY1	LLY2	LLY3	LLY4	LLY5	LLY6	LLY7	LLY8	LLY9	LLY10	LLY11	LLY12	LLY13
HSC 3	4+	4+	1+	4+	4+	-	4+	4+	4+	+	1+	4+	4+
SCC4	4+	4+	3+	4+	4+	-	4+	4+	3+	-	4+	3+	3+
SCC10A	4+	3+	1+	4+	3+	-	2+	4+	3+	-	1+	3+	4+
Hok313	4+	1+	1+	-	4+	2+	2+	2+	2+	-	2+	4+	4+
Mok101	2+	3+	-	+	±	-	±	+	2+	-	±	±	2+
NHK	-	±	-	+	-	+	+	-	2+	-	-	-	±
HUVEC	-	-	-	-	-	-	-	-	-	-	-	-	-
NUFF	-	-	-	-	-	-	-	-	+	-	-	-	+
WBC	-	-	-	-	-	-	-	-	-	-	-	-	-

Six peptides were selected for further studies for their strong binding ability to OSCC cells but not bind to normal human cells (highlighted red)

4+: whole cell binding on bead; 3+: 3/4 cell binding on beads; 2+: 2/4 cell binding on beads; 1+:1/4 cell binding on bead; and ±: fewer cell binding.

LLY1 to LLY 13 are the names of OSCC binding peptides.

SCC: oral squamous carcinoma cells line; NHK: human keratinocytes; HUVEK: human endothelial cells; NUFF: human fibroblast cells; WBC: human granulocytes.

.
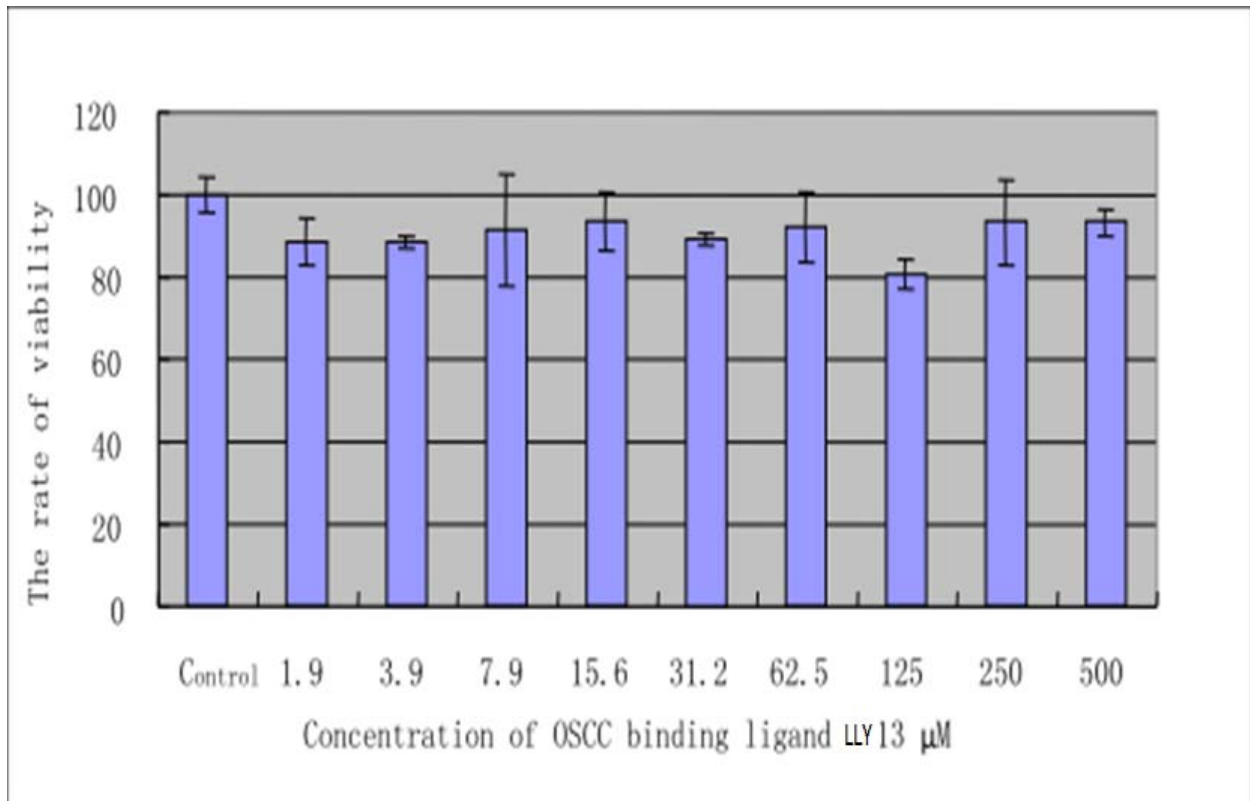
Figure 3.9: MTT assays showed that OSCC binding ligand LLY13 has no cytotoxicity to NHK cells at up to the concentration of 500 μM.

CHAPTER 4. DEVELOPING OSCC OPTICAL PROBE - *In vitro* and *in vivo* STUDIES OF THEIR TARGETING EFFICACY

4.1. Abstract: Background: OSCC is often first diagnosed at late stages of the disease (advanced regional disease and/or metastasis). Delayed diagnosis decreases the probability of successful treatment and favorable outcomes. Current diagnostic techniques against OSCC utilize light-based detection systems, fluorescent visualizations and brush cytology. Unfortunately, only 35% of cases are caught in the earlier phase. The gold standard for the diagnosis of OSCC is invasive biopsy and histological analysis. Non-invasive early detection of OSCC is a highly sought goal. Indeed, specific biomarkers for OSCC are essential for the development of optical probes. Through screening twenty-four OBOC combinatorial libraries against different intact live OSCC cells, six peptide ligands were identified with the properties of binding to different human OSCC cells lines, without binding to human keratinocytes, endothelial cells and WBC, therefore, these six putative OSCC ligands were selected for the further development of the OSCC optical probes. **Material and Methods**: The optical OSCC probes were generated by biotinylating the peptides at the carboxyl end via hydrophilic spacer to minimize the interference by streptavidin. Briefly, the six biotinylated OSCC peptides were synthesized on Rink resins using standard Fmoc solid phase peptide synthesis method. The peptides were then deprotected and cleaved off the resins with trifluoroacetic acid cocktail. The cleaved peptides were then precipitated and washed with cold ether, dried and disulfide cyclized with CLEAR-OX resins. The cyclized peptides were then purified on a C18-reverse phase column with HPLC, and molecular weights confirmed by mass spectrometry. Peptide-histochemistry was

employed *in vitro* to evaluate these OSCC probes' targeting efficacy and specificity to different human OSCC cells grown on the chamber slides. Mice bearing orthotopic and subcutaneous OSCC models were used to evaluate the *in vivo* the targeting efficacy and specificity of the OSCC probes. **Results**: Two OSCC probes, LLY12 and LLY13 were able to stain OSCC grown on the chamber slides at a concentration of 1 μM after 30 min incubation. Also, LLY13 exhibited the ability to penetrate OSCC cells grown on chamber slides, probably via endocytosis. Data from *In vivo* and *ex vivo* near infra-red fluorescence optical imaging studies confirmed the LLY13's targeting efficiency and specificity on subcutaneous and orthotropic mice xenograft models. H&E staining of mouse tongue tumor tissues revealed that LLY13-derived imaging probe was localized within the tumor tissue as well as demarcated the OSCC tumor margins. **Conclusion**: LLY13 has promising targeting activity against OSCC *in vitro* and *in vivo.* In addition, LLY13 is also able to penetrate into cancer cells, probably through endocytosis. LLY13 is an excellent candidate lead compound for the development of OSCC tumor targeted theranostic agents after further modification.

4.2. Introduction

Oral squamous cell carcinoma (OSCC) has a remarkably high incidence worldwide, and a fairly poor prognosis, encouraging further research into advanced technologies for noninvasive methods of early detection of this disease, ideally in primary care settings. Current techniques or methods used for diagnosis of OSCC are as follows: 1. Vital staining techniques in which a range of pigments are used to stain cells with high proliferative rate such as neoplastic cells, thus it can direct the physician or dentist to examine and biopsy the suspicious areas of the oral cavity (77). 2. Light-

based detection systems the utilize the device featuring special light source designed according to principles of tissue reflectance to enhance the oral examination process (78). 3. Histological techniques are the good standard for diagnostic methods for OPMD or OSCC lesions by incisional (IB) or excisional biopsy (79). 4. Cytological techniques involved microscopic study of cell samples collected from mucosal surfaces (via smears, scrapings or lavage) or from internal sites via fine-needle aspiration (80). 5. Molecular analysis involves molecular profiling studies that incorporate genetic and epigenetic alterations (81). 6. Imaging diagnostic techniques include radiographic techniques, nuclear medicine, magnetic resonance and ultrasonography. Imaging modalities used to evaluate the oral cavity include plain radiography (panoramic radiography and intraoral radiography), nuclear medicine scintigraphy, ultrasound (US), computed tomography (CT), magnetic resonance imaging (MRI), and positron emission tomography (PET) (82). The most common methods for diagnosing OSCC are summarized in Table 4.1 (83). However, even though OSCC is more accessible to visualization compared to most other tumors, only 35% of patients are diagnosed in the earlier phase (6). Currently, the earlier diagnosis of malignant lesion or OSCC depends on invasive biopsy. Replacing this approach by non-invasive techniques such as surface spray or optical imaging, will therefore allow dentists to perform over-chair, screening of OSCC. The six OSCC probes discovered through our OBOC screening, if proven to bind OSCC tissue with high specificity and affinity can potentially be developed into optical imaging probes for early detection of OSCC. In this study both *in vitro* and *in vivo* imaging studies were performed to assess the OSCC probes' targeting efficacy.

4.3. Material and methods

4.3.1. Development of OSCC optical probes.

Materials: Rink amide MBHA resin (0.5 mmol/g), Fmoc-protected amino acids, and N-hydroxybenzotriazole (HOBt) were purchased from GL Biochem (shanghai, China). 1-3-Diisopropylcarbodiimide (DIC) was purchased from Advanced Chem Tech (Louisville, KY, USA). TentaGel S NH_2 resin (0.24 mmol/g, 1% DVB cross-linked 90 um) was purchased from Rapp Polymere (Tubingen, Germany). The other chemical reagents were purchased from Aldrich (Milwaukee, WI, USA) and were of analytical grade.

Generation of OSCC probes using the six peptides discovered from screening OBOC combinatorial libraries. The schematic illustration of generation of OSCC probes is shown in Figure 4.1. Briefly, OSCC probes, named as LLY1, LLY 2, LLY5, LLY8, LLY12 and LLY13 were synthesized on Rink resin (loading 0.5 mmol/g) using Fmoc chemistry. Peptide-linker-lysine(biotin) was prepared on Rink resin using Fmoc-Lys(Alloc) as the first building block. After Alloc deportation, biotin was coupled to the amino group at the ε position of lysine. Fmoc-Ebes linker and Fmoc amino acids were coupled to resin sequentially, followed by Fmoc deprotection. The probes were finally cleaved from the Rink resins using the TFA cocktail and then precipitated in cold ether. Disulfide peptide cyclization was carried out using CLEAR-OX resin (Peptides Intl. Louisville, KY, USA). OSCC probes were purified by preparative reverse-phase (C18) high-performance liquid chromatography (RP-HPCL). Matrix-assisted laser desorption/ionization time of flight mass spectrometry (MALDI-TOF MS) was employed to verify the final biotinylated OSCC probes.

4.3.2. Peptide-histochemistry studies. To evaluate binding efficacy and specificity of optical probes on different human OSCC cell lines and normal cells (49). Optical OSCC probes generated from 4.3.1 were used for these studies. Human OSCC cells, normal human keratinocytes (HaCat) and endothelial cells (Huvec) were seeded on culture chamber slide. At 70% confluency, OSCC cells were incubated with 5% BSA to block non-specific binding. After washing with PBS 3X, OSCC probes at different concentrations were added to the OSCC cells grown in the chamber slides and incubated for half an hour, then washed 3X with PBS, followed by adding 1:500 dilution of streptavidin-Alexa 488 and incubation for half hour. Specimens were washed 3X with PBS and fixed briefly with 4% formaldehyde before adding the DAPI. Confocal microscopy was then performed.

4.3.3. OSCC peptide induced cell endocytosis assay. To investigate endocytic uptake of the targeting ligand by live OSCC cells (50, 51), biotinylated peptide LLY-13 (50 μM) was first pre-incubated with streptavidin-PE (1mg/mL) for 2 hours at RT and at 4º C overnight to form the biotin-peptides-streptavidin complex. OSCC cells HCS-3 and MOK101 cells were seeded in chamber slides at a concentration of $2x10^4$ cells / well. After 60% confluency, biotin-peptides-streptavidin complex were added at different time intervals (0, 30 min, one hour, two hours and three hours). By the end of the experiments, 1:2000 dilution of DAPI was added to the specimens. Endocytic uptake of LLY13 by OSCC was observed under a confocal laser scanning microscope.

4.3.4. Establish subcutaneous and bioluminescent orthotopic mice OSCC models. All animal experiments were performed in compliance with the institutional guidelines according to protocol No. 07-13119 and No. 09-15584 approved by the

Animal Use and Care Administrative Advisory Committee at the University of California, Davis. Twenty athymic nude mice (*nu/nu*), were obtained from Harlan (Hayward,CA,USA) at 5 to 6 weeks of age. OSCC subcutaneous tumors was established by injecting HSC-3 ($1x10^6$ cells) into the right flank of the mouse (n=10) (52, 53). To establish OSCC orthotopic bioluminescent nude mice model in tongue, HSC-3 cells were infected with lentiviral vectors that express green fluorescent protein (GFP)/firefly luciferase fusion proteins. 20 µl of $1x10^5$ infected HSC-3 cells mixed with Matrigel at 1:1, and were implanted into mice tongue (n=10) (54, 55). Tumors were measured with calipers in 3 orthogonal diameters 2 times per week and the volume was calculated by the formula for hemiellipsoids (84). The schematic illustration shows the plasmid used to establish the bioluminescent orthotopic mice model was shown in Figure 4.9a.

    4.3.5. *Near*-infrared (NIR) optical imaging of OSCC cancer xenografts. *In vivo* and *ex vivo* optical imaging studies were performed to evaluate the biodistribution and binding efficacy and specificity of the OSCC targeting ligands against OSCC xenografts (56, 57, 58, 59). After tumors developed (2 x2 x2 mm) in mice tongues and 8x8x8 mm in mice flanks, tetravalent ligand-biotin-Cy5.5 complex prepared by mixing 7.2 nmol of biotinylated peptide with 1.8 nmol of streptavidin-Cy5.5 in PBS overnight at 4°C, was injected into the mice via the tail vein. Twenty four hours after injection, the mice were anesthetized by an injection of 30 µL Nembutal (50 mg/mL) and images were acquired with a Kodak IS2000MM Image Station with excitation filter 625/20 band pass, emission filter 700WA/35 band pass, and 150 W quartz halogen lamp light source set at maximum. The mice were then sacrificed and the organs were excised for *ex vivo*

imaging. Data are collected and analyzed using the Kodak ID 3.6 software by mapping the region of interest on the images.

4.3.6. Histological study. H&E staining of excised OSCC bearing tongue was performed to evaluate targeting efficacy of the peptides (60). Six mice with OSCC tumors implanted in the tongue were randomly selected from each group, and sacrificed by cervical dislocation. The tumor specimen from mice tongues were excised by cutting the tongue root and bathed in a neutral buffered 10% concentrated formalin solution and paraffin embedded. The specimens were sectioned for hematoxylin and eosin staining. Histological assessment was conducted using optical microscopy.

4.4. Representative results

Six OSCC probes were generated using the compounds discovered from screening OBOC combinatorial libraries. Their molecular weights were confirmed by MS. As shown in Figure 4.2, OSCC probe LLY13 has molecular weight 1814. Six OSCC probes were used to evaluate the targeting efficacy and specificity by adding the different concentration of probes into the OSCC cells grown on the chamber slides. Initial peptide-histochemistry studies revealed that LLY12 and LLY13 were able to detect OSCC cells grown on chamber slides at the concentration of 1 µM. As showed in Figure 4.3, there are strong fluorescent signals on the MOK 101, followed by HSC 3, SCC4 and SCC 10a, but weak or background binding to NHK and human endothelial cells.

In addition, confocal microscope images indicated that probe LLY13 not only can bind OSCC, but also had the capability of penetrating into HSC-3 cells as well as

MOK101 cells, probably via endocytosis. In order to observe the cell penetration ability of LLY13, LLY13-biotin/streptavidin 488 complex was added to HSC-3 cells at varying time intervals. After three hours of incubation, LLY13-biotin/streptavidin488 complex had significant accumulation in the cytoplasm and nucleus of HSC-3 cells, while in the control group, composed of bacterial binding peptide (imipq-biotin/streptavidin488 complex), no fluorescent signal was observed in the HSC-3 cells. Figure 4.3 demonstrated that LLY13 penetrated into the HSC-3 cells as a function of time and accumulated in the cytoplasm as well as in the nucleus compared to the control group. LLY13's cell penetration ability was also seen in OSCC cell line MOK101. Figure 4.4 shows that LLY13-biotin/streptavidin488 complex was able to penetrate into MOK101 cells and localized in the perinuclear region and inside of the nucleus after 2-hours of incubation.

To compare the *in vivo* bio-distribution and targeting efficacy of LLY12 and LLY13, LLY12-biotin/SA-Cy5.5 complex and LLY13-biotin/SA-Cy5.5 complex were each injected into nude mice bearing subcutaneous HSC-3 xenograft tumors. The MFI of LLY12 and LLY13 in the ROI of each xenograft was quantified. Figure 4.5 shows illustrated that LLY13 had a narrower distribution profile than LLY12 and localized at the HSC-3 tumor site.

In vivo tumor-targeting effect of LLY13 on orthotopic luciferase transfected xenograft tumor of HSC3 cells was assessed by optical imaging. Briefly, HSC-3 cells were stable infected with luciferase reporter plasmid and inoculated into to tongue to generate orthotopic GFP luciferase positive xenograft tumor (Figure 4.6). After tumor growth to 2 x 2 x 2 mm, LLY13-biotin/SA-Cy5.5 was injected. The mice were subjected

to both *in vivo* and *ex vivo* bioluminescent imaging and optical NIRF imaging. Orthotopic

xenograft tumors of HSC-3 cells showed that LLY13 accumulated heavily at the tongue

as compared to the control group where Steptavidin-Cy5.5 alone, without ligand was

administered (Figure 4.7). There was co-localization or overlap signals between the

GFP tumor signal and the optical NIRF signal in the orthotopic xenograft tumors (Figure

4.7 A, B). We quantified the NIRF images and found that orthotopic xenografts had

significantly higher uptakes of LLY13-biotin/SA-Cy5.5 compared to that of the biotin-

/SA-Cy5.5 control (1.87-fold) (Figure 4.7 C, D, E). H&E staining of excised OSCC

bearing tongue clearly demonstrated that the LLY13-biotin/SA-Cy5.5 complex was

localized within the tumor tissue as well as demarcated the OSCC tumor margins (Fig.

4.8).

4.5. Discussion:

Optical imaging is useful as a non-invasive preclinical imaging tool to evaluate or

screen tumor-targeting ligands. Optical probes are technically easy to develop, non-

radioactive and relatively inexpensive. In this report, we use six OSCC probes

generated from screening OBOC libraries to staining OSCC cells grown on chamber

slides. LLY12 and LLY13 were able to detect OSCC cells at 1 µM, including HSC-3,

SSC4, SSC10a and Mok101, while there were only weak or background binding on the

normal human keratinocyte and endothelial cells. The limitation of this study is that all of

the cell lines used have been screened with OBOC libraries. Therefore, we need to

employ more cell lines to evaluate the OSCC probe's sensitivity and specificity. More

importantly, it is imperative to evaluate the probe's targeting specificity with pre-OSCC

lesions (leukoplakia, erythroplasia (high malignant potential), benign ulcer in patients

and OSCC. If these ligands are not specific enough, we will generate more focused OBOC libraries using LLY13 as the template to screen for more highly specific ligands against OSCC. In addition, we will also create diverse OBOC libraries to screen for ligands against other tumor-associated receptors.

During the peptide-histochemistry studies of the OSCC probes, we accidently found scattered fluorescent signals inside of live OSCC cells, which gave us some hints that LLY 13 might be able to penetrate into the cancer cells via endocytosis. To further prove this phenomenon, we added LLY13-biotin/streptavidin388 complex to the HSC-3 cells grown on the chamber slide at different time intervals. Under confocal microscope examination, we found fluorescent uptake inside of the cytoplasm as well as in the nucleus. In contrast, no fluorescent signal was detected in the control group, made of bacterial binding ligand (imipq-biotin/Stresptavidin488). These observations indicated that LLY13 not only targeted the surface of tumor cells but also internalized into the cells given longer time of interaction. This OSCC cancer cell penetrating peptide might help to construct targeting drug-loaded nanoparticle, which not only facilitate the delivery of nanocarriers to the tumor site via EPR effects and attachment to the tumor cell surface, but also enhance endocytic uptake of the drugs into the tumor cells, where they will be released.

To evaluate the targeting efficacy of OSCC probes, we established mice bearing subcutaneous xenograft OSCC model as well as orthotopic GFP luciferase positive xenograft model on mice tongues using athymic mice. Athymic mice lack mature T-cells that are believed to be involved in tumor immune surveillance and are critical to "self" recognition and destruction of grafted non-self-tissues. This loss of T-cell function

enables cross-species "xenograft" tissues, including tumor cells, to be tolerated by the immune system of the recipient animal (84, 85). Subcutaneous tumor models are advantages because of their ease of tumor establishment, measurement, and reproducibility. However, ectopic subcutaneous xenograft models are less useful for studying agents that modulate the tumor microenvironment, as an ectopic site does not reproduce the primary tumor site microenvironment as well as an orthotopic site. Orthotopic xenograft model can represent a more clinically relevant tumor model with respect to the tumor's primary site and metastasis (86). In orthotopic xenograft models, host microenvironments are more closely mimicked by implanting tumor cells into the original anatomical sites when compared to subcutaneous xenograft models. In this study, we successfully constructed orthotopic xenograft model on mice tongues by inoculating HSC-3 cancer cells derived from human tongue tumors.

Modern optical imaging techniques offer real-time and high-resolution imaging of fluorophores embedded in tissues. Near-infrared (NIR) fluorescence-based imaging is useful for non-invasive *in vivo* imaging in small animals because of modest tissue penetration (~2mm) and minimal auto-fluorescence with NIR light. Cy5.5 has been used previously by several groups as a convenient NIR fluorescent dye for *in vivo* detection of tumors (27, 44, 58, and 59). Here, we used *in vivo* and *ex vivo* NIR optical imaging to investigate targeting efficiency of LLY13 in nude mice bearing HSC-3 subcutaneous and orthotropic xenografts. After given intravenously approximately 7.2 nmol OSCC probe complex (LLY13-biotin/streptavidin-Cy5.5) to the mice, tumor uptake of the NIR signal was found to peak at about 24 hours post-injection followed by slow clearance; significant fluorescent signal remained at the tumor site even after 72 hours. The LLY13

targeting efficacy and specificity were further confirmed by H&E staining. As shown in Figure 4.8, there was a clearly mapping area of field cancerization with lesion margins.

4.6. Conclusion: LLY13 has promising targeting activity against OSCC *in vitro* and *in vivo* studies. In addition, it is likely that LLY13 is also able to penetrate into cancer cells and might be via endocytosis. This cancer cell penetrating peptide might help in constructing targeting drug loaded nanoparticles, which not only help to deliver nanoparticle loading drugs to the tumor site, but also enhance endocytic uptake of drugs by tumor cells, where they will be released. Therefore, The LLY13 developed from this study is an excellent lead peptide for the development of an OSCC tumor targeting theranostic after further optimization.

4.7. Figures and Tables

Table 4.1. Techniques that contribute to the diagnosis of oral cancer in addition toconventional oral examination

1.	VITAL STAINING	5% Acetic acid - Toluidine Blue - Methylene Blue - Lugol's Iodine - Rose Bengal - Iodine staining - Tolonium chloride
2.	LIGHT-BASED DETECTION SYSTEMS	- Tissue fluorescence imaging (Velscope, identafi 3000) - Chemiluminiscence (ViziLite plus, Microlux/DL) - Tissue fluorescence spectroscopy (NBI)
3.	HYSTOLOGICAL TECHNIQUES	- Incisional biopsy - Excisional biopsy
4.	CYTOLOGICAL TECHNIQUES	- Oral Brush biopsy (Oral CDX) - Liquid Based Cytology - Laser Microdisection (LCMd)
5.	MOLECULAR ANALYSES	- Gene alterations - Epigenetic alterations, loss of Heterozygosity and Microsatellite instability - Viral genome studies - Proliferation index and AgNOR Analysis - Immunohistochemical identification of tumor markers.
6.	IMAGING TECHNIQUES	- FDG-PET - Optical Coherence Tomography (OCT)
7.	OTHER TECHNIQUES	Onco-chips
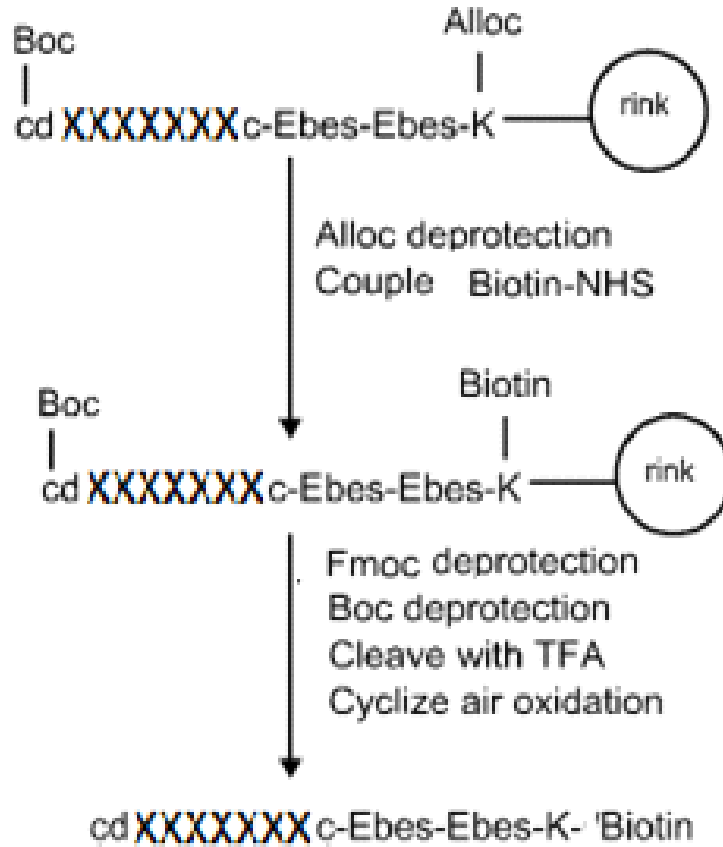
Figure 4.1: Schematic illustration of the generation of OSCC probes. OSCC probes were developed by biotinylating the carboxyl end of the six ligands via a hydrophilic linker to form ligand-linker lysine (biotin).
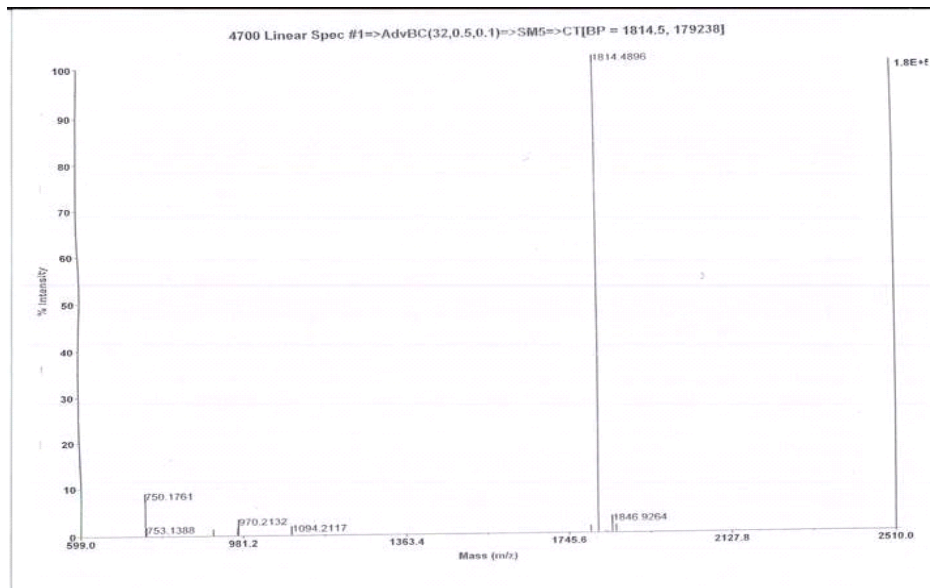
Figure 4.2: MALDI-TOF MS analysis of OSCC probe LLY-13 with MW of 1814.
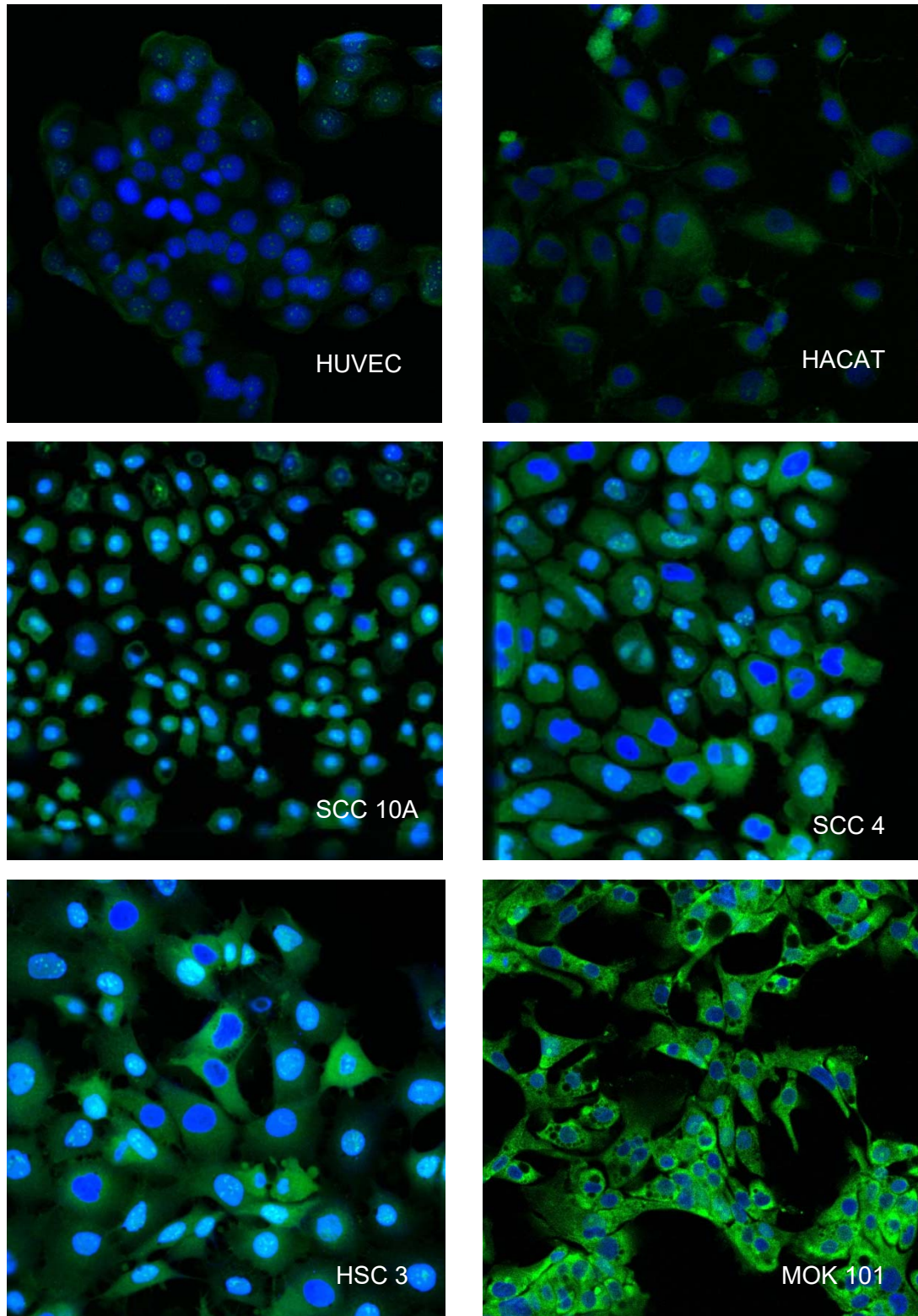
Figure 4.3: Confocal microscopy of different OSCC cell line and normal cells stained with OSCC probe LLY-13; nuclei were counter stained by DAPI. Strong staining of OSCC cells with probe LLY 13 were observed in HSC 3, SCC 4, SCC1A, and MOK 101, and only weak or background staining to HUVEC and human HaCat cells was observed.
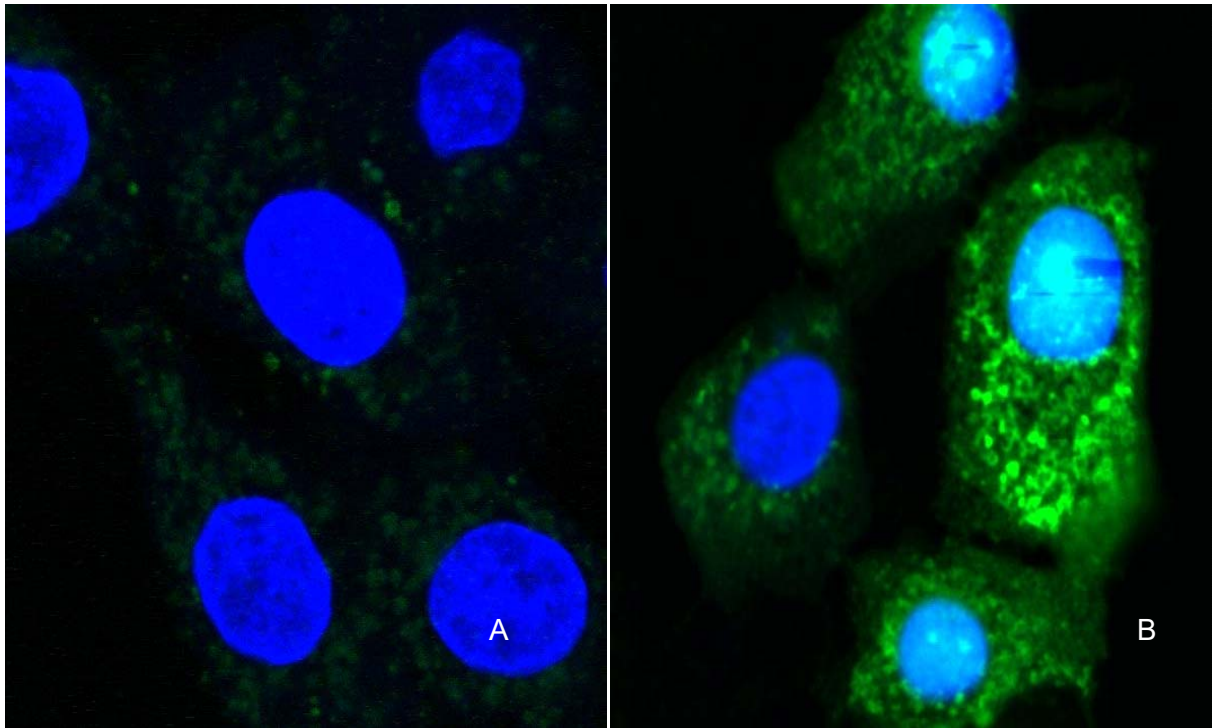
Figure 4.4: Confocal microscopy showed bioptinylated LLY-13-streptavidin-488 complex started to penetrate into HSC3 cells after 1hour incubation (a) and accumulated in the cytoplasm and nucleus after 3 hours incubation (b).
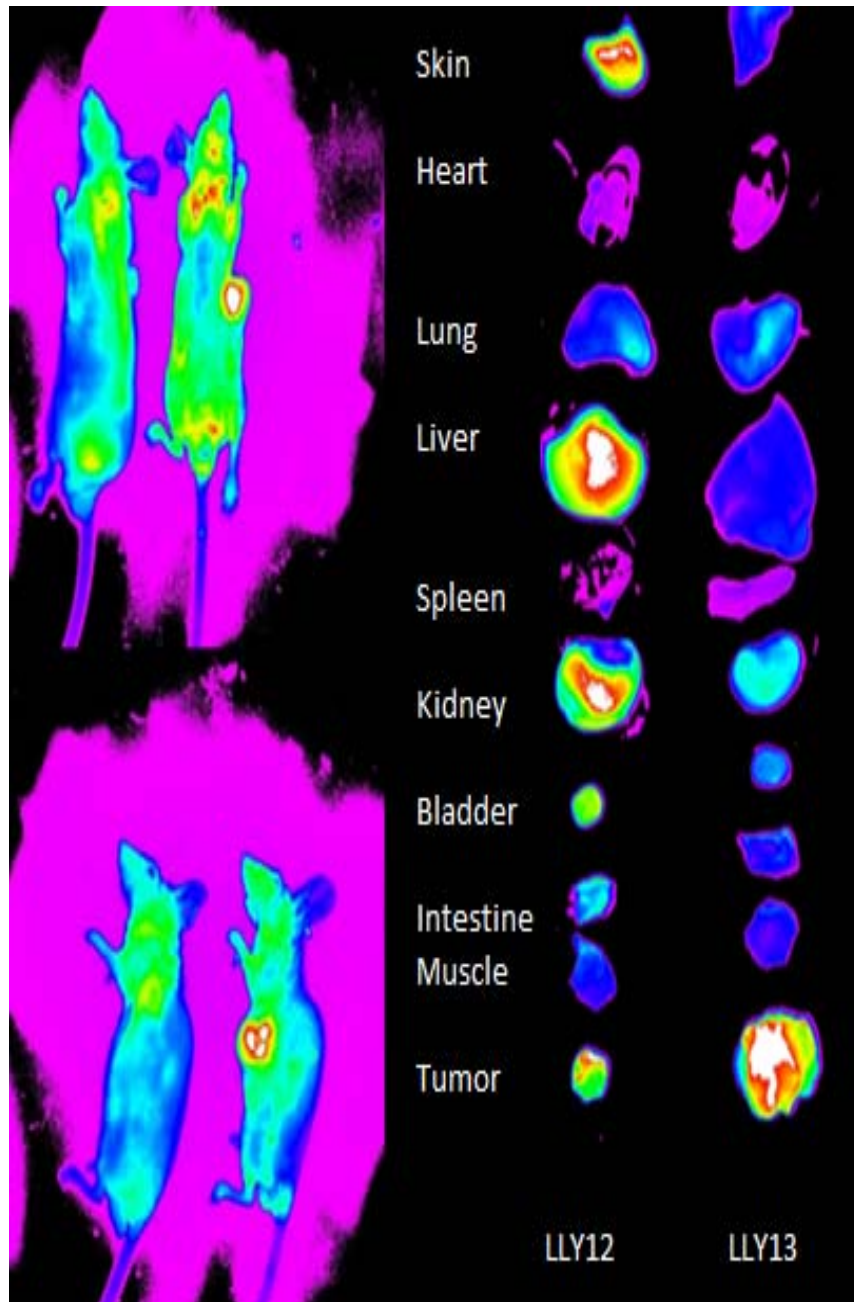
Figure 4.5: Comparison of LLY12 (left) and LLY13 (right)
targeting effects on the subcutaneous xenograft tumors
of HSC-3 cells. *In vivo* and *ex vivo* imagines showed that
LLY13 has more specificity to target subcutaneous
xenograft tumors than LLY 12.
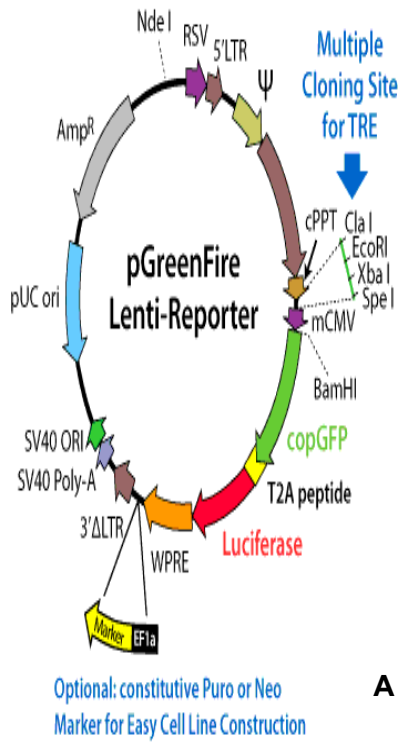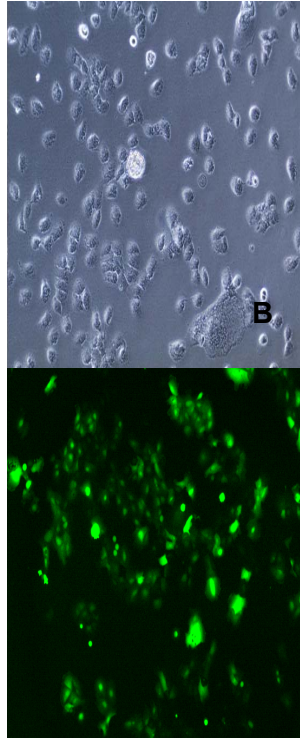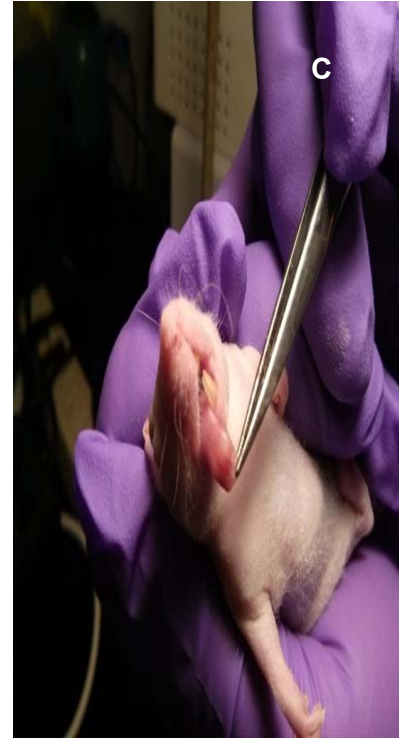
Figure 4.6: (a) Schematic illustration of bioluminescent reporter plasmid used to generate orthotopic mice OSCC model; (b) microphotograph of transfected HSC 3 cells (top): light microscope; bottom: fluorescent microscope with fluorescent signals. (c) Bioluminescent report plasmid infected HSC3 orthotropic tumor grown in mice tongue.

Fluorescent Cy 5.5 Signal   **Fluorescent GFP Tumor Signal**

Tongue	1.87	0.26
Heart	1.06	0.37
Lung	1.36	0.44
Liver	0.83	0.19
Spleen	1.13	0.50
Kidney	0.67	0.29
Bladder	0.85	0.22
Intestine	0.69	0.11
Muscle	0.82	0.03
Skin	0.89	0.06
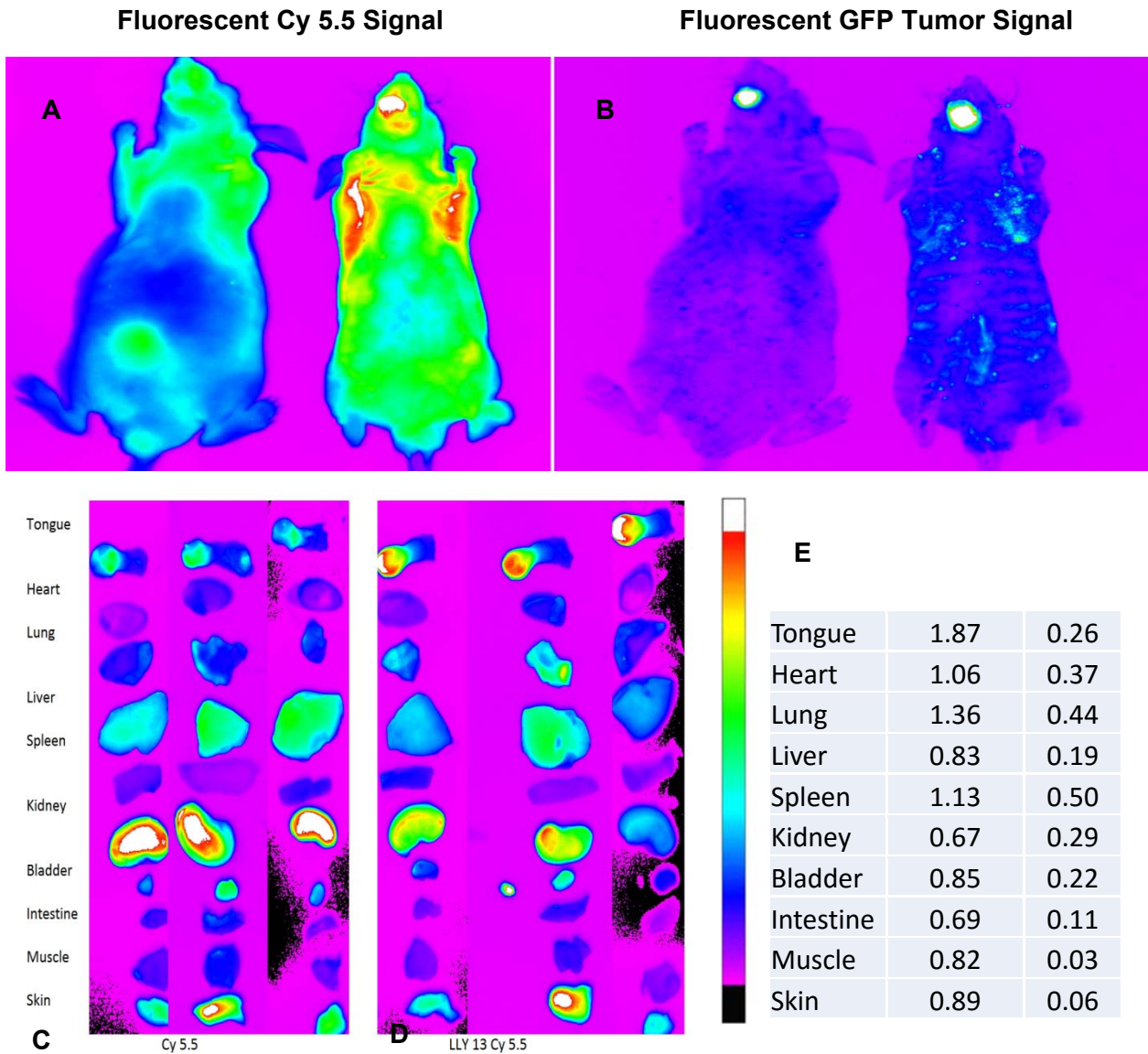
Figure 4.7: *In vivo* and *Ex vivo* bioluminescence imaging (BLI) and optical NIRF imagine after LLY13 –biotin/SA-Cy5.5 was injected. There was an overlap between LLY13 Cy 5.5 signal co-localize with HSC-3 GFP signal (A,B). Compared to the control group with biotin-cy5.5, LLY 13 signal was 1.87 fold higher within the orthotopic tumor (C,D, E).
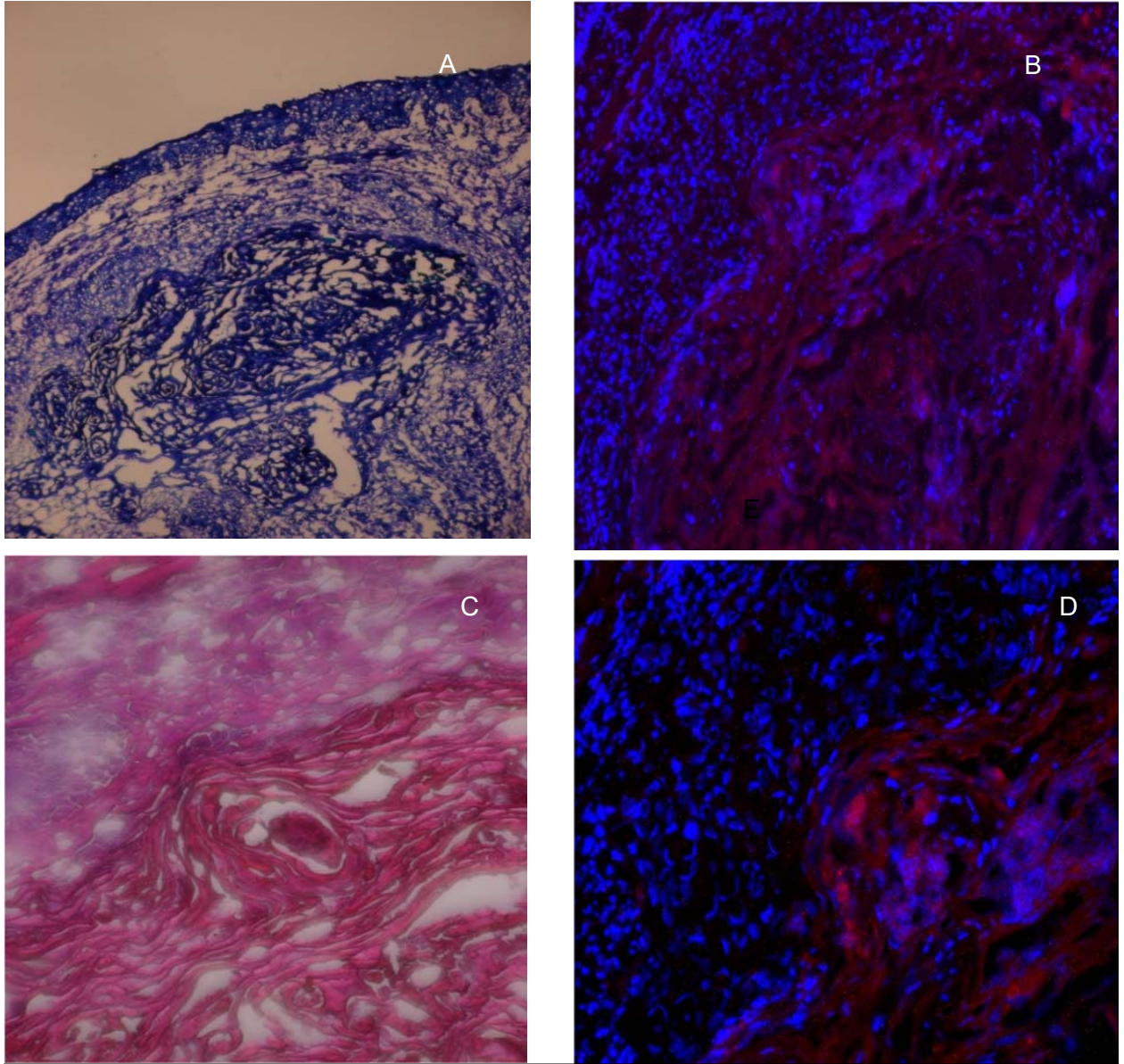
Figure 4.8: Light microscopy of H&E staining of excised HSC-3 bearing tongue: left (10X); right (20x). The LLY13 localized within the tumor tissue as well as clearly demarked the HSC3 tumor margins.

CHAPTER 5. INVESTIGATION OF OSCC LIGANDS-RECEPTOR INTERACTION

5.1. Abstract: Background: Integrins are associated with tumor cell survival and progression, and their expressions has been shown to be increased in tumors. Integrins are involved in a wide range of cell to extracellular matrix (ECM) and cell–to-cell interactions, mediating cell adhesion, signal transduction, tumorigenesis, tumor growth, and metastasis. X1 library, from which the OSCC binding ligand LLY13 was identified, is a focused library designed based on a cyclic peptide motif that bind preferentially to ovarian cancer with high specificity against α3 integrin. Therefore, we expect that LLY13 might interact with α3 integrin during the binding with OSCC cells. **Material and methods**: A panel of anti-integrin antibodies was employed to evaluate their ability to block OSCC cell binding to the LLY13 beads. In addition, we have performed differential binding studies of the LLY13 to α3- integrin transfected K562 cell lines vs un-transfected parent K562 cells. **Result**: Of the antibody panel tested, including anti-α1, α2, α3, α4, α5, α6, αV, β1 antibodies, only anti-α3 antibody was able to block most of the HSC3 cells binding to LLY13-beads. After incubation with LLY13 beads, the α3 integrin-transfected K562 cells were found to bind moderately to LLY13 beads, while parent K562 cells did not. **Conclusion**: Taken together, the data suggested that LLY13 partially interacts with α3 integrin on OSCC cells. Further studies are warranted to examine the possibility of somatic mutation, and expression pattern among the α3 integrins of HSC-3 cells in comparison to normal cells to elucidate the precise mechanism for our OSCCs' binding specificity.

5.2. Introduction: Cell surface receptors are excellent theranostic targets for cancers. One class of candidate targets are integrins, a family of adhesion molecules consisting

of non-covalent bound transmembrane subunits, which are involved in a wide range of cell to extracellular matrix (ECM) and cell-to-cell interactions, mediating cell adhesion, signal transduction, tumorigenesis, tumor growth, and metastasis (87). Its dysregulation is involved with chronic inflammation, tumor angiogenesis, and metastasis. Integrins are thus attractive targets for the treatment and prevention of several diseases, including cancers. At least twenty-four different integrin heterodimers can be formed from the 18-α and 8-β chains that have been identified (88) (Table 5.1). The pairing of α and β subunits determines the ligand binding specificity of integrin. This cell surface receptor mediates the interaction of cells with the extracellular matrix allowing for cell migration via intracellular trafficking through various endocytic and cell-signaling pathways. Our whole exome sequence analysis of integrin family in TCGA's published date of patient with head and neck cancer showed 186 non-synonymous mutations being found in 127 patients (127/509; 25%) (Table 5.2). Focused analysis on the whole exome sequence analysis of α3, β1 integrins showed 71% non-synonymous α3 mutations and 29% of the α3 aberrations were deleterious; 93% non-synonymous β1 mutations and 25% of the aberrations were deleterious (Table 5.3). This change in somatic sequence of integrin in oral cancer patients supports the findings in recent studies that alterations in certain integrin expression are implicated in neoplasia and the progression of oral cancer. Furthermore, studies of integrin expression and function are increasing our understanding of cell interactions in oral cancer and may pave the way for novel therapeutic interventions to arrest the progression of individual tumors. X1 library in which we have identified LLY13 is a highly focused library designed based on a disulfide-cyclic peptide motif of $cdGX_1GX_2X_3c$ that bind preferentially to ovarian cancer

with high specificity against α3 integrin (76). We therefore expect that LLY13 might elicit α3 integrin in its binding interaction to oral cancer cells.

5.3. Material and methods

5.3.1. Material. Anti-α1, α2, α3, α4, α5, α6, αV, β1 integrin antibodies were purchased from Chmicon (CHEMICON international, Inc). K562 cell line and α3-integrin transfected K562 cell line were generous gifts from Dr. Yoshikazu Takada.

5.3.2 Solid binding-blocking assay. Solid beads binding blocking assay was conducted to explore the functional inhibition using a panel of anti-integrin antibodies. HSC-3 cells adherent to the bottom of a T75 flask were trypsinized with 0.05% trypsin and washed with culture medium. Floating cells were collected, spun down and re-suspended in 200 μl of culture media containing anti-α1, α2, α3, α4, α5, α6, αV, β1 integrin antibodies and incubation at a rotating platform (speed of 40 rpm) inside an incubator at 37° C under 5% CO_2. After one hour of incubation, HSC-3 cells were spun down and washed three times with culture media and re-suspended in in 5 ml culture medium in a Petri dish. The LLY13 compound beads were then added and incubated with suspended HSC-3 cells. The entire dish was placed on a rotating platform (speed of 40 rpm) inside an incubator at 37° C under 5% CO_2. The plate was then examined under an inverted microscope every 15 minutes.

5.3.3. Specific α3 integrin-transfected cells confirmation assay. Stably α3 integrin transfected K562 cells were generated by electroporation of parent cell lines with a DNA construct containing full-length murine α3 cDNA cloned from murine lung cDNA and a neomycin selectable marker. Stably transfected cells were selected by

passaging cells in culture medium containing 1 mg/ml G418 (Invitrogen) for 14 days

followed by flow cytometry to isolate cells expressing the highest level of surface-

expressed murine α3. Transfected K562 cells were cultured in DMEM supplemented

with 4 mm L-glutamine adjusted to contain 1.5 g/liter sodium bicarbonate, 4.5 g/liter

glucose, 1.0 mm sodium pyruvate, 10% FBS, 2.5% mouse IL-3 culture supplement, and

1.5 mg/ml active G418. Stably α3 integrin transfected K562 cells were cultured in RPMI

media. After 2 passages, 3 * 10^5 α3 integrin transfected K562 cells were incubated with

LLY13 for three hours. Cell binding on LLY13 were observed under inverted

microscope. Parent K562 cells were used as a control.

5.4. Representative results

Before conducting the molecular receptor interaction study between LLY13 and

HSC-3, we used flow cytometry to obtain evidence that the HSC-3 cancer cells

expressed α3-integrin (data not shown). On the *in vitro* bead binding-blocking assay, as

shown in Figure 5.1, a panel of anti-integrin monoclonal antibodies (anti-α1, α2, α3, α4,

α5, α6, αV, and β1) were incubated with HSC-3 cancer cells prior to addition of LLY13

compound beads. Marked cell binding inhibition was observed only with anti-α3 integrin

antibody blocked HSC-3 cells. The inhibition of α3-integrin function was further

confirmed by incubation of α3-transfected K562 cells and parent K562 cells with LLY13

compound beads. K562 cells transfected with α3 integrin showed moderate binding to

LLY13 bead, while parent K562 cells did not (Figure 5.2).

5.5. Discussion:

Integrins are heterodimeric cell-surface receptors that have been implicated in regulating a variety of processes by mediating cell adhesion, migration, and signaling. At least twenty four different integrin heterodimers can be formed from the 18-α and 8-β chains that have been identified. The pairing of α and β subunits determines the ligand binding specificity of integrins (87, 88). For example, some integrin heterodimers specifically bind to ligands containing the tripeptide sequence RGD (89).   X1 OBOC combinatorial library in which we identify LLY13 is designed based on the binding motif of cdGXGXXc for α3β1 integrin in lung and ovarian cancers (76). The structure of the X1 OBOC combinatorial library is cdGXGXXcXX. Since LLY13 contains the same cdGXGXXc motif, α3β1 integrin is likely to be the corresponding receptor for LLY13 and OSCC cell interaction. To confirm this, HSC-3 oral cancer cells were treated separately with a panel of anti-integrin monoclonal antibodies (anti-α1, α2, α3, α4, α5, α6, αV, β1) prior to incubation with LLY13 peptide-beads. We found that only anti-α3 antibody could partially block HSC-3 cancer cell binding to LLY13-beads, indicating that the molecular target for LLY13 might be α3 integrin. However, anti β1antibody did not block the HSC-3 binding to LLY13, therefore, β1 integrin most likely is not the partial corresponding receptor involved for LLY13. Molecular interactions between LLY13 and α3 integrin was further elucidated using K562 myeloid leukemia cells transfected with mutant α3-integrins. K562 cells transfected with α3 integrin and parent K562 cells were incubated with LLY13 compound beads and as shown in Figure 5.2, only α3-transfected K562 cells exhibited moderate binding to LLY13 compound beads, whereas K562 parent cells did not. This further demonstrated the binding specificity of LLY13 to α3-integrin on HSC3 cells.

Since α3 integrins are commonly expressed in many epithelial cells and endothelial cells, and our OSCC binding ligands have thus far indicated strong binding to OSCC cells but not normal cells. Further studies are warranted to examine the possibility of somatic mutation, and expression pattern among the α3 integrins of OSCC cells in comparison to normal cells to elucidate the precise mechanism for our OSCCs' binding specificity.

5.6. Conclusion: Of the antibody panel tested, including anti-α1, α2, α3, α4, α5, α6, αV, β1 antibodies, only anti-α3 antibody was able to block most of the HSC3 cells binding to LLY13-beads. After incubation with LLY13 beads, the α3 integrin-transfected K562 cells were found to bind moderately to LLY13 beads, while parent K562 cells did not. Taken together, the data suggested that LLY13 partially interacts with α3 integrin on OSCC cells. Further studies are warranted to examine the possibility of somatic mutation, and expression pattern among the α3 integrins of HSC3 cells in comparison to normal cells to elucidate the precise mechanism for our OSCCs' binding specificity

5.7. Figures and Tables

Integrin Symbol	Integrin Names	Chromosome	Function
ITGA1	α1	5	Laminin Receptor
ITGA2	α2	5	Laminin, Collagen receptors
ITGA2B	α2b	17	Platelet glycoprotein IIIa complex
ITGA3	α3	17	Fibronectin, Laminin, Collagen, Epiligrin, Thrombospondin, CSPG4 Receptor
ITGA4	α4	2	Fibronectin Receptor
ITGA5	α5	12	Fibronectin, Fibrinogen receptor
ITGA6	α6	2	Laminin Receptors
ITGA7	α7	12	Laminin Receptors
ITGA8	α8	10	Tenascin, Fibronectin, Vitronectin Receptors
ITGA9	α9	13	
ITGA10	α10	1	Collagen Receptor
ITGA11	α11	15	Collagen Receptor
ITGAD	αD	16	ICAM-3 Receptor
ITGAE	αE	17	E Cadherin Receptor
ITGAL	αL	16	ICAM-3 Receptor
ITGAM	αM	16	Complement System
ITGAV	αV	2	Vitronectin Receptor
ITGAX	αX	16	Complement System
ITGB1	β1	10	
ITGB2	β2	X	
ITGB3	β3	21	
ITGB4	β4	17	
ITGB5	β5	3	
ITGB6	β6	2	
ITGB7	β7	12	
ITGB8	β8	7	

Table 5.1: Integrin heterodimers can be formed from the 18-α and 8-β chains and have different known functions.

Integrin	Pt percentage	Mutation %	Silent %	Missense %	Frameshift %	Nonsense%	Splicing%	Damage %
ITGA1	1.79%	2.51%	28.57%	71.43%	0.00%	0.00%	0.00%	57.14%
ITGA2	4.66%	5.02%	42.86%	50.00%	0.00%	0.00%	7.14%	35.71%
ITGA2B	2.51%	3.23%	22.22%	77.78%	0.00%	0.00%	0.00%	44.44%
ITGA3	2.51%	3.23%	22.22%	55.56%	0.00%	22.22%	0.00%	22.22%
ITGA4	5.38%	6.45%	22.22%	66.67%	0.00%	0.00%	11.11%	38.89%
ITGA5	2.15%	2.15%	33.33%	50.00%	0.00%	0.00%	16.67%	33.33%
ITGA6	1.43%	1.43%	0.00%	100.00%	0.00%	0.00%	0.00%	50.00%
ITGA7	4.30%	4.66%	38.46%	46.15%	0.00%	15.38%	0.00%	38.46%
ITGA8	8.60%	10.04%	3.57%	60.71%	7.14%	17.86%	7.14%	21.43%
ITGA9	2.15%	2.51%	57.14%	42.86%	0.00%	0.00%	0.00%	14.29%
ITGA10	4.66%	5.02%	14.29%	78.57%	7.14%	0.00%	0.00%	42.86%
ITGA11	4.30%	4.30%	8.33%	83.33%	8.33%	0.00%	0.00%	16.67%
ITGAD	3.23%	3.58%	20.00%	60.00%	0.00%	0.00%	20.00%	20.00%
ITGAE	1.79%	1.79%	20.00%	60.00%	20.00%	0.00%	0.00%	0.00%
ITGAL	4.66%	5.73%	43.75%	25.00%	12.50%	12.50%	6.25%	0.00%
ITGAM	3.94%	4.66%	23.08%	53.85%	0.00%	15.38%	7.69%	15.38%
ITGAV	3.23%	3.58%	20.00%	70.00%	10.00%	0.00%	0.00%	20.00%
ITGAX	2.51%	2.87%	0.00%	87.50%	12.50%	0.00%	0.00%	37.50%
ITGB1	6.09%	7.89%	4.55%	68.18%	4.55%	18.18%	4.55%	22.73%
ITGB1B2	1.79%	2.15%	16.67%	83.33%	0.00%	0.00%	0.00%	66.67%
ITGB2	2.15%	2.51%	28.57%	42.86%	0.00%	0.00%	28.57%	28.57%
ITGB3	2.87%	3.23%	0.00%	77.78%	11.11%	11.11%	0.00%	44.44%
ITGB4	6.09%	6.81%	52.63%	42.11%	5.26%	0.00%	0.00%	36.84%
ITGB5	1.08%	1.43%	75.00%	25.00%	0.00%	0.00%	25.00%	25.00%
ITGB6	3.94%	3.94%	45.45%	45.45%	0.00%	0.00%	0.00%	18.18%
ITGB7	1.08%	1.08%	66.67%	33.33%	0.00%	0.00%	0.00%	33.33%
ITGB8	3.58%	3.58%	30.00%	50.00%	0.00%	0.00%	20.00%	30.00%
ITGBL1	1.79%	1.79%	0.00%	0.00%	0.00%	0.00%	0.00%	60.00%

Table 5.2: Whole exome sequence analysis of integrin family in patient with head and neck cancer shows 186 non-synonymous mutations being found in 127 patients (127/509; 25%);

Integrin	Reference	Alternate	Codon Change	Mutation Change	Prediction
ITGA3	C	T	GGG T[C/T]A GAA	Single AA Change	Neutral
ITGA3	C	G	CAG A[C/G]C TAC	Single AA Change	Neutral
ITGA3	G	A	CCC [G/A]GT GCC	Single AA Change	Deleterious
ITGA3	C	T	ATT [C/T]AG CGC	Nonsense	NA
ITGA3	G	A	AAG CT[G/A] AGC	Synonymous	Neutral
ITGA3	C	T	AAA [C/T]GG AAC	Single AA Change	Deleterious
ITGA3	G	A	CCA GG[G/A] AGC	Synonymous	Neutral

	Reference	Alternative	Codon Change	Mutation Type	Prediction
ITGB1	G	C	AAT TT[C/G] AAG	Single AA Change	Neutral
ITGB1	CT	-		Frameshift	NA
ITGB1	C	T	AAC [G/A]AG GTC	Single AA Change	Neutral
ITGB1	A	C	TTC TA[T/G] TTT	Nonsense	NA
ITGB1	G	A	GTC [C/T]AA CCT	Nonsense	NA
ITGB1	G	A	TTT [C/T]AA GGG	Nonsense	NA
ITGB1	C	T	TGT [G/A]AA GCC	Single AA Change	Neutral
ITGB1	G	A	AAA TT[C/T] TGC	Synonymous	Neutral
ITGB1	C	T	GGC [G/A]CG TGC	Single AA Change	Neutral
ITGB1	C	T	AAG [G/A]AT TCT	Single AA Change	Neutral
ITGB1	T	-		Frameshift	NA
ITGB1	C	A	GAT [G/T]CA TAC	Single AA Change	Neutral
ITGB1	G	C	TTG AT[C/G] ATT	Single AA Change	Deleterious
ITGB1	C	G	CAG TT[G/C] ATC	Single AA Change	Deleterious
ITGB1	A	C	AAT G[T/G]A AAA	Single AA Change	Deleterious
ITGB1	C	T	GAC [G/A]AT TTG	Single AA Change	Deleterious
ITGB1	C	T	GAC [G/A]AT TTG	Single AA Change	Deleterious

Table 5.3: Whole Exome Sequence Analysis of α3, β1 integrins show 71% non-synonymous α3 mutations and 29% of the α3 aberrations were deleterious; 93% non-synonymous β1 mutations and 25% of the aberrations were deleterious.
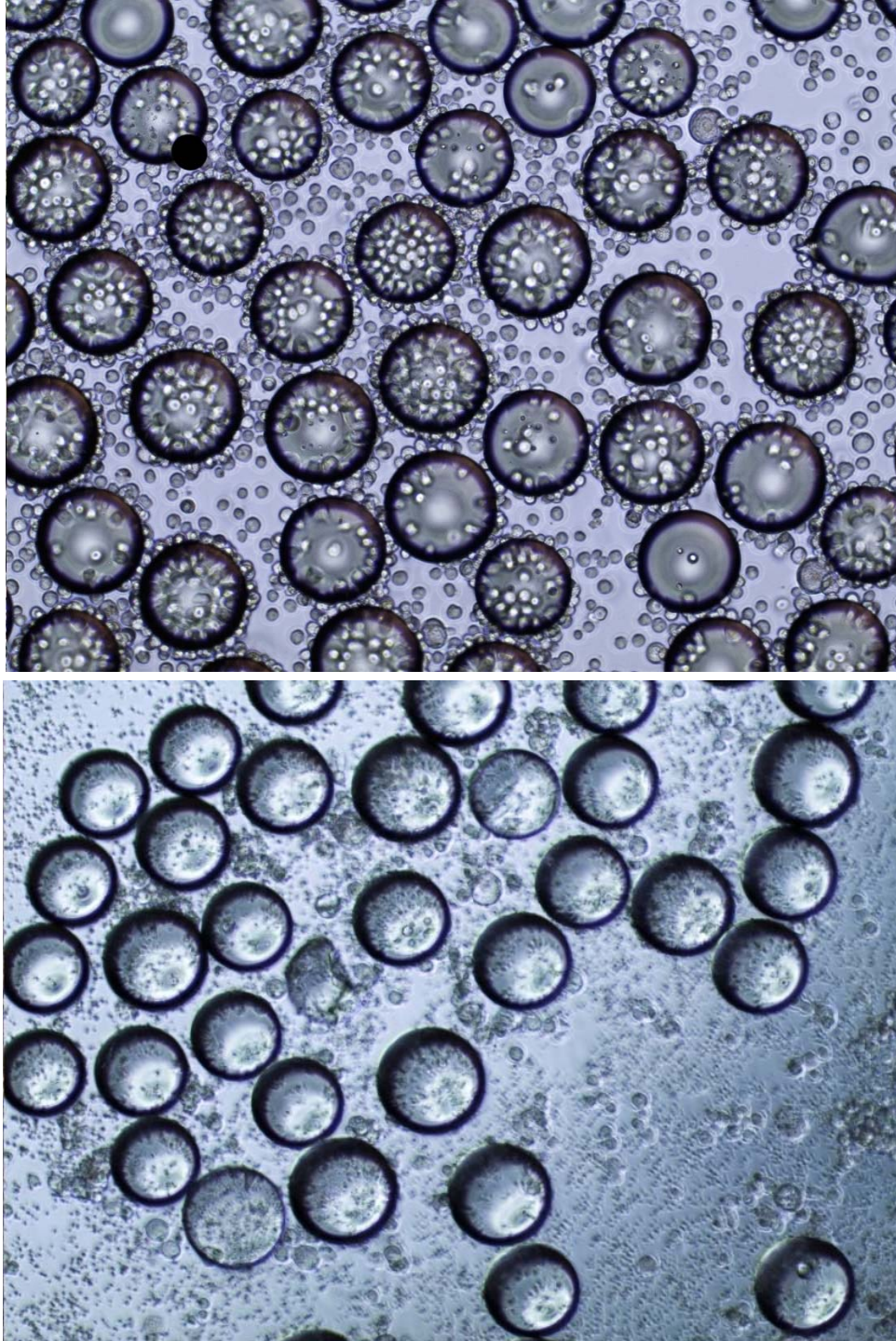
Figure 5.1: On the *in vitro* whole bead binding-blocking assay, a panel of anti-integrin monoclonal antibodies (anti α1, α2, α3, α4, α5, α6, αV, and β1) was incubated with HSC-3 cells prior to incubation with LLY13 compound beads. Top picture was the HSC-3 cells bind to the LLY13 compound beads; while there was a marked cell binding inhibition observed on anti-α3 integrin antibody blocked HSC-3 cancer cell (bottom).
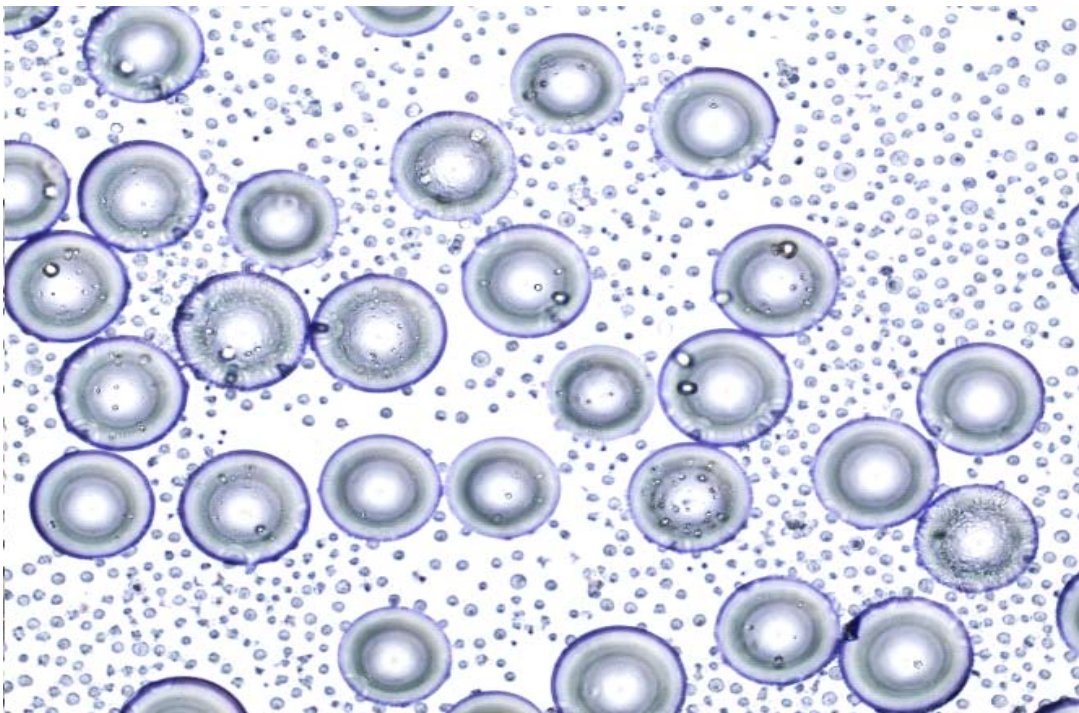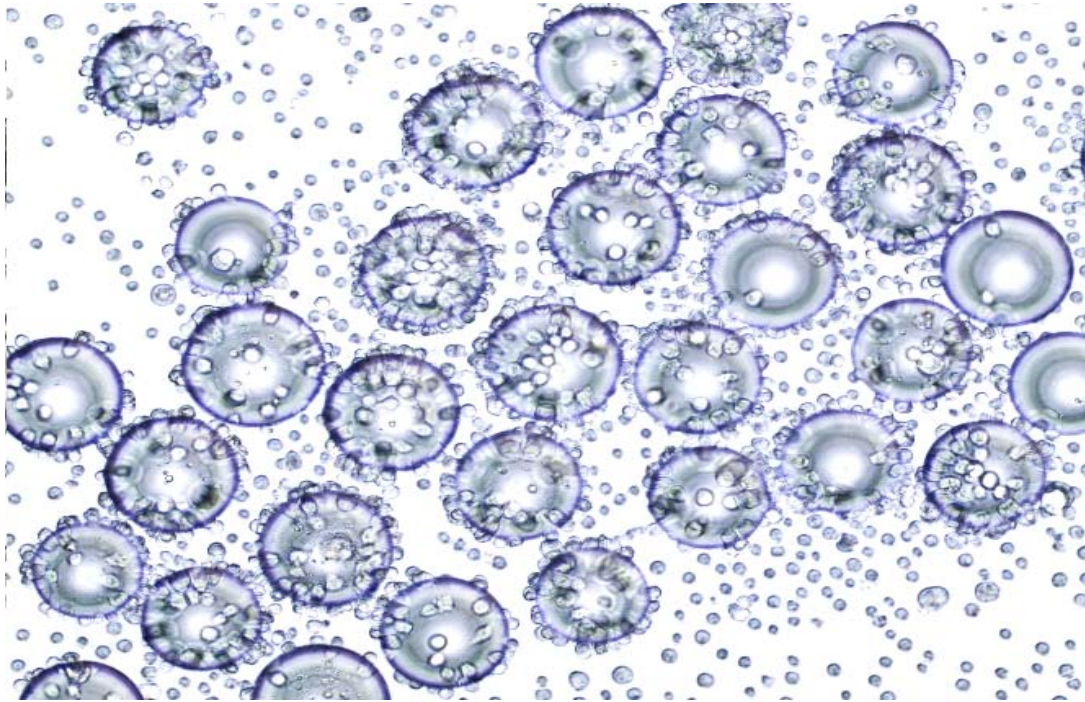
Figure 5.2: *in vitro* solid binding-blocking assay using α3 transfected K562 cells. α3 transfected K562 cells shows moderately binding to LLY13 compound beads (top), while K562 parent cells did not bind to LLY13 compound beads (bottom).

CHAPTER 6. DEVELOPMENT OF TARGETING NANO PROPHYRINS WITH BOTH IMAGING AND TERHAPEUTIC POTENTIAL AGAINST OSCC

6.1. Abstract: **Background**: Using OBOC combinatorial library techniques, we identified cancer-specific ligand, LLY13. *In vitro* studies indicated that LLY13 was able to bind to different OSCC cell lines, but not bind to normal human keratinocytes, endothelial cells and granulocytes. Cancer cell targeting capability of LLY13 was further confirmed on subcutaneous and orthotopic mice xenografts. In addition, LLY13 was found to have the ability to penetrate into OSCC cells and therefore might induce endocytosis. In this study, we assessed whether the targeting micelles decorated with LLY13 on the surface could enhance targeting mice OSCC cells or tissues. **Material and methods**: The traditional porphyrin/CA hybrid telodendrimer (PEG^{5k}-Por_4-CA_4), and the ligand conjugated porphyrin/CA hybrid telodendrimer (L-PEG^{5k}-CA_4)/ PEG^{5k}-Por_4-CA_4), were synthesized through solution-phase condensation reaction from MeO-PEG-NH_2 and N_3-PEG-NH_2 using peptide chemistry. After lyophilization, telodendrimer and ligand-porphyrin-telodendrimer were self-assembled in an aqueous solution to form non-targeting, targeting NPs micelles. **Results**: Targeting LLY13 micelles (25± 4nm in diameter) were more efficient in binding to HSC-3 cancer cells compared to non-targeting micelles. *Ex vivo* images demonstrated that both non-targeted micelles and targeting micelles exhibited relatively high uptake in the HSC-3 orthotopic tumors as compared to normal organs except for liver, while xenografts from the mice with targeting micelles appeared to have higher signals than the non-targeting groups, i.e., the median fluorescence intensity of tumors for targeting micelles is 2.44 folds higher than that for non-target micelles. **Conclusion**: NPs decorated with LLY13 is able to

enhance targeting OSCC cells *in vitro* and *in vivo*. Therefore, LLY13-NP is an excellent candidate for clinical development as a theranostic agent against OSCC after further optimization.

6.2. Introduction

In current treatment for oral cancer, anti-cancer drug or/ cocktail of drugs are used such as cisplatin, cetuximab, fluorouracil, paclitaxel, docetaxel, and methotrexate (90). These cytotoxic agents act through inhibiting protein synthesis by mimicking building blocks, to preventing cell replication by acting as alkylating agents that covalently link alkyl group in nucleic acids/proteins to crosslinking DNA strands, and inhibiting the disassembly of microtubules, to antimetabolites that inhibit proliferation of cells. The cocktail of drugs to treat cancers expose cells to different mechanism of action and overlapping toxicities; reducing the development of drug resistance, and increase the synergistic cytotoxic effect to achieve higher therapeutic efficacy (90). Unfortunately the limitation of cytotoxic agents are the safety profile and efficacy of chemotherapeutic agents, and most notably the high incidence of adverse effects including bone marrow suppression, alopecia, mucositis, nausea and vomiting (91). Nanomedicine has become a field of interest to overcome the limitation of current cancer treatment techniques. Nanoparticles, in definition are "unltradispersed solid supramolecular structures with a submicrometer size ranging from 10 to 1,000 um" (92). Different reported recipes for nanoparticles include dispersion of preformed polymers, the polymerization of monomers, ionic gelation and coacervation of hydrophilic polymers, and etc. The precise control of the size of these nanocarriers allows them to travel systemically yet limit their crossing of healthy region of the organism with tight

spacing of 15-30 nm (92). In case of inflammation in pathological regions such as in tumors, the endothelial cells are less tightly packed thereby allowing the accumulation of nanoparticles in the tumor tissue near blood vessels leading to the enhanced permeability and retention effect (EPR) (93). In the recent decades, oncology nanomaterial research has focused on: 1) synthesis of novel smart nanocarriers using organic and inorganic molecules; 2) surface functionalization through passive pegylation or active conjugation with biomolecules; 3) encapsulation of various first line hydrophobic chemotherapeutics with the design goal of enhance tumor uptake of these biocompatible nanoparticles that can deliver therapeutic agents of interest (94).

Clinically, major techniques used for oral cancer detection and diagnoses are computed tomography, magnetic resonance imaging, and position emission tomography (95). Inorganic nanoparticles such as iron oxide, gold oxide, titanium oxide, quantum dots, platinum oxides, have been shown to have unique physicochemical properties that include increase surface plasmon resonance that when localized in tissue will serve as valuable fluorescent probes, contrast agents and photo-absorbers when coupled with traditional imaging tools (96). However, unfavorable biodistribution, high background noise, and most importantly, concerns about the safety of the inorganic nanoparticles have drastically limited their broad clinical application (97). Organic nanoparticles such as paclitaxel (PTX) loaded polymeric micelles, liposomal doxorubicin (Doxil), liposomal vincristine (Marqibo) and PTX –loaded albumin nanoaggregate have been approved or are currently in clinical trials for the treatment of human cancers because of their excellent biocompatibility and drug-loading capacity

(98). However, there are mostly used as drug carriers and lack imaging functions and intrinsic light absorbing ability.

Theranostic agents are emerging as a paradigm towards personalized nanomedicine for patient specific diagnosis and treatment of cancer and other diseases. To truly achieve multifunctionality of theranostic, the nanoparticles should be prepared to overcome *in vivo* biological barriers such as interaction with blood proteins, lipoproteins, blood cells, blood vessel walls and the reticuloendothelial system, and be able to deliver drugs and imaging agents efficiently in a targeted manner to diseased tissues (99). For example, organic nanoparticles such as porphysome nanovesicles and conductive polymer have been recently studied as theranostic agents for their ability to be auto-fluoresce and transduce light to heat for photothermal therapy against cancer (100). However, those theranositc nanoparticles, like traditional imaging and therapeutic nanoparticles reported in the literature, have only been able to 'integrate a limited number of clinically useful functions" largely due to 1) complexity of fabrication, 2) their high liver and spleen accumulation resulting in non-specific clearance by the reticuloendothelial system, hence unfavorable biodistribution, and 3) high background noise and lack of an amplification strategy to increase the target's signal output (101).

Recently, a new nanoplatform developed by the Lam lab was reported as a 'robust, smart and highly versatile all in one porphyrin based organic nanoconstruct' that can be self-assembled from a novel hybrid amphiphilic polymer called teldodendrimer, comprised of dendritic cholic acid and porphyrin linked to a linear PEG. These porphyrin-based nanoparticle allows (i) efficient encapsulation of hydrophobic chemotherapeutic drugs, (ii) near-infra red fluorescent (NIRF) detection of the tumor

based on the intrinsic fluorescence of porphyrins, (iii) efficient free radical and heat generation at tumor site upon activation with light for photodynamic therapy (PDT) and photothermal therapy (PTT), respectively, and (iv) convenient ligation of cancer-targeting ligands to the surface of the micelle for cancer-specific targeted delivery (Figure 6.1) (102). This new porphyrin based nanoparticle when loaded with paclitaxel (PTX) and decorated with ovarian cancer binding ligands (discovered through OBOC library technique), exhibits superior anti-tumor efficacy and lower systemic toxicity profile in nude mice bearing ovarian cancer tumor xenograft when compared with equivalent doses of non-targeted PTX nanoparticles as well as clinical PTX formulation (44). This versatile porphyrin/cholic acid hybrid telodendrimer can self-assemble in aqueous solution by design, thereby integrating a variety of imaging and therapeutic function that includes imaging (near-infrared fluorescent imaging (NIFI), positron emission tomography, magnetic resonance tomography (MRI), dual modal PET-MRI, PTT and PDT as well as targeted drug delivery (102). In this study, we explore the potential targeting efficacy after novel OSCC targeting ligand, LLY13, is conjugated to this novel nanoplatofrm called nanoporphyrin (NP) as "nanoagents" for early diagnosis and treatment of OSCC.

6.3. Material and Methods

6.3.1. Materials: Bifunctional polyethylene glycol was purchased from Rapp Polymere (*Tübingen*, Germany). Cy5.5 Mono NHS ester was purchased from Amersham Biosciences (Piscataway, NJ). Paclitaxel was purchased from AK Scientific Inc. (Mountain View, CA). Taxol® (Mayne Pharma, Paramus, NJ) was obtained from the UC Davis Cancer Center Pharmacy. Cholic acid, MTT [3-(4, 5-dimethyldiazol-2-yl)-2, 5

diphenyl tetrazolium bromide] and all other chemicals were purchased from Sigma-Aldrich.

6.3.2. Generation of NPs: The traditional porphyrin/CA hybrid telodendrimer (PEG^{5k}-Por_4-CA_4), and the ligand conjugated porphyrin/CA hybrid telodendrimer (L-PEG^{5k}-CA_4)/ PEG^{5k}-Por_4-CA_4), were synthesized through solution-phase condensation reaction from MeO-PEG^{5k}-NH_2 and N_3-PEG^{5k} -NH_2 using peptide chemistry (Figure 6.2). In brief, Fmoc)Lys(Fmoc)-OH(3 eq.) was coupled on the N terminus of PEG using DIC and HOBt as coupling reagents until a negative Kaiser test result was obtained, thereby indicating completion of the coupling reaction. PEGylated molecules were precipitated by adding cold ether and then washed with cold ether twice. Fmoc groups were removed by the treatment with 20% (v/v) 4-methylpiperidine in dimethylformamide (DMF), and the PEGylated molecules were precipitated and washed three times by cold ether. White powder precipitate was dried under vacuum and one coupling of (Fmoc)Lys(Fmoc)-OH and one coupling of (Fmoc)lys(Boc)-OH were carried out, respectively, to generate a third generation of dendritic polylysine terminated with four Boc and Fmoc groups on one end of PEG. CA NHS ester were coupled to the terminal end of dendritic polylysine after the removal of Fmoc with 20% (v/v) 4-methylpiperidine and the removal of Boc groups with 50% (v/v) trifluoroacetic acid in dichloromethane, respectively. The telodendrimer solution was filtered and then dialysed against 4 L of water in a dialysis tube with MWCO of 3.5 KDa; reservoir water was refreshed completely four times in 24 h. Finally, the telodendrimer was lyophilized. Alkyne modified OSCC ligands (cdG-Nle-G-Hyp-c-Ebes-K-alkyne) was synthesized *via* solid-phase synthesis on Fmoc-Rink Amide MBHA Resins using the

standard Fmoc chemistry as described previously (40). 5-hexanoic acid was coupled onto the ε-amino group of lysine on the peptide. Alkyne modified ligands was conjugated to the N_3-PEG^{5k}-CA$_8$ telodendrimer *via* Cu^I catalyzed cyloaddition. The conjugation was confirmed by the amino acid analysis (AAA). To prepare NP and LNP, 20 mg porphyrin-telodendrimer or ligand-porphyrin-telodendrimer were dissolved in 1 ml PBS followed by sonication for 10 min to form NPs.

6.3.3. Characterization of NPs: In all, 20 mg porphyrin–telodendrimer were first dissolved in CHCl$_3$/MeOH, mixed and evaporated on rotavapor to obtain a homogeneous dry polymer film. The film was reconstituted in 1 ml PBS, followed by sonication for 30 min, allowing the sample film to disperse into NP solution. Finally, the NP solution was filtered with a 0.22-µm filter to sterilize the sample. Dynamic light scattering (DLS) was used to measure the size of nanoparticles synthesized. The absorbance spectra of the ligand porphyrin/CA hybrid telodendrimer was measured through UV-spectroscopy.

6.3.4. Cell targeting assay: HSC 3 oral cancer cells were seeded in 8-well chamber slides until confluent and then incubated with 2 µM porphyrin -telodendrimer nanoparticles and ligand (LLY13)-telodendrimer (L-PEG^{5k}-CA$_8$ with PEG^{5k}-Por$_4$-CA$_4$ (1:1)),for 0, 30, 1 hr and 2 hr at 37 °C with 5% CO$_2$, respectively. Then, cells were washed three times with cold PBS, fixed with 4% paraformaldehyde for 10 min, and the nuclei were counterstained by DAPI. The slides were mounted with coverslips and observed by Olympus FV1000 confocal microscopy. In a separate experiment, different concentration of porphyrin – telodendrimer (PEG^{5k}-Por$_4$-CA$_4$), and ligand – porphyrin –

telodendrimer ((L-PEG^{5k}-CA$_8$ with PEG^{5k} -Por$_4$-CA$_4$ (1:1)), (0, 0.05, 0.5, 5 µM) were incubated with HSC- 3 to study the uptake ability of these targeted NPs.

6.3.5. NIRF imaging: After nude mice (n= 12) developed established tumors (2 mm in diameter), they were subjected to *in vivo* NIRF imaging by injecting 100 µl of NPs via tail vein. At different time points post injection of NPs, mice were scanned using a Kodak multimodal imaging system IS2000MM with an excitation bandpass filter at 625/20 nm and an emission at 700/35 nm under anesthesia. After *in vivo* imaging, animals were killed. Tumors and major organs were excised and imaged with the Kodak imaging station.

6.3.6. Statistical analysis: Statistical analysis was performed by Student's *t*-test for two groups, and one-way analysis of variance for multiple groups. All results were expressed as the mean± s.d. unless otherwise noted. A value of *P*<0.05 was considered statistically significant.

6.3. Representative results

Synthesis and Characterization of Nanoparticles: Both non-targeted nanoporphyrin (NP) and ligand-decorated targeting nanoporphyrin (LNP) were assembled from hybrid telodendrimers comprised of linear polyethylene glycol (PEG) and dendritic oligomers of pyropheophorbide (a porphyrin analogue) and cholic acid (CA) (Figure 6.3). Alkyne modified OSCC ligands (Figure 6.3 A) were synthesized via stepwise solution-phase condensation reaction as reported previously, and its molecular weight from MALDI-TOF MS was identical to the theoretical value (Figure 6.3 B). Click chemistry was used to covalently conjugate alkyne-containing OTSCC ligand onto the

azide group at the PEG terminus of the N_3-PEG^{5k}-CA$_8$ (Figure 6.3 C), resulting in the LLY13-PEG^{5k}-CA$_8$ telodendrimer (Figure 6.3 D). High-Performance liquid chromatography was used to monitor the completion of the cyclo-addition of alkyne-modified OSCC ligand LLY13 to N_3-PEG^{5k}-CA$_8$ (Figure 6.3 E); with a 50 folds decrease in alkyne-LLY13. This self-assembled nanocarrier has a hydrophobic core and a hydrophilic shell. Dynamic light scattering (DLS) measurement revealed a particle size of 25± 4nm (Figure 6.3 F), that is consistent with previously published result from the Lam lab (102). The absorbance spectra of ligand porphyrin/CA hybrid telodendrimer is around 680 nm that is also consistent with previously published result from the Lam lab (102).The conjugation of LLY13 onto PEG^{5k}-CA$_8$ telodendrimer was further confirmed by quantitative amino acid analysis (AAA). LLY13-PEG^{5k}-CA$_8$ telodendrimer was hydrolyzed with HCl and quantitatively measured by HPLC.

Evaluation of NP vs LLY13- NPs targeting efficacy to human HSC-3 cancer cells: To evaluate targeting efficacy, HSC 3 cancer cells were incubated with targeting and non-targeting micelles for one hour before washing. Both targeting and non-targeting micelles were able to deliver porphyrin to the cells in a dose and time-dependent manner. The uptake for targeting micelles could be observed in as early as 5 mins while the uptake of non-targeting micelles was observed at 30 mins (Figure 6.4). In addition, the uptake of targeting micelles was observed at 0.05μM while non-targeting micelles was observed at 0.5 μM after 1 hr incubation. This data indicate LLY13, when linked to the surface of NP, can enhance its targeting efficacy to HSC3 cancer cells compared to non-targeting NP.

Imaging efficacy of NP in xenograft models: NIRF optical imaging is an important tool for visualizing molecular processes *in vivo*, as NIRF dyes has deeper tissue penetrating property, low auto-florescence, and low tissue absorption and scattering enable the high-resolution tissue imaging. Biodistribution of porphyrin–telodendrimer in mice bearing GFP positive orthotopic oral cancer showed the co-localization of porphyrin NP (red) with GFP positive tumor cells (red) (Figure 6.6). Fluorescent microscopy of tongue section of orthotopic xenograft of GFP positive HSC-3 cells shows porphyrin–telodendrimer accumulate around the peripheral of tumor but does not penetrate into the tumor tissue (Figure 6.7).

Imaging efficacy of LLY13-NP in xenograft models: Comparing to the non-targeting NP micelles, both of our non-targeting NP micelles and targeting LLY-13 NP micelles distributed throughout the body of the mice immediately after the intravenous injection, and gradually accumulated at tumor site as visualized by the localization of the GFP (green) signal from the GFP-transfected HSC-3 tumors and the NIRF signal from the LLY13-NPs. After 24hr, near infra-red uptake of tumors over background in in LLY13-NP injected mice was substantially higher than that of mice injected with non-targeting NPs. *Ex vivo* images at 24 hr demonstrated that both non-targeting NPs micelles and targeting LLY13-NPs micelles exhibited relatively high uptake in the HSC3 orthotopic tumor compared to normal organs (except for liver, possibly due to macrophage uptake) as a result of the EPR effect. Furthermore, ex vivo NIR images of xenografts from LLY13-NP injected mice was found to be 2.44 folds higher than that of non-targeting NP (Figure 6.8).

6.4. Discussion:

The major goal of this study is to identify cancer-specific ligands to develop theranostic agents against OSCC for early detection and treatment. We discovered LLY13, an oral cancer-targeting ligand from high throughput screening of combinatorial cyclic peptide library. It has high affinity and selectivity toward different human oral tongue cancer cell lines as well as cancer tissues from orthotopic mice xenografts. In addition, LLY13 showed the capability to penetrate to the human oral cancer cells via endocytosis. Here, we assessed whether the targeting micellar nanoporphyrin (NP) decorated with LLY13 on the surface could specifically target human oral cancer cells *in vitro* using cells grown on the chamber slides and *in vivo* using orthotopic mice xenograft model. The nanoporphyrin platform (24 +/- 4 nm) has several unique favorable features making it a highly versatile multifunctional nanoplatform: building blocks of the telodendrimer are non-toxic, scale up preparation to 50 gram level easily achievable, high-loading for many hydrophobic drugs or imaging probes, stability of NPs in the blood circulation, modular preparation via self-assembly of hybrid telodendrimer makes it easy to control the density and kinds of ligands on the surface of the nanoparticles, multi-modality imaging (MRI, PET, fluorescent) possible, non-specific uptake to normal organs relatively low when compared to tumors, and can afford efficient phototherapy (photodynamic and photothermal therapy). Thus NP is a smart nano-platform that can be useful for drug-delivery, imaging, image-guided surgery, and intra-operative phototherapy.

In this pilot study, we first examined the OSCC targeting efficiency of non-targeting nanoparticles. NIF imaging of the biodistribution of non-targeting porphyrin–telodendrimer in mice bearing GFP positive orthotropic oral cancer showed the co-

localization of porphyrin NP (red) with GFP positive tumor cells (red) . However, fluorescent microscopy of the tongue section of orthotopic xenograft of GFP positive HSC-3 cells only showed porphyrin–telodendrimer accumulate around the peripheral of tumor but did not penetrate into the tumor tissue. We therefore expected that the penetrating ligand LLY13 might help to deliver NPs into the tumors. Hence, we combined oral cancer-targeting ligand, LLY13, with a novel micelle drug delivery system. When decorated with LLY13 on the surface of micelles, targeting micelles NPS could not only adhere to the human oral cancer cells surface, but were also taken into the target cancer cells. *In vivo* studies show that targeting NPs were more efficient in delivering the imaging agents into the orthotropic tongue cancer xenografts in nude mice, compared to the non-targeting NPs.

The *in vivo* data indicates that LLY13 is an excellent cell surface targeting ligands against oral cancers. It has great potential to be developed into effective imaging and therapeutic agents against this disease. Targeting delivery of imaging agents has already been used in clinical setting. For example, octreotide, a cyclic peptide against somatostatin receptors, has been radiolabeled with indium-111 via the diethylene triamine penta-acetate chelate for imaging and detection of neuroendocrine tumors. Lin at al also reported that targeting PLZ4 micelles loaded with the imaging agent DID concentrated in the bladder in the tumor xenografts, but not uptake by liver and lungs (103).

Targeting NPs can be developed into therapeutic agents as well. This is can be done by the decoration of oral cancer specific ligand on the surface of NPs micelles loaded with chemotherapeutic drug such as paclitaxel, doxorubicin, and vincristine, to

facilitate the precise delivery of nano-encapsulated drugs to tumor site while sparing normal organs. Xiao et al reported that PTX-loaded OA02-nanomicelles exhibited superior antitumor efficacy and lower systemic toxicity profile in nude mice bearing SKOV-3 tumor xenografts when compared with equivalent doses of non-targeted PTX-nanomicelles as well as clinical paclitaxel formulation (44). Since LLY13 can target OSCC cancer cells *in vitro* via endocytosis, they can be conjugated to nanoporphyrins to deliver high concentration of drug to the target cells; it is reasonable to believe that such treatment may be able to overcome tumors that are drug resistant to standard chemotherapeutic regimens. Furthermore, for those tumors that are accessible to near infra-red light illumination, phototherapy can be performed to further enhance the anti-cancer efficacy. Due to the anatomical location, OSCC tumors in oral cavity is ideally suited for such combined photo-chemo-therapy, including the incorporation of heat shock protein inhibitors and/or chemotherapy inside LLY13-NPs.

6.5. Conclusion: NPs decorated with LLY13 is able to enhance targeting OSCC cells *in vitro* and *in vivo*. Therefore, LLY13-NP is an excellent candidate for clinical development as a theranostic agent against OSCC.

6.7. Figures and Tables:
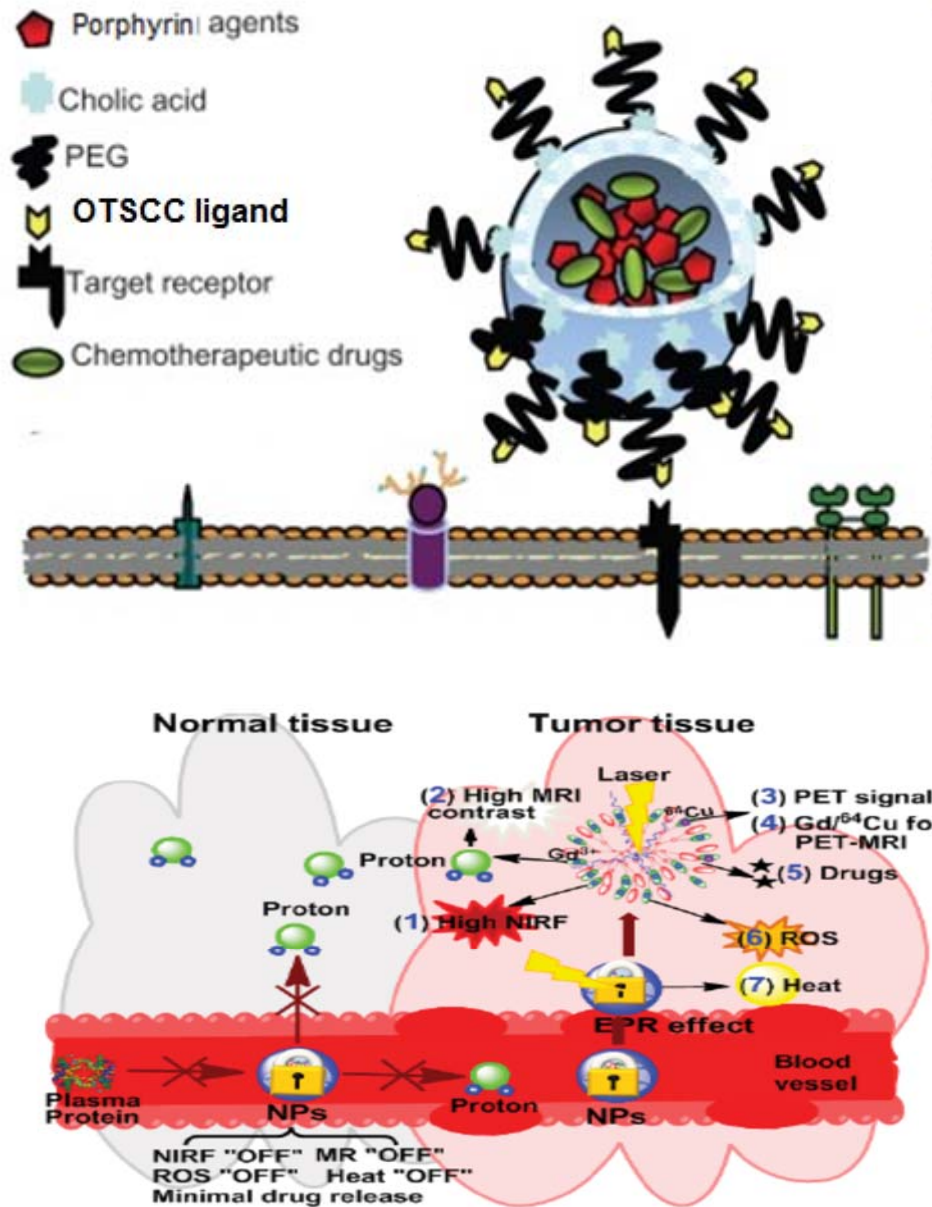
Figure 6.1: Design schematic of multifunctional porphyrin-based micellar nanoplatform: (1) near-infra red fluorescent (NIRF) detection of the tumor based on the intrinsic fluorescence of porphyrins.(2) efficient encapsulation of hydrophobic chemotherapeutic drugs. (3) efficient free radical and heat generation at tumor site upon activation with light for photodynamic therapy (PDT) and photothermal therapy (PTT), respectively, and (4) convenient ligation of cancer-targeting ligands to the surface of the micelle for cancer-specific targeted delivery.

Figure 6.2: The traditional porphyrin/CA hybrid telodendrimer (PEG^{5k}-Por$_4$-CA$_4$), and the ligand conjugated porphyrin/CA hybrid telodendrimer (L-PEG^{5k}-Por$_4$-CA$_4$), were synthesized through solution-phase condensation reaction from MeO-PEG-NH$_2$ and N$_3$-PEG-NH$_2$ using peptide chemistry. Alkyne modified ligands was conjugated to the N$_3$-PEG^{5k}-CA$_8$ telodendrimer via CuI catalyzed cyloaddition.
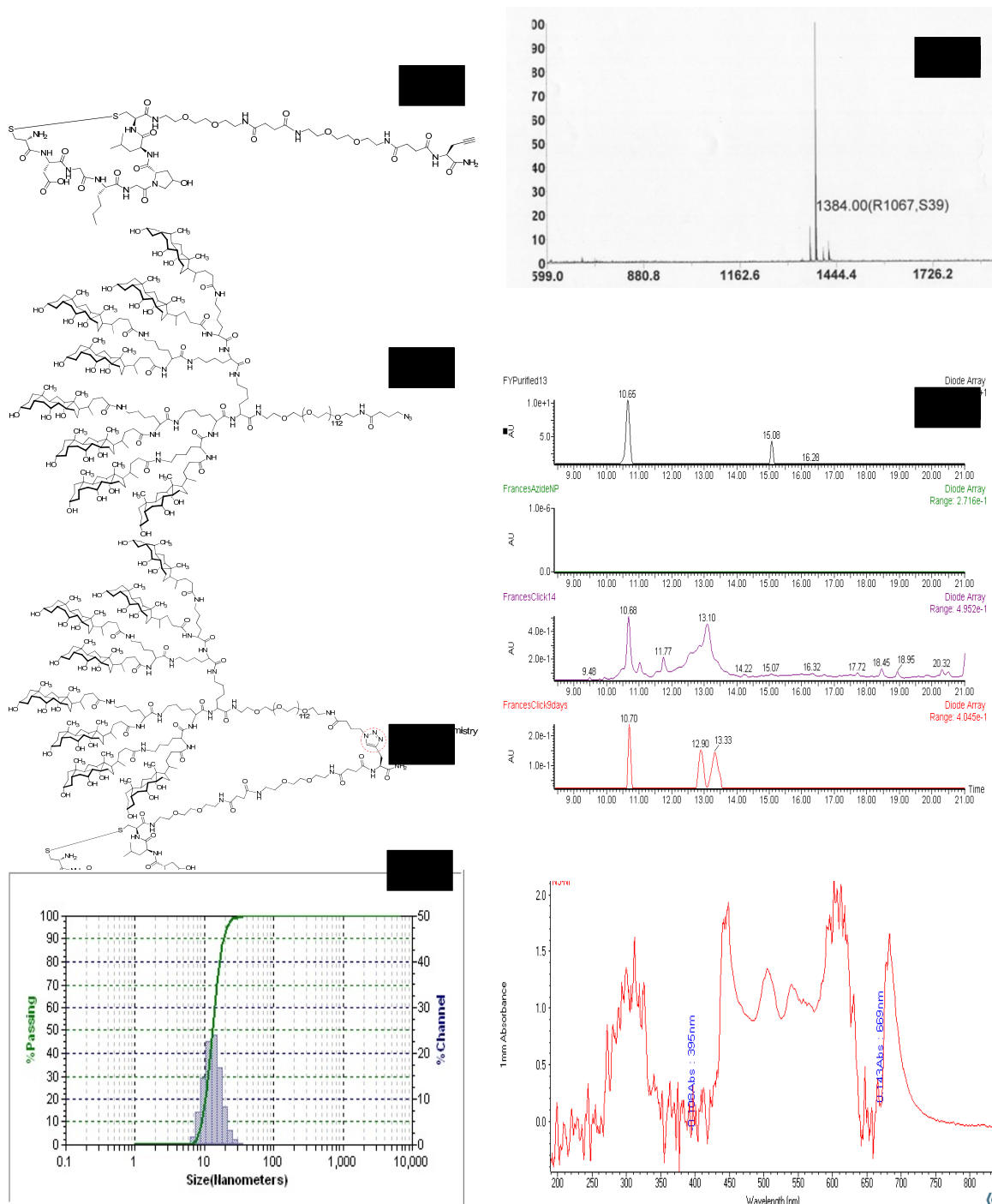
Figure 6.3: Schematic of a) alkyne modified OSCC ligands (cdG-Nle-G-Hyp-c-Ebes-K-alkyne); b) MS was used to confirm that alkyne modified OSCC ligands (cdG-Nle-G-Hyp-c-Ebes-K-alkyne; e) are of correct molecular weight; c) azide modified porphyrin/CA hybrid telodendrimer; d) ligand porphyrin/CA hybrid telodendrimer; e) High-Performance liquid chromatography was used to monitor the completion of the cyclo addition of alkyne modified OTSCC ligand and the azide modified porphyrin-telodendrimer as the concentration of the starting produced decreased by 50 folds; f) Dynamic light scattering shows the ligand porphyrin/CA hybrid telodendrimer is about 25+/- 4 nm in diameter; g) The absorbance spectra of ligand porphyrin/CA hybrid telodendrimer is around 680 nm.
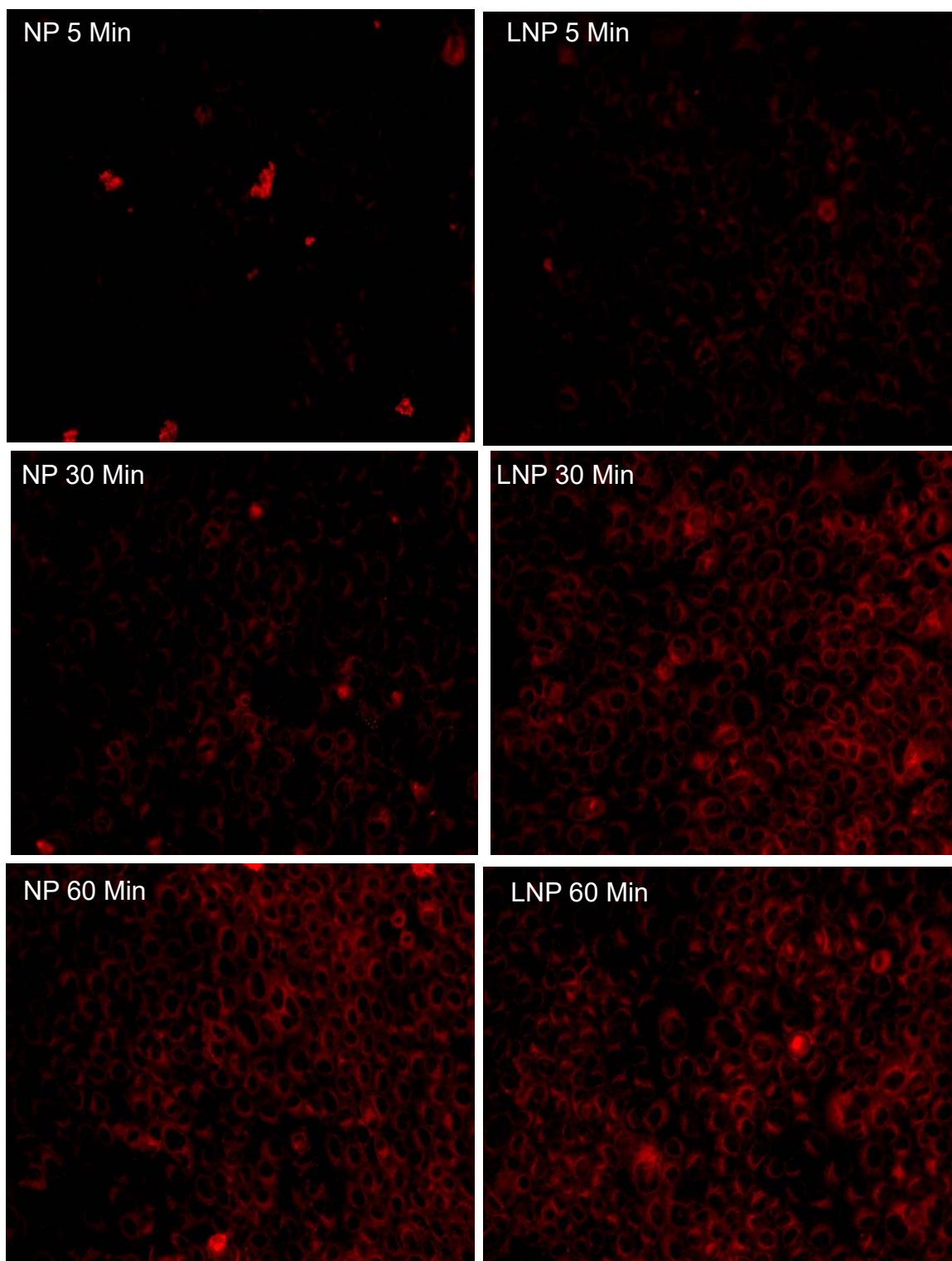
Figure 6.4: HSC-3 cells uptake of non-targeting and targeting micelles. The cellular uptake of targeting micelles could be observed as early as 5 min whereas the uptake of non-targeting micelles was observed at 30 min.
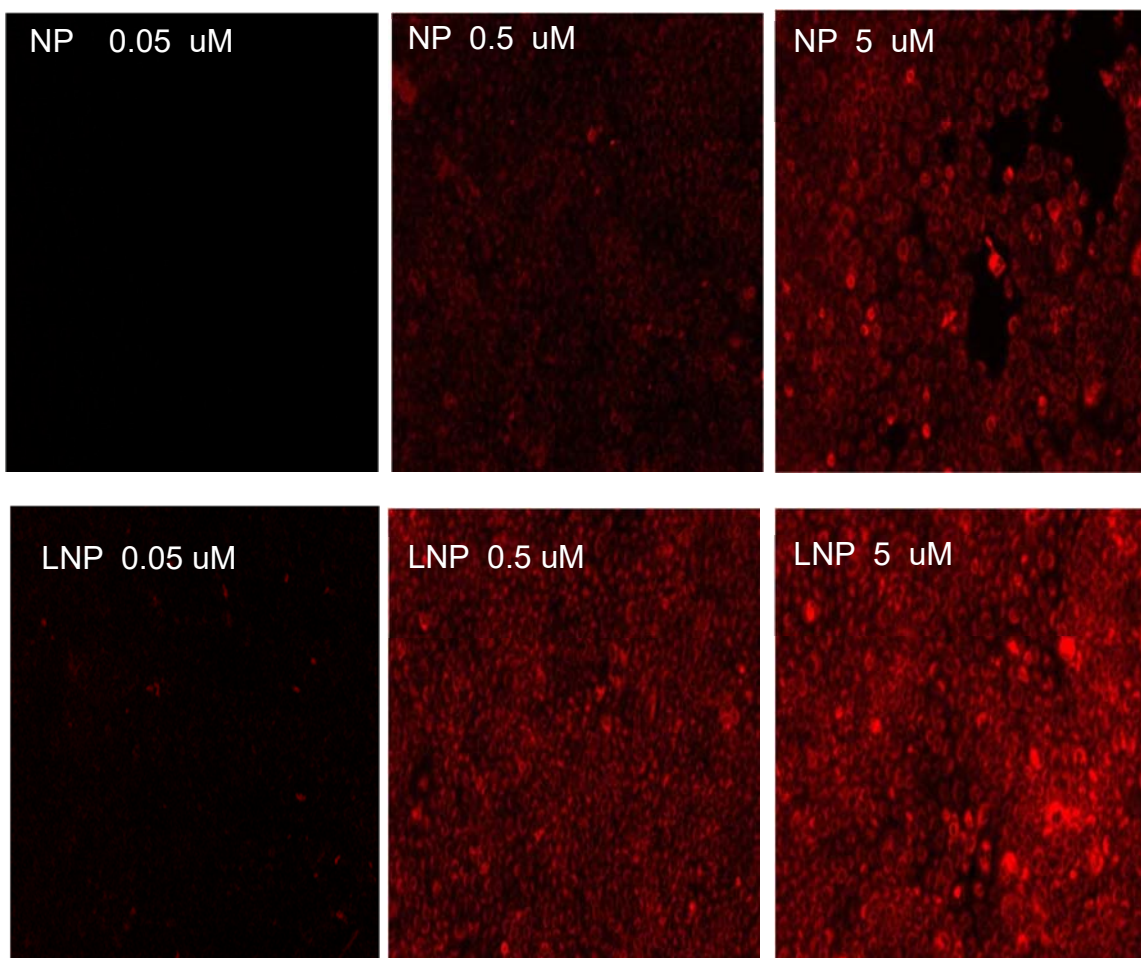
Figure 6.5: Both targeting and non-targeting micelles were able to deliver porphyrin to the cells in a dose dependent manner. The uptake for targeting micelles could be observed in as early as 5 mins at 0.05 uM after incubation, while the uptake for non-targeting micelles was shown up after 15 min at 5 uM after incubation.
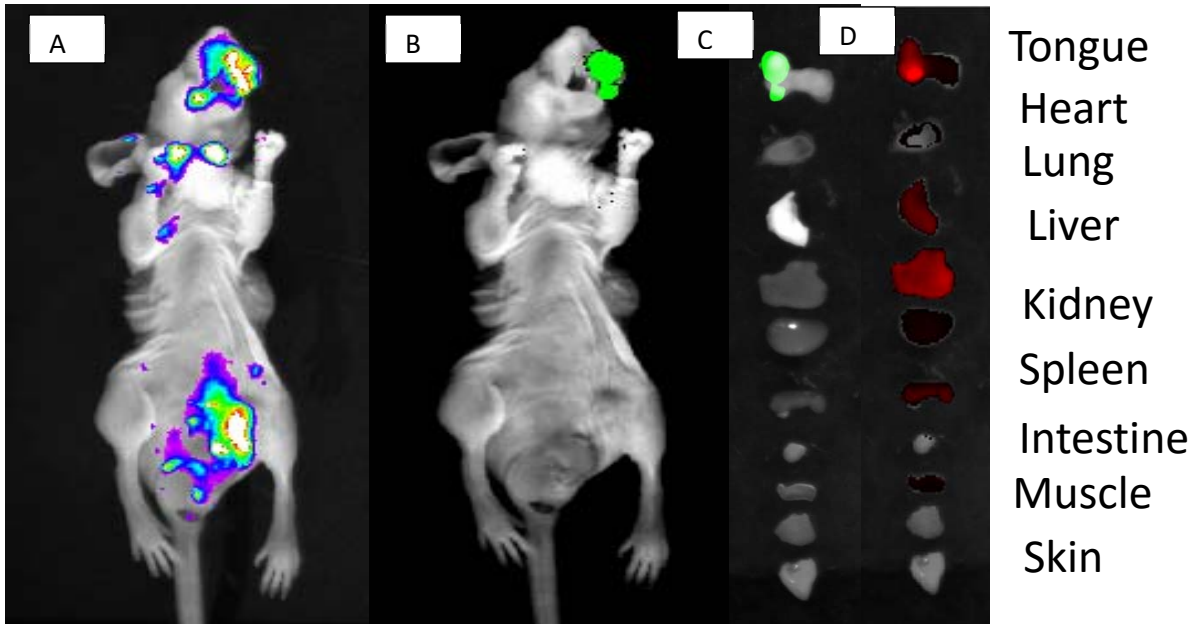
Figure 6.6: Biodistribution of porphyrin–telodendrimer in mice bearing GFP positive orthotopic oral cancer shows the co-localization of porphyrin NP (red) with GFP positive tumor cells (red).
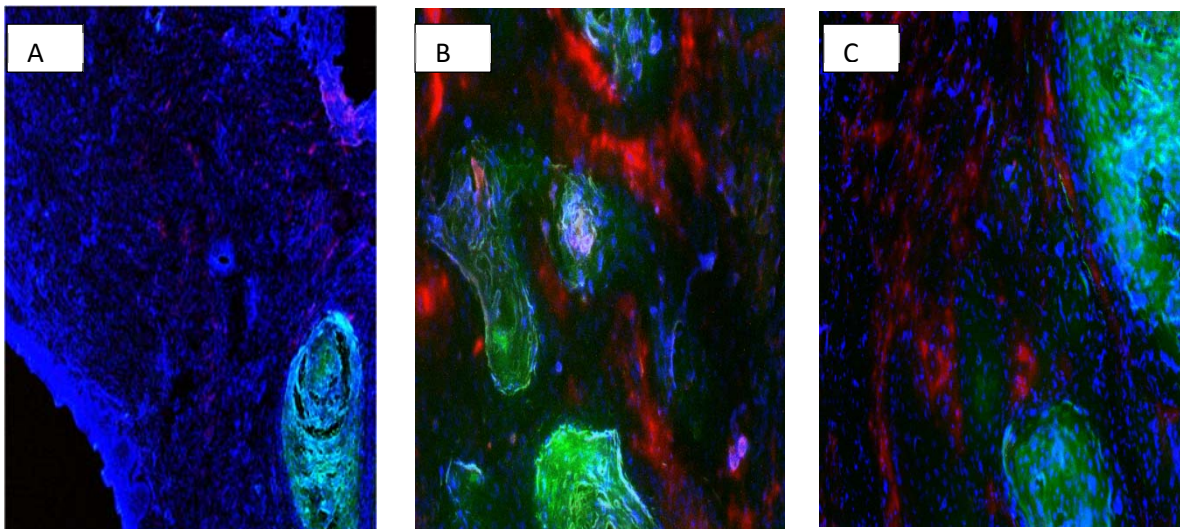
Figure 6.7: a) Fluorescent microscopy of tongue section of orthotropic xenograft o GFP positive HSC3 cells: b) porphyrin–telodendrimer accumulate around the peripheral of tumor but c) does not penetrate into the tumor tissue.
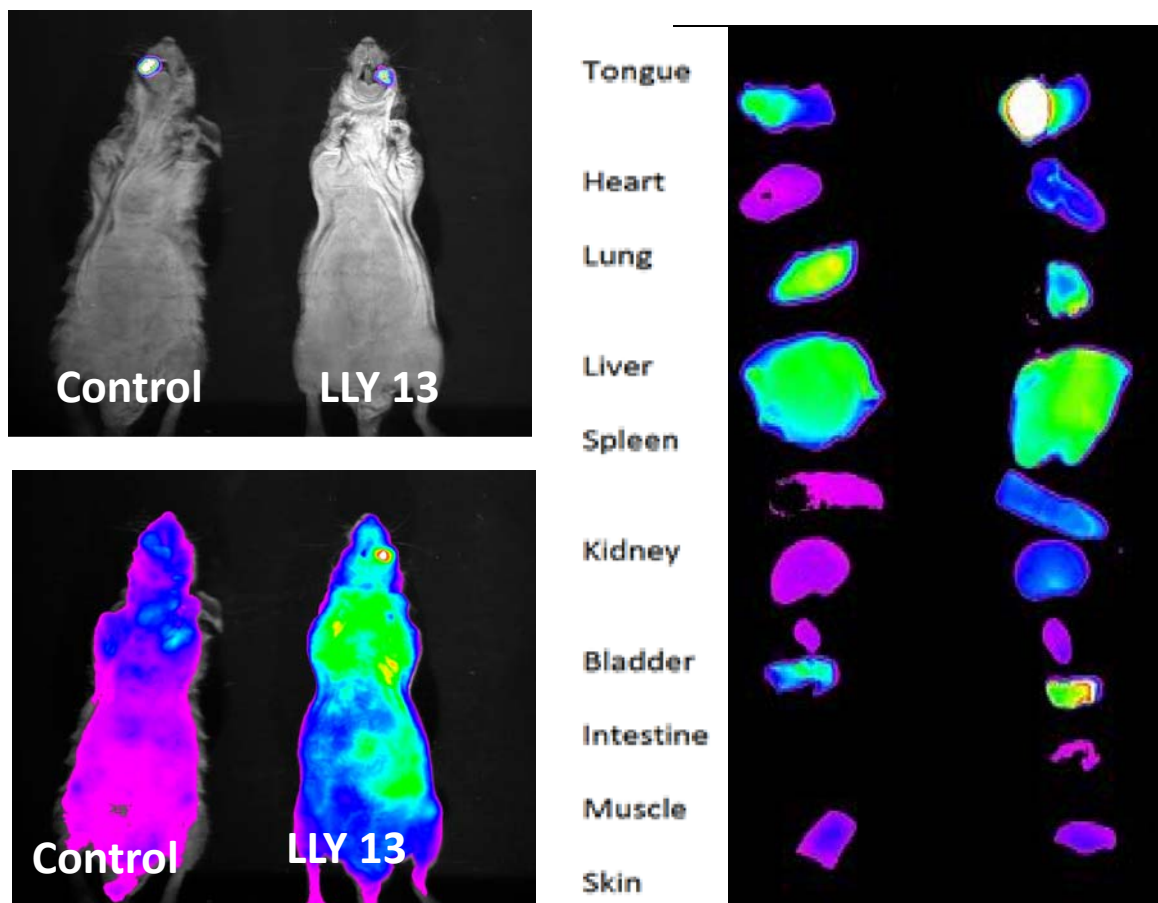
Figure 6.8: Ex vivo images at 24 h demonstrated that both non-targeted micelles and targeting micelles exhibited relatively high uptake in the HSC3 orthotopic tumor compared to normal organs except for liver, possibly due to macrophage uptake as result of EPR effect, while xenografts from the mice with targeting micelles appeared to have higher signals than the non-targeting groups, ie, the median fluorescence intensity of tumors for targeting micelles is 2.44 folds higher than that for non-targeting micelles.

CHAPTER 7. CONCLUSION AND FUTURE PERSPECTIVES

7.1 **Conclusion**: Oral cancer is one of the 10th most common cancers in the world, mostly attributed to delayed clinical detection, poor prognosis, lack of specific biomarkers for the disease and expensive therapeutic alternatives. This study focuses on the synthesis and screening of OBOC libraries with the aim to find specific peptidomimetic compounds that binds to oral squamous carcinoma cancer cells (OSCC), in an attempt to develop theranostic agents to improve the tumor targeting imaging and consequently the anti-tumor efficacy. Through screening twenty-four OBOC peptide libraries against four different OSCC cell lines, six cyclic peptide ligands were identified and developed as the OSCC optical imaging probes. Two of these probes, LLY12 and LLY13 are able to specifically bind to different OSCC cell lines grown on the chamber slides at 1 μM. *In vivo* and *ex vivo* near infra-red fluorescence optical imaging studies have confirmed the targeting efficiency and specificity of LLY13 in HSC-3 subcutaneous xenografts as well as in HSC-3 orthotopic xenografts. NPs micelles decorated with LLY13 is able to enhance targeting and uptake into OSCC cells in our *in vitro* and *in vivo* studies. Also, LLY13 has been proven to be capable of penetrating into HSC-3 and Mok-101 cancer cells grown on chamber slides and may induce endocytosis, making it an excellent candidate for use as efficient vehicle to deliver drug loaded-nanoparticles for OSCC therapy. Overall, the novel OSCC targeting ligand LLY13 disclosed here represents as a promising candidate for further advancement study in the domain of targeted tumor imaging as well as anti-tumor targeting therapy.

Work is currently underway in our laboratory to evaluate the binding profile of LLY13 to cancer tissues obtained directly from primary human OSCC tumors. Since LLY13 does not bind to normal keratinocytes, should it prove to bind strongly to a significant portion of clinical OSCC cancer specimens, it will have great translational potential. First, LLY13 based optical probe can be developed as a simple non-invasive method for early detection of OSCC. This test can potentially be performed by primary care providers. Second, LLY13 can be developed into a PET imaging probe for detection of both local and metastatic diseases, making it a valuable tool for staging workup. Third, since LLY13 is able to bind and penetrate OSCC cells, it can be used as vehicle for the delivery of potent toxin such as MMAE, for systemic therapy. In addition, it can also be used as vehicle for delivery of nanocarriers with encapsulated anti-cancer drugs. Finally, as detailed in the previous chapters, LLY13 can be used to decorate nanoporphyrin and used as highly effective photosensitizer for phototherapy of oral cancers. Since LLY13 is cyclic and composed of natural and unnatural amino acids, it resists proteolytic degradation and be stable for *in vivo* application. Therefore, LLY13 is an excellent peptide ligand that has great translational potential in tumor-specific imaging and chemotherapy drug delivery to the tumor sites while sparing the normal tissues.

7.2 FUTURE PERSPECTIVES

The critical future requirements for effective early detection of OSCC include development of high-quality molecular markers, noninvasive methods for specimen procurement, economical, high-throughput, robust platform for testing, social recognition of need, economic support of testing and availability of expert diagnosticians, and

availability of effective preventive measures for precancerous lesions. Through screening OBOC combinatorial libraries, we identified LLY13 that can specifically target OSCC cells as demonstrated in our *in vitro* and *in vivo* studies. More works have been proposed here for the future studies:

1. Optimization of LLY13. The structure activity relationship study (SAR) will be performed to find the essential amino acid residues that are necessary to keep the OSCC cell binding functions.   Based on the information obtained from SAR, highly focused OBOC combinatorial libraries will be designed and screened under higher stringency conditions by lowering the bead surface substitution, shorter incubation time or add soluble competing receptor specific antagonist against OSCC, so that ligands with higher affinity and higher specificity can be identified.

2. Validation of LLY13-receptor interaction. *In vitro* study indicated that only anti-α3 antibody was able to block the most of OSCC cells binding to the LLY13 compound beads, while β1 integrin antibody didn't block the OSCC cell binding. More anti-β integrin antibodies, such as β1, β2, β3, β4, β5 integrin antibodies binding to different epitopes will be employed to better define the LLY-3 receptor involved. *In vivo* study will be further employed by administrating anti-α3 integrin blocking antibody prior to add the LLY13-biotin/SA-Cy5.5 complex to the orthotropic xenograft model. Fluorescent density will be compared to the controls.

3. Elucidation of the mechanism of action of the cell penetrating process through the application of known endocytosis pathway inhibitors. In order to determine whether the cell penetration are mediated by endocytosis, we can apply the inhibitors, such as

dynasore , chlorpromazine (clathrin dependent endocytosis) , filippin and nystatin (caveolar dependent endocytosis), amiloride and wortmanin (micropinocytosis) to the cells prior to application of our fluorescent-labeled LLY13. Inhibition profile of LLY13-triggered cell uptake will enable us to define the mechanisms of uptake.

4. Evaluation of binding profile of LLY13 to a series of pre-cancerous lesions (such as leukoplakia, erythroplakia, or combined pathologies) and OSCC using peptide-histochemistry or fluorescent microscopy. Hematoxylin and eosin-stained sections will be used to confirm clinical diagnosis and to grade the specimens. OSCC samples are graded as well, moderately or poorly differentiated. Oral epithelial dysplasia samples are histopathologically graded as mild, moderate or severely dysplastic. Colleagues from Department of Somatology, Medical Center of Tianjing Medical University, P.R.China will be able to provide human biopsy specimens for such study. Five-micron thickness of human OSCC samples will be obtained in paraffin-embedded tissues and placed on 3-amino propyl triethoxy silane coated slides. The sections will be de-paraffinised and brought to water. The sections will be placed in sodium citrate buffer (pH 6) and antigen retrieval will be done using an autoclave at 15 psi for 15 min. The slides will be washed three times inris buffer saline solution. The endogenous blocking will be performed with avidin and biotin provided in the endogenous biotin blocking kit. The sections will be incubated with LLY13-biotin at room temperature for 1 h and then incubated with streptavidin-PE for 30 min. Counterstained with hematoxylin will be used as positive control. Standard benchmark will be used to evaluate the intensity of staining among the study group.

REFERENCES

1.   Warnakulasuriya S. Global epidemiology of oral and oropharyngeal cancer. Oral Oncol. 2009; 45:309–316.

2.   Chi AC, Day TA, Neville BW. Oral cavity and oropharyngeal squamous cell carcinoma--an update. CA Cancer J Clin. 2015; 65:401-21.

3.   Chaturvedi AK, Anderson WF, Lortet-Tieuleut J. Worldwide trends in incidence rates for oral cavity and oropharyngeal cancers J. Clin. Oncol. 2013:31:4550-4559.

4.   Lingen MW, Kalmar JR, Karrison T and Speight PM. Critical evaluation of diagnostic aids for the detection of oral cancer. Oral Oncol 2008;44:10-22.

5.   Dissanayaka WI, Pitiyage G, Kumarasiri PV, Layanage RL, Dias KD and Tilakaraene WM. Clinical and histopathologic parameters in survival of oral squamous cell carcinoma. Oral Surg Oral Med Oral Pathol Oral Radiol 2012; 113:518-525.

6.   Jemal A, Bray F, Center MM, Ferlay J, Ward E, Forman D. Global cancer statistics. CA Cancer J Clin 2011; 61:69–90.

7.   Ganly I, Patel S, Shah J. Early stage squamous cell cancer of the oral tongue - clinicopathologic features affecting outcome. Cancer. 2012; 118:101–111.

8.   Chandler, C. Vance, S. Budnick, S. Muller. Muscle invasion in oral tongue squamous cell carcinoma as predictor of nodal status and local recurrence: just as effective as depth of invasion? Head Neck Pathol. 20; 5: 359–363.

9.   Ferlay J, Shin HR, and Bray F. Estimates of worldwide burden of cancer in 2008 Int J Cancer. 2010; 127: 2893–2917.

10.   Mishra A, Meherotra R. Head and neck cancer: global burden and regional trends in India. Asian Pac J Cancer Prev. 2014; 15(2): 537–550.

11.   Osuna T, Kopkins S. Oral cancer diagnosis technologies. CDHA J. 2008; 24(1) 12-8.

12.   Lane P. Simple device for the direct visualization of oral-cavity fluorescence. J Biomed Opt. 2006; 11:240.

13.   Rivera C, Venegas B. Histological and molecular aspects of oral squamous cell carcinoma. Oncol Lett. 2014; 8:7-11.

14.   Patel SG, Shah JP. TNM staging of cancers of the head and neck: striving for uniformity among diversity. CA Cancer J Clin. 2005; 55(4):242-58.

15.   Taghavi N, Yazdi I. Prognostic factors of survival rate in oral squamous cell carcinoma: clinical, histologic, genetic and molecular concepts. Arch Iran Med. 2015 ;18:314-9.

16.   Yu CH, Lin HP, Cheng SJ, Sun A, Chen HM. Cryotherapy for oral precancers and cancers. J Formos Med Assoc. 2014;113: 272-7.

17.   Napier SS, Speight PM. Natural history of potentially malignant oral lesions and conditions: an overview of the literature. J Oral Pathol Med. 2008; 37:1-10.

18.   Mithani SK, Mydlarz WK, Grumbine FL, Smith IM, Califano JA. Molecular genetics of premalignant oral lesions. Oral Dis. 2007;13(2):126-33.

19.   Damphousse KE, Mowls DS, Beebe LA. An Ecological Analysis of Tobacco Use and Oral Cavity and Pharynx Cancers in U.S. Males. J Okla State Med Assoc. 2015;108(11):488-9.

20.   Varoni EM, Lodi G, Iriti M.Ethanol versus Phytochemicals in Wine: Oral Cancer Risk in a Light Drinking Perspective. Int J Mol Sci. 2015; 27; 17029-47.

21.   Manvikar V, Kulkarni R, Koneru A, Vanishree M. Role of human papillomavirus and tumor suppressor genes in oral cancer.J Oral Maxillofac Pathol. 2016; 20(1):106-10.

22.   Ajila V, Shetty H, Babu S, Shetty V, Hegde S.Human. Papilloma Virus Associated Squamous Cell Carcinoma of the Head and Neck. J Sex Transm Dis. 2015 2015:791024.

23.   Çankaya H, Güneri P, Epstein JB. Adjunctive methods and devices for clinical detection of oral squamous cell carcinoma. Oral Health Prev Dent. 2015; 13(1):29-39

24.   Liu CH, Chen HJ, Wang PC, Chen HS, Chang YL. Patterns of recurrence and second primary tumors in oral squamous cell carcinoma treated with surgery alone. Kaohsiung J Med Sci. 2013;29(10):554-9.

25.   Aina O.H., R. Liu, J.L. Sutcliffe, J. Marik, C.X. Pan, K.S. Lam. From combinatorial chemistry to cancer-targeting peptides. Mol. Pharm. 2007;4:631–651.

26.   Lam KS, Salmon SE. A new type of synthetic peptide library for identifying ligand-binding activity. Nature. 1991; 354:82-4.

27.   Peng L, Liu R, et al. Combinatorial chemistry identifies high-affinity peptidomimetics against alpha4beta1 integrin for in vivo tumor imaging. Nat Chem Biol. 2006 ;2(7):381–9.

28.   Wu CY, Wang DH, Wang X, Dixon SM, Meng L, Ahadi S, Enter DH, Chen CY, Kato J, Leon LJ, Ramirez LM, Maeda Y, Reis CF, Ribeiro B, Weems B, Kung HJ, Lam KS. Rapid Discovery of Functional Small Molecule Ligands against Proteomic Targets through Library-Against-Library Screening. ACS Comb Sci. 2016; 3. [Epub ahead of print].

29.   Mendes K, Ndungu JM, Clark LF, Kodadek T. Optimization of the Magnetic Recovery of Hits from One-Bead-One-Compound Library Screens. ACS Comb Sci. 2015;17(9):506-17.

30.   Cho CF, Amadei GA, Breadner D, Luyt LG, Lewis JD. Discovery of novel integrin ligands from combinatorial libraries using a multiplex "beads on a bead" approach. Nano Lett. 2012 14;12:5957-65.

31.   Lam, K. S.; Lebl, M.; Krchnak, V.The "One-Bead-One-Compound" Combinatorial Library Method Chem. Rev. 1997; 97: 411– 448.

32.   Lam, K. S.; Liu, R.; Miyamoto, S.; Lehman, A. L. Tuscano, J. M. Applications of one-bead one-compound combinatorial libraries and chemical microarrays in signal transduction research Acc. Chem. Res. 2003;36:370– 377.

33.   Meldal, M.; Svendsen, I.; Breddam, K.; Auzanneau, F. I. Portion-mixing peptide libraries of quenched fluorogenic substrates for complete subsite mapping of endoprotease specificity. Proc Natl Acad Sci. 1994; 91:3314– 3318.

34.   Olsen, J. A.; Jensen, K. J.; Nielsen, J. Combinatorial solid-phase synthesis of hapalosin mimetics J Comb Chem. 2000; 2:143–150.

35.   Copeland, G. T.; Miller, S. J. Selection of enantioselective acyl transfer catalysts from a pooled peptide library through a fluorescence-based activity assay: an approach to kinetic resolution of secondary alcohols of broad structural scope. J Am Chem Soc. 2001; 123: 6496– 6502.

36.   Evans, C. A.; Miller, S. J. Proton-activated fluorescence as a tool for simultaneous screening of combinatorial chemical reactions Curr Opin Chem Biol. 2002; 6: 333– 338.

37.   Tozzi, C.; Anfossi, L.; Baggiani, C.; Giovannoli, C.; Giraudi, G.A combinatorial approach to obtain affinity media with binding properties towards the aflatoxins Anal. Bioanal. Chem. 2003; 375: 994– 999.

38.   Kaufman, D. B.; Hentsch, M. E.; Baumbach, G. A.; Buettner, J. A.; Dadd, C. A.; Huang, P. Y.; Hammond, D. J.; Carbonell, R. G.Affinity purification of fibrinogen using a ligand from a peptide library. Biotechnol Bioeng. 2002; 77: 278– 289.

39.   Li Y, et al. A novel size-tunable nanocarrier system for targeted anticancer drugs delivery. J Control Release. 2010 15; 144(3):1314–23.

40.   Li Y, Xiao K, et al. Well-defined, reversible disulfide cross-linked micelles for on-demand paclitaxel delivery. Biomaterials. 2011; 32(27):6633–45.

41.   Xiao K, Li Y, et al. The effect of surface charge on in vivo biodistribution of PEG-oligocholic acid-based micellar nanoparticles. Biomaterials. 2011;32(13):3435–46.

42.   Xiao K, Luo J, et al. A self-assembling nanoparticle for paclitaxel delivery in ovarian cancer. Biomaterials. 2009;30:6006–16.

43.   Luo J, Xiao K, et al. Well-defined, size-tunable, multifunctional micelles for efficient paclitaxel delivery for cancer treatment. Bioconjug Chem. 2010 21;21(7):1216–24.

44.   Xiao K, Li Y, Lee J, Lam K. OAO2 peptide facilitates the precise targeting of paclitaxel-loaded micellar nanoparticles to ovarian cancer in vivo. Cancer Res. 2012; 15; 72(8):2100-10.

45.   Luo J, Zhang H, et al. Rainbow beads: a color-coding method to facilitate high-throughput screening and optimization of one-bead one-compound combinatorial libraries. J Comb Chem. 2008; 10(4):599–604.

46.   Almutary A, Sanderson BJ. The MTT and Crystal Violet Assays: Potential Confounders in Nanoparticle Toxicity Testing. Int J Toxicol. 2016 May 20. pii: 1091581816648906. [Epub ahead of print].

47.   Gibbs S. *In vitro* irritation models and immune reactions. Skin Pharmacol Physiol. 2009; 22(2):103-13

48.   Palek J, Liu SC. Red cell membrane skeleton: structure-function relationships. Prog Clin Biol Res. 1980; 43:21-44

49.   Carvajal-Hausdorf DE, Schalper KA, Neumeister VM, Rimm DL. Quantitative measurement of cancer tissue biomarkers in the lab and in the clinic.Lab Invest. 2015; 95(4):385-9

50.   Robers MB, Binkowski BF, Cong M, Zimprich C, Corona C, McDougall M, Otto
G, Eggers CT, Hartnett J, Machleidt T, Fan F, Wood KV A luminescent assay for real-
time measurements of receptor endocytosis in living cells. Anal Biochem. 2015;15;
489:1-8.

51.   Fujioka Y, Nanbo A, Nishide SY, Ohba Y. Fluorescent protein-based biosensors
to visualize signal transduction beneath the plasma membrane. Anal Sci.
2015;31(4):267-74.

52.   Sano D, Myers J. Xenograft models of head and neck cancers. Head & Neck
Oncology 2009; 13;1-32.

53.   Sano D, Fooshee DR, Zhao M, Andrews GA, Frederick MJ, Galer C, Milas ZL,
Morrow PK, Myers JN.Targeted molecular therapy of head and neck squamous cell
carcinoma with the tyrosine kinase inhibitor vandetanib in a mouse model. Head Neck.
2011;33(3):349-58.

54.   Wang Y, Zhu Y, Lv P, Li L. Targeting miR-21 with AS-miR-21 suppresses
aggressive growth of human tongue squamous cell carcinoma *in vivo*. Int J Clin Exp
Pathol. 2015;1;8(5):4773-81.

55.   Weng J, Wang C, Wang Y, Tang H, Liang J, Liu X, Huang H, Hou J.Beclin1
inhibits proliferation, migration and invasion in tongue squamous cell carcinoma cell
lines. Oral Oncol. 2014;50(10):983-90.

56.   Xiao W, Li T, Bononi F, Lac D, Kekessie A, Liu Y, Sanchez E, Lam K, Liu R.
Discovery and characterization of a high-affinity and high-specificity peptide ligand

XXY30 for *in vivo* targeting of alfa 3 integrin-expressing human tumor. EJNMMI Res. 2016 Dec; 6(1):18. doi: 10.1186/s13550-016-0165-z. Epub 2016 Feb 27.

57. Xiao W, Wang Y, Lau EY, Luo J, Yao N, Shi C, Meza L, Tseng H, Maeda Y, Kumaresan P, Liu R, Lightstone FC, Takada Y, Lam KSMo The use of one-bead one-compound combinatorial library technology to discover high-affinity αvβ3 integrin and cancer targeting arginine-glycine-aspartic acid ligands with a built-in handle. Cancer Ther. 2010;9(10):2714-23.

58. Xiao W, Yao N, Peng L, Liu R, Lam KS. Near-infrared optical imaging in glioblastoma xenograft with ligand-targeting alpha 3 integrin. Eur J Nucl Med Mol Imaging. 2009;36(1):94-103.

59. Yao N, Xiao w, Wang X, Marik J, Park S, Lam K. Discovery of targeting ligands for breast cancer cells using the one-bead one-compound combinatorial method J Med Chem 2009;8:126-133

60. Yellapurkar S, Natarajan S, Boaz K, Baliga M, Shetty P, Manaktala N, Prasad M, Ravi M.Tumour-Associated Tissue Eosinophilia in Oral Squamous Cell Carcinoma- A Boon or a Bane? J Clin Diagn Res. 2016;10(4):65-8.

61. Sumedha S, Kotrashetti VS, Somannavar P, Nayak R, Babji DA histochemical comparison of methyl green-pyronin, and hematoxylin and eosin for detecting apoptotic cells in oral squamous cell carcinoma, oral leukoplakia, oral submucous fibrosis and normal oral mucosa. Dent Res J. 2013; 10(6):784-9.

62.   Dyce OH, Ziober AF, Weber RS, Miyazaki K, Khariwala SS, Feldman M, Ziober BL. Integrins in head and neck squamous cell carcinoma invasion. Laryngoscope. 2002; 112(11):2025-32.

63.   Oliveira CR, Marqueti Rde C, Cominetti MR, Douat ES, Ribeiro JU, Pontes CL, Borghi-Silva A, Selistre-de-Araujo HS. Effects of blocking αvβ3 integrin by a recombinant RGD disintegrin on remodeling of wound healing after induction of incisional hernia in rats. Acta Cir Bras. 2015; 30(2):134-42.

64.   Yao N, Xiao W, Wang X, Marik J, Park SH, Takada Y, Lam KS. Discovery of targeting ligands for breast cancer cells using the one-bead one-compound combinatorial method. J Med Chem. 2009; 52(1):126-33.

65.   Irimie A, Braicu C, Cojocneanu-petric R. Novel technologies for oral squamous carcinoma biomarkers in diagnostic and prognostics. Acta Odontologica Sandinavica 2015;73(3):161-8.

66.   Boy S.C. Leukoplakia and erythroplakia of the oral mucosa—a brief overview SADJ. 2012; 67:558–560.

67.   L. Feller, J. Lemmer. Oral Squamous cell carcinoma: epidemiology, clinical presentation and treatment. J Can Ther. 2012;3:263-268.

68.   Mahomed F. Oral submucous fibrosis—a potentially malignant condition of growing concern. SADJ. 2012; 67:562–5.

69.   Scully. C., Bagan, J. Oral squamous cell carcinoma overview. Oral Oncology, 2009; 45:301–308.

70.   Van der Waal I. Potentially malignant disorders of the oral and oropharyngeal mucosa; terminology, classification and present concepts of management. Oral Oncology, 2009;45: 317–323.

71.   Hughes PE, Caenepeel S, Wu LC. Targeted Therapy and Checkpoint Immunotherapy Combinations for the Treatment of Cancer. Tren ds Immunol. 2016 May 20. pii: S1471-4906(16)30033-3.

72.   Levêque D. Off-label use of targeted therapies in oncology. World J Clin Oncol. 2016;10;7(2):253-7.

73.   Fujii M. [New therapeutic strategy for head-and-neck neoplasms--Molecular target therapy]. Nihon Jibiinkoka Gakkai Kaiho. 2015;118 (11):1369-74.

74.   Liu R, Li X, Xiao W, Lam KS. Tumor-targeting peptides from combinatorial libraries. Adv Drug Deliv Rev. 2016 May 19. pii: S0169-409X(16)30151-X. doi: 10.1016/j.addr.2016.05.009. [Epub ahead of print].

75.   Aina OH, Marik J, Liu R, Lau DH, Lam KS. Identification of novel targeting peptides for human ovarian cancer cells using "one-bead one-compound" combinatorial libraries.Mol Cancer Ther. 2005;4(5):806-13.

76.   Aina OH, Marik J, Gandour-Edwards R, Lam KS Near-infrared optical imaging of ovarian cancer xenografts with novel alpha 3-integrin binding peptide "OA02".Mol Imaging. 2005;4(4):439-47.

77.   Cheng YS, Rees T, Wright J. Updates Regarding Diagnostic Adjuncts for Oral Squamous Cell Carcinoma. Tex Dent J. 2015 Aug; 132(8):538-49.

78.   Rethman MP, Carpenter W, Cohen EE, Epstein J, Evans CA, Flaits CM. Evidence-based clinical recommendations regarding screening for oral squamous cell carcinaoma. J Am Dent Assoc. 2010;141:509-20

79.   Carreras-Torras C, Gay-Escoda C.Techniques for early diagnosis of oral squamous cell carcinoma: Systematic review. Med Oral Patol Oral Cir Bucal. 2015; 20(3):305-15

80.   Lingen MW, Kalmar JR, Karrison T, Speigh PM. Critical evaluation of diagnostic aids for the detection of oral cancer. Oral Oncol. 2008;44:10-22

81.   Irimie AI1, Braicu C, Cojocneanu-Petric R, Berindan-Neagoe I, Campian RS. Novel technologies for oral squamous carcinoma biomarkers in diagnostics and prognostics. Acta Odontol. Scand.2015;73(3):161-8.

82.   Rumboldt Z1, Day TA, Michel M.Oral Oncol. Imaging of oral cavity cancer. 2006 ;42(9):854-65.

83.   Carreras-Tprras C, Gay-Escpda C. Tecjmoques for early diagnosis of oral squamous cell carcinoma: systematic review. Med Oral Patol Oral Cir Bucal 2015; 20:305-15.

84.   Pelleitier M, Montplaisir S. The nude mouse: a model of deficient T-cell function. Methods Achiev Exp Pathol. 1975; 7:149-66.

85.   Rolstad B.The athymic nude rat: an animal experimental model to reveal novel aspects of innate immune responses? Immunol Rev. 2001; 84:136-44.

86.   Sano D, Myer J. Xenograft models of head and neck cancers. Head &Neck Oncology Head Neck Oncol. 2009;13:1:32. doi: 10.1186/1758-3284-1-32.

87.   Akiyama SK Integrins in cell adhesion and signaling. Hum Cell. 1996 Sep; 9(3):181-6.

88.   Takada Y, Ye X, Simon S. The integrins. Genome Biol. 2007;8:215-222

89.   Kunicki TJ1, Ely KR, Kunicki TC, Tomiyama Y, Annis DS.J Biol Chem. The exchange of Arg-Gly-Asp (RGD) and Arg-Tyr-Asp (RYD) binding sequences in a recombinant murine Fab fragment specific for the integrin alpha IIb beta 3 does not alter integrin recognition.1995;14;270(28):16660-5.

90.   Huang SH, O'Sullivan B. Oral cancer: Current role of radiotherapy and chemotherapy. Med Oral Patol Oral Cir Bucal. 2013; 1; 18(2):e233-40.

91.   Mao L.Oral squamous cell carcinoma - progresses from risk assessment to treatment. Chin J Dent Res. 2012; 15(2):83-8.

92.   Lim WQ, Phua SZ, Xu HV, Sreejith S, Zhao Y. Recent advances in multifunctional silica-based hybrid nanocarriers for bioimaging and cancer therapy. Nanoscale. 2016 Jan 11 [Epub ahead of print].

93.   Maeda H, Fang J, Ulbrich K, Etrych T, Nakamura H. Missile-Type Tumor-Targeting Polymer Drug, P-THP, Seeks Tumors via Three Different Steps Based on the EPR Effect. Gan To Kagaku Ryoho. 2016; 43(5):549-57.
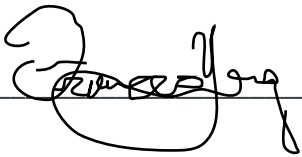
94. Mocan T, Matea CT, Iancu C, Agoston-Coldea L, Mocan L, Orasan R.Hypersensitivity and nanoparticles: update and research trends. Clujul Med. 2016; 89(2):216-9.

95. Zygogianni AG, Kyrgias G, Karakitsos P, Psyrri A, Kouvaris J, Kelekis N, Kouloulias V. Oral squamous cell cancer: early detection and the role of alcohol and smoking. Head Neck Oncol. 2011 Jan 6;3:2. doi: 10.1186/1758-3284-3-2.

96. Peng HS, Chiu DT. Soft fluorescent nanomaterials for biological and biomedical imaging. Chem. Soc. Rev. 2015 Jul 21;44(14):4699-722. doi: 10.1039/c4cs00294.

97. Huang X, El-Sayed M. Gold nanoparticles: Optical properties and implementations in cancer diagnosis and photothermal therapy. J Adv Res. 2010:1:13–28.

98. Zarschler K, Rocks L, Licciardello N, Boselli L. Ultrasmall inorganic nanoparticles: State-of-the-art and perspectives for biomedical applications, Nanomedicine: Nanotechnology. Bio Med. 2016. 22. pii: S1549-9634(16)30010-7. doi: 10.1016/j.nano.2016.02.019. [Epub ahead of print].

99. Xie J, Lee S, Chen X. Nanoparticle-based theranostic agents. Adv Drug Deliv Rev. 2010 Aug 30; 62(11): 1064–1079.

100. Calixto GMF, Bernegossi J, Freitas LM, Fontana C, Chorilli M. Nanotechnology-Based Drug Delivery Systems for Photodynamic Therapy of Cancer: A Review. Molecules. 2016 Mar 11;21(3). pii: E342. doi: 10.3390/molecules21030342.

101. Abrahamse H, Hamblin M. New photosensitizers for photodynamic therapy. Biochem J. 2016; 473:347–364.

102. Li YP, Lin TY, Lam KS. A Smart and Versatile Theranostic Nanomedicine Platform based on Nanoporphyrin. 2014 Aug 26;5:4712. doi: 10.1038/ncomms5712.

103. Lin TY, Zhang H, Luo J, Li Y, Gao T, Lara PN Jr, de Vere White R, Lam KS, Pan CX. Multifunctional targeting micelle nanocarriers with both imaging and therapeutic potential for bladder cancer. Int J Nanomedicine. 2012;7:2793-804.

Publishing Agreement

It is the policy of the University to encourage the distribution of all theses, dissertations, and manuscripts. Copies of all UCSF theses, dissertations, and manuscripts will be routed to the library via the Graduate Division. The library will make all theses, dissertations, and manuscripts accessible to the public and will preserve these to the best of their abilities, in perpetuity.

I hereby grant permission to the Graduate Division of the University of California, San Francisco to release copies of my thesis, dissertation, or manuscript to the Campus Library to provide access and preservation, in whole or in part, in perpetuity.

Author Signature_____ Date _6/10/16_